

Quantum Spin Liquid States

Yi Zhou,^{1,2} Kazushi Kanoda,³ and Tai-Kai Ng⁴

¹*Department of Physics and Zhejiang Institute of Modern Physics,
Zhejiang University,
Hangzhou, 310027,
P. R. China*

²*Collaborative Innovation Center of Advanced Microstructures,
Nanjing 210093,
China*

³*Department of Applied Physics,
University of Tokyo,
Hongo 7-3-1, Bunkyo-ku,
Tokyo 113-8656,
Japan*

⁴*Department of Physics,
Hong Kong University of Science and Technology,
Clear Water Bay Road,
Kowloon, Hong Kong,
China*

(Dated: March 18, 2019)

This article is an introductory review of the physics of quantum spin liquid (QSL) states. Quantum magnetism is a rapidly evolving field, and recent developments reveal that the ground states and low-energy physics of frustrated spin systems may develop many exotic behaviors once we leave the regime of semi-classical approaches. The purpose of this article is to introduce these developments. The article begins by explaining how semi-classical approaches fail once quantum mechanics become important and then describes the alternative approaches for addressing the problem. We discuss mainly spin 1/2 systems, and we spend most of our time in this article on one particular set of plausible spin liquid states in which spins are represented by fermions. These states are spin-singlet states and may be viewed as an extension of Fermi liquid states to Mott insulators, and they are usually classified in the category of so-called $SU(2)$, $U(1)$ or Z_2 spin liquid states. We review the basic theory regarding these states and the extensions of these states to include the effect of spin-orbit coupling and to higher spin ($S > 1/2$) systems. Two other important approaches with strong influences on the understanding of spin liquid states are also introduced: (i) matrix product states and projected entangled pair states and (ii) the Kitaev honeycomb model. Experimental progress concerning spin liquid states in realistic materials, including anisotropic triangular lattice systems (κ -(ET)₂Cu₂(CN)₃ and EtMe₃Sb[(Pd(dmit)₂)₂]), kagome lattice systems (ZnCu₃(OH)₆Cl₂) and hyperkagome lattice systems (Na₄Ir₃O₈), is reviewed and compared against the corresponding theories.

PACS numbers: 75.10.Kt, 71.10.-w, 71.10.Ay, 71.30.+h

CONTENTS

I. Introduction	2	III.2. $U(1)$ gauge fluctuations	14
II. From semi-classical to non-linear- σ model approaches for quantum antiferromagnets	3	III.2.1. Mott transition: relation between Fermi and spin liquids	16
II.1. Two-spin problem	3	III.3. Z_2 spin liquid states	18
II.2. Berry's phase	4	III.4. Numerical realization of Gutzwiller projection: variational Monte Carlo method and some results	19
II.3. Non-linear- σ -model	4	III.4.1. One-dimensional lattice	20
II.3.1. Topological term	5	III.4.2. Triangular lattice	21
II.4. Quantum spin chains and the Haldane conjecture	6	III.4.3. Kagome lattice	22
II.4.1. Integer spin chains	6	III.5. Classification of spin liquid states: quantum orders and projective symmetry groups	23
II.4.2. Half-odd-integer spin chains	7	IV. Beyond RVB approaches	25
II.4.3. Open spin chains and end states	7	IV.1. RVB and its generalization to spin systems with strong spin-orbit coupling	25
II.5. Higher dimensions and frustrated quantum antiferromagnets	8	IV.2. RVB approach to $S > 1/2$ systems	27
III. Resonant valence bond (RVB) states	8	IV.3. Matrix product state (MPS) and projected entangled pair state (PEPS)	29
III.1. RVB theory and gauge Theory	11	IV.3.1. Valence-bond solids and MPSs in one	

dimension	29
IV.3.2. PEPSSs in higher dimensions and beyond	31
IV.4. Kitaev honeycomb model and related issues	32
 V. QSL states in real materials	 35
V.1. Anisotropic triangular lattice systems:	
κ -(ET) ₂ Cu ₂ (CN) ₃ and EtMe ₃ Sb[(Pd(dmit) ₂) ₂	35
V.2. Kagome-lattice system: ZnCu ₃ (OH) ₆ Cl ₂	41
V.3. Hyperkagome-lattice system: Na ₄ Ir ₃ O ₈	44
V.4. Experimental summary	46
 VI. Summary	 49
Acknowledgments	50
 A. Path integral for a single spin	 50
References	51

I. INTRODUCTION

Quantum spin liquid (QSL) states in dimensions of $d > 1$ have been a long-sought dream in condensed matter physics. The general idea is that when acting on spin systems, quantum mechanics may lead to exotic ground states and low-energy behaviors that cannot be captured by traditional semi-classical approaches. The difficulty in implementing this idea is that we have no natural place to start once we have left the comfort zone of semi-classical approaches, at least in dimensions larger than one. Except for a few exactly solvable models, we must rely heavily on numerical or variational approaches to “guess” the correct ground state wavefunctions and on a combination of sophisticated numerical and analytical techniques to understand the corresponding low-energy excitations.

Several excellent reviews are available on QSLs (Balents, 2010; Lee, 2008a) and frustrated magnetism (Diep, 2004; Lacroix *et al.*, 2011). This article complements those mentioned above by providing a pedagogical introduction to this subject and reviews the current status of the field. We explain, at an introductory level, why sophisticated approaches are needed to study QSL states, how these approaches are implemented in practice, and what new physics may be expected to appear. The experimental side of the story and the drawbacks or pitfalls of the theoretical approaches are also discussed. We concentrate mainly on spin 1/2 systems and study in detail one particular set of plausible spin liquid states that are usually termed resonating valence bond (RVB) states. The spins are treated as fermions in these states, which may be viewed as an extension of Fermi liquid states to Mott insulators. They are usually classified in the category of $SU(2)$, $U(1)$ or Z_2 spin liquid states. Because of the intrinsic limitations of the fermionic RVB approach, many other approaches to spin liquid states have been developed by different authors. These approaches often lead to other exotic possibilities not covered by the simple fermionic approach. Two of these approaches are introduced in this article for completeness: (i) matrix

product states and projected entangled pair states and (ii) the Kitaev honeycomb model.

The article is organized as follows. In section II, we introduce the semi-classical approach to simple quantum antiferromagnets, and we explain the importance of the spin Berry phase and how one can include it in a semi-classical description to obtain the correct theory. In particular, we show how it leads to the celebrated Haldane conjecture. The existence of end excitations as a natural consequence of the low-energy effective theory of these systems is discussed. One-dimensional quantum spin systems are of great interest at present because they provide some of the simplest realizations of symmetry-protected topological (SPT) phases in strongly correlated systems.

The limitations of the semi-classical approach when applied to systems with frustrated interactions are discussed in section III, where we introduce the alternative idea of constructing variational wavefunctions directly. We introduce Anderson’s famous idea of the RVB wavefunction for spin 1/2 systems and discuss how this idea can be implemented in practice. The difficulty of incorporating the $SU(2)$ spin algebra in the usual many-body perturbation theory is noted, and the trick of representing spins by particles (fermions or bosons) with *constraints* to avoid this difficulty is introduced. The non-trivial $SU(2)$ gauge structure in the fermion representation of RVB states and the resulting rich structure of the low-energy effective field theories for these spin states ($SU(2)$, $U(1)$ and Z_2 spin liquids) are discussed. An interesting linkage of the $U(1)$ spin liquid state to the (metallic) Fermi liquid state through a Mott metal-insulator transition is introduced.

The difficulty of finding controllable approaches for studying spin liquid states has led to an extension of the RVB approach and a search for alternative approaches. Some of these approaches are reviewed briefly in section IV, including (i) the extension of the RVB approach to include the effect of spin-orbit coupling and to higher spin ($S > 1/2$) systems, (ii) the concepts of matrix product states and projected entangled pair states, and (iii) the Kitaev honeycomb model. The main message of this section is that a larger variety of exotic spin states become possible when we leave the paradigm of spin 1/2 systems with rotational symmetry. The $U(1)$ and Z_2 spin liquid states belong to merely a very small subset of the plausible exotic states once we leave the paradigm of semi-classical approaches.

Section V is devoted to a survey of experimental research on spin liquid states. Special attention is paid to the $U(1)$ spin liquid state, on which most experimental efforts have been focused. The best studied examples are a family of organic compounds denoted by κ -(ET)₂Cu₂(CN)₃ (ET) (Shimizu *et al.*, 2003) and Pd(dmit)₂(EtMe₃Sb) (dmit salts) (Itou *et al.*, 2008). Both materials are Mott insulators near the metal-insulator transition and become superconducting (ET)

or metallic (dmit) under modest pressure. Despite the large magnetic exchange $J \approx 250$ K observed in these systems, there is no experimental indication of long-range magnetic ordering down to a temperature of ~ 30 mK. A linear temperature dependence of the specific heat and a Pauli-like spin susceptibility have been found in both materials at low temperature, suggesting that the low-energy excitations are spin-1/2 fermions with a Fermi surface (Watanabe *et al.*, 2012; Yamashita *et al.*, 2008b). This Fermi-liquid-like behavior is further supported by their Wilson ratios, which are close to one. In addition to ET and dmit salts, the kagome compound $\text{ZnCu}_3(\text{OH})_6\text{Cl}_2$ (Helton *et al.*, 2007) and the three-dimensional hyperkagome material $\text{Na}_4\text{Ir}_3\text{O}_8$ (Okamoto *et al.*, 2007) are also considered to be candidates for QSLs with gapless excitations. Experimental surveys on these QSL candidate materials are presented in this article, including their thermodynamics, thermal transport and various spin spectra. We also briefly introduce the discoveries of a few new materials and discuss the existing discrepancies between experiments and theories. The paper is summarized in section VI.

II. FROM SEMI-CLASSICAL TO NON-LINEAR- σ MODEL APPROACHES FOR QUANTUM ANTIFERROMAGNETS

Here, we consider simple Heisenberg antiferromagnets on bipartite lattices (with sublattices A and B) with the Hamiltonian

$$H = J \sum_{\langle i,j \rangle} \mathbf{S}_i \cdot \mathbf{S}_j, \quad (1)$$

where $J > 0$ and $\langle i,j \rangle$ describes a pair of nearest neighbor sites in the bipartite lattice. In a bipartite lattice, any two nearest neighbor sites always belong to different sublattices. \mathbf{S} is a quantum spin with magnitude $S = n/2$, where n = positive integer. Examples of bipartite lattices include 1D spin chains, 2D square or honeycomb lattices, and 3D cubic lattices.

II.1. Two-spin problem

The semi-classical approach begins with the assumption that the quantum spins are “close” to classical spins, and it is helpful to start by first analyzing the corresponding classical spin problem. For simplicity, we start by considering only two classical spins coupled by the Heisenberg interaction

$$H = J \mathbf{S}_A \cdot \mathbf{S}_B. \quad (J > 0).$$

The classical spins obey Euler’s equation of motion:

$$\frac{\partial \mathbf{S}_{A(B)}}{\partial t} = J \mathbf{S}_{B(A)} \times \mathbf{S}_{A(B)}. \quad (2)$$

This equation can be solved most easily by introducing the magnetization and staggered magnetism vectors $\mathbf{M}(\mathbf{N}) = \mathbf{S}_A + (-)\mathbf{S}_B$, where it is easy to show from Eq. (2) that

$$\begin{aligned} \frac{\partial \mathbf{M}}{\partial t} &= 0, \\ \frac{\partial \mathbf{N}}{\partial t} &= J \mathbf{M} \times \mathbf{N}, \end{aligned} \quad (3)$$

indicating that classically, the staggered magnetization vector \mathbf{N} rotates around the (constant) total magnetization vector \mathbf{M} . Let $\mathbf{S}_{A(B)} = S_{A(B)} \hat{r}_{A(B)}$, where $S_{A(B)}$ are the magnitudes of the spins $\mathbf{S}_{A(B)}$ and $\hat{r}_{A(B)}$ are unit vectors indicating the directions of $\mathbf{S}_{A(B)}$; then, the classical ground state has $\hat{r}_A = -\hat{r}_B$ with $\mathbf{M} = 0$, i.e., the two spins are antiferromagnetically aligned. Note that the equation of motion given in Eq. (3) implies that $\frac{\partial(\mathbf{N}^2)}{\partial t} = 0$, i.e., the magnitude of \mathbf{N} remains unchanged during its motion. Therefore, if we write $\mathbf{N} = N \hat{n}$, where N is the magnitude of \mathbf{N} and \hat{n} is the unit vector denoting its direction, we find that only \hat{n} changes under the equation of motion given in Eq. (3).

The effects of quantum mechanics can be seen most easily by observing that the equation of motion given in Eq. (3) describes the dynamics of a free rotor (a rigid rod with one end fixed such that the rod can rotate freely around the fixed end). A free rotor can be represented by a vector $\mathbf{r} = r_0 \hat{r}$, where $r_0 = \text{constant}$ is the length of the rod and \hat{r} is the unit radial vector describing the orientation of the rod. The rod has an angular momentum of

$$\mathbf{L} = \mathbf{r} \times \mathbf{p} = r_0 \hat{r} \times \mathbf{p}, \quad (4)$$

where $\mathbf{p} = m r_0 \dot{\hat{r}}$ is the momentum and m is the mass. Using Eq. (4), we obtain

$$\hat{r} \times \mathbf{L} = -r_0 \mathbf{p} = -mr_0^2 \dot{\hat{r}}. \quad (5a)$$

We also have

$$\dot{\mathbf{L}} = 0 \quad (5b)$$

(conservation of angular momentum). Comparing Eqs.(3) and (5), we find that the equation of motion for two spins is equivalent to the equation of motion for a free rotor if we identify $\mathbf{L} \rightarrow \mathbf{M}$, $\hat{r} \rightarrow \hat{n}$ and $J = I^{-1}$, where $I = mr_0^2$ is the moment of inertia of the rotor.

The quantum Hamiltonian of the free rotor is

$$H_{\text{rotor}} = \frac{1}{2I} \mathbf{L}^2,$$

and its solution is well known. The eigenstates are the spherical harmonics $Y_{lm}(\theta, \phi)$ (where θ and ϕ specify the direction of the unit vector \hat{r}) with eigenvalues

$$\mathbf{L}^2 = l(l+1)\hbar^2, \quad L_z = m\hbar,$$

and corresponding energies $E_l = l(l+1)\hbar^2/2I$, where l and m are integers such that $l \geq 0$ and $l \geq |m|$. In particular, $\mathbf{L}(\mathbf{M}) = 0$ for the ground state of the quantum rotor, but the direction of the vector $\mathbf{r}(\mathbf{N})$ is completely uncertain ($Y_{00}(\theta, \phi) = \frac{1}{\sqrt{4\pi}}$) as a result of quantum fluctuations, indicating a breakdown of the classical solution, in which \mathbf{n} is fixed in the ground state. (Alternatively, one can gain this understanding from the Heisenberg uncertainty principle, $\langle \delta\hat{r} \rangle \langle \delta\mathbf{L} \rangle > \hbar$. With $\mathbf{L} = 0$ in the ground state, $\delta\mathbf{L} \equiv 0$ and $\delta\hat{r} \rightarrow \infty$, the direction of the vector \hat{r} becomes completely uncertain.)

A moment of thought indicates that our mapping of the spin problem to the rotor problem cannot be totally correct. What happens if \mathbf{S}_A is an integer spin and \mathbf{S}_B is a half-odd-integer spin? Elementary quantum mechanics tells us that the ground state should carry half-odd-integer angular momentum. The possibility of such a scenario is missing in our rotor mapping, in which the spin magnitudes $S_{A(B)}$ do not appear.

II.2. Berry's phase

The missing piece in our mapping of the two-spin problem to the rotor model is the Berry's phase (Berry, 1984), which is carried by spins but is absent in rotors. The correct spin-quantization rule is recovered only after this piece of physics is properly added into the rotor problem. First, let us review the Berry's phase carried by a single spin.

We recall that for a spin tracing out a closed path \mathbf{C} on the surface of the unit sphere, the spin wavefunction acquires a Berry's phase $\gamma(\mathbf{C}) = S\Omega(\mathbf{C})$, where S is the spin magnitude and $\Omega(\mathbf{C})$ is the surface area under the closed path \mathbf{C} on the unit sphere (see Fig. 1). $S\Omega(\mathbf{C})$ can be represented more conveniently by imagining the spin trajectory as the trajectory of a particle carrying a unit charge moving on the surface of the unit sphere. In this case, the Berry's phase is simply the phase acquired by the charged particle if a magnetic monopole of strength S (i.e., $\mathbf{B}(\mathbf{r}) = (S/r^2)\hat{r}$) is placed at the center of the sphere. The Berry's phase acquired is the magnetic flux enclosed by the closed path \mathbf{C} .

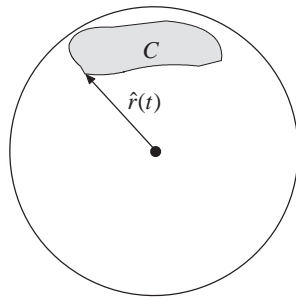


FIG. 1 Berry's phase with a magnetic monopole.

Let $S\mathbf{A}_M(\mathbf{r})$ be the vector potential associated with the monopole, i.e., $\nabla \times \mathbf{A}_M = \hat{r}/r^2$; then, in the “charge + gauge field” representation, the effect of the Berry's phase can be described by a vector-potential term in the action:

$$S_B = \hbar S\Omega(C) = \hbar S \int dt \mathbf{A}_M(\hat{r}) \cdot \dot{\hat{r}}. \quad (6)$$

This is an example of a Wess-Zumino term for quantum particles. A more rigorous derivation of the Wess-Zumino action is given in Appendix A, where the action for a single spin in a magnetic field is derived *via* a path integral approach.

We now revisit the two-spin problem. With the Berry's phases included, the Lagrangian of the corresponding rotor problem becomes

$$L = \frac{1}{2J}(\hat{n} \times \dot{\hat{n}})^2 + \hbar S_A \mathbf{A}_M(\hat{r}_A) \cdot \dot{\hat{r}}_A + \hbar S_B \mathbf{A}_M(\hat{r}_B) \cdot \dot{\hat{r}}_B, \quad (7)$$

where $\mathbf{N} = N\hat{n} = \mathbf{S}_A - \mathbf{S}_B$. To simplify the problem, we adopt the semi-classical approximation $\hat{r}_A = -\hat{r}_B$ in the Berry's phase terms, which is a reasonable approximation for states close to the classical ground state. With this approximation, we obtain

$$L \rightarrow \frac{1}{2J}(\hat{n} \times \dot{\hat{n}})^2 + \hbar \Delta S \mathbf{A}_M(\hat{n}) \cdot \dot{\hat{n}}, \quad (8)$$

where $\hat{n} = \hat{r}_A$ and $\Delta S = S_A - S_B$. The Hamiltonian of the system is

$$H_M = \frac{J}{2}(\mathbf{\Pi} - \hbar \Delta S \mathbf{A}_M(\hat{n}))^2, \quad (9)$$

where $\mathbf{\Pi} = \dot{\hat{n}}/J$ is the canonical momentum of the rotor.

H_M is the Hamiltonian of a charged particle moving on the surface of a unit sphere with a magnetic monopole of strength $|\Delta S|$ located at the center of the sphere. The eigenstates of the Hamiltonian are well known and are called the monopole spherical harmonics (Wu and Yang, 1976). The most interesting feature of the monopole spherical harmonics is that they allow half-odd-integer angular momentum states (which occur when $|\Delta S|$ is a half-odd-integer). The ground state carries an angular momentum of $L = |\Delta S|$ and is $(2|\Delta S| + 1)$ -fold degenerate, corresponding to the degeneracy of a quantum spin of magnitude $|\Delta S|$, in agreement with the exact result for the two-spin problem.

II.3. Non-linear- σ -model

The two-spin problem tells us that there are two important elements that we must keep track of when a classical spin problem is replaced with the corresponding quantum spin problem: a) quantum fluctuations, originating from the (non)-commutation relation between the canonical coordinates (\mathbf{N}) and momenta (\mathbf{M}), and b) Berry's

phase, which dictates the quantization of the spins. In the following, we generalize the rotor approach to the many-spin systems described by the antiferromagnetic (AFM) Heisenberg model, keeping in mind the above two elements.

Following Haldane (Haldane, 1983a,b), we here consider Heisenberg antiferromagnets on a bipartite lattice described by the Hamiltonian given in Eq. (1). As in the two-spin problem, we introduce the magnetization vectors $\mathbf{M}(\mathbf{x}_i)$ and the staggered magnetization vectors $\mathbf{N}(\mathbf{x}_i)$ such that

$$\begin{aligned}\mathbf{S}_i^A &= \mathbf{M}(\mathbf{x}_i) + \mathbf{N}(\mathbf{x}_i), \\ \mathbf{S}_i^B &= \mathbf{M}(\mathbf{x}_i) - \mathbf{N}(\mathbf{x}_i),\end{aligned}\quad (10)$$

where $\mathbf{S}^{A(B)}$ denote spins on the $A(B)$ sublattices of the bipartite lattice. We assume that the ground state of the quantum system is “classical-like” with nearly anti-parallel spins on two nearest neighboring sites such that $\mathbf{M}(\mathbf{x}_i) \ll \mathbf{N}(\mathbf{x}_i)$, where both $\mathbf{M}(\mathbf{x})$ and $\mathbf{N}(\mathbf{x})$ are very slowly varying functions in space. (We show that this assumption can be justified in the following section.) The classical equation of motion for the spin at lattice site i is

$$\frac{\partial \mathbf{S}_i^{A(B)}}{\partial t} = J \left(\sum_{j=\text{NN}(i)} \mathbf{S}_j^{B(A)} \right) \times \mathbf{S}_i^{A(B)}, \quad (11)$$

where $j = \text{NN}(i)$ means that j represents the nearest neighbor sites of i .

Using Eq. (10), after some straightforward algebra and taking the continuum limit, we obtain

$$\begin{aligned}\frac{\partial \mathbf{N}(\mathbf{x})}{\partial t} &\sim Jz\mathbf{M}(\mathbf{x}) \times \mathbf{N}(\mathbf{x}), \\ \frac{\partial \mathbf{M}(\mathbf{x})}{\partial t} &\sim -\frac{Ja^2}{2}(\nabla^2 \mathbf{N}(\mathbf{x})) \times \mathbf{N}(\mathbf{x}),\end{aligned}\quad (12)$$

where a is the lattice spacing and $z = 2d$ is the coordination number. We have assumed a square (cubic)-type lattice and have adopted the slowly varying approximation

$$\mathbf{M}(x_{i+1}) + \mathbf{M}(x_{i-1}) \sim 2\mathbf{M}(x_i),$$

$$\mathbf{N}(x_{i+1}) + \mathbf{N}(x_{i-1}) \sim 2\mathbf{N}(x_i) + a^2 \partial_x^2 \mathbf{N}(x_i),$$

etc. in deriving the above result. We have also assumed $\mathbf{M}(\mathbf{x})$ to be small and have neglected all non-linear terms in $\mathbf{M}(\mathbf{x})$ in deriving Eq. (12).

To proceed further, we consider the situation in which all spins have the same magnitude S . Then, it is easy to see from Eq. (10) that $\mathbf{N}(\mathbf{x})^2 + \mathbf{M}(\mathbf{x})^2 = S^2$ and $\mathbf{N}(\mathbf{x}) \cdot \mathbf{M}(\mathbf{x}) = 0$. Assuming that $M = |\mathbf{M}(\mathbf{x})| \ll N = |\mathbf{N}(\mathbf{x})| \sim S$, we find from Eq. (12) that $M \sim \omega/(zJ)$ and $\omega \sim \sqrt{z}JaS|\mathbf{k}|$, where ω and \mathbf{k} are the frequency and wavevector, respectively, of the fluctuations in \mathbf{N} .

In particular, $M \ll N$ when $ak \ll \sqrt{z}$, i.e., when $\mathbf{N}(\mathbf{x})$ is slowly varying in space.

In the following, we adopt the approximation $N \sim S$ and write $\mathbf{N}(\mathbf{x}) = S\hat{\mathbf{n}}(\mathbf{x})$, where $\hat{\mathbf{n}}^2 = 1$. Eliminating $\mathbf{M}(\mathbf{x})$ from Eq. (12), we obtain

$$\frac{\partial^2 \hat{\mathbf{n}}(\mathbf{x}, t)}{\partial t^2} = \frac{z(SJa)^2}{2} \nabla^2 \hat{\mathbf{n}}(\mathbf{x}, t), \quad (13a)$$

corresponding to the following classical action for the vector field $\hat{\mathbf{n}}$:

$$S_\sigma = \frac{1}{2} \int dt \int d^d x \left(\frac{1}{J} \left(\frac{\partial \hat{\mathbf{n}}}{\partial t} \right)^2 - \frac{zJ(Sa)^2}{2} (\nabla \hat{\mathbf{n}})^2 \right), \quad (13b)$$

with the constraint $\hat{\mathbf{n}}^2 = 1$. S_σ is the non-linear- σ model (NL σ M) for the unit vector field $\hat{\mathbf{n}}(\mathbf{x})$.

Comparing Eqs.(13b) and (8), we see that the NL σ M can be viewed as a continuum model describing coupled rotors $\hat{\mathbf{n}}(\mathbf{x})$. The first term in the action gives the kinetic energy for the rotors, which we have discussed in detail for the two-spin model. The second term represents the coupling between nearest neighboring rotors in the lattice spin model. We note that the term for the coupling between rotors has a magnitude of $\sim S^2$ and dominates over the kinetic energy in the limit of large S .

A more systematic derivation of the NL σ M starting from Eq. (10) can be achieved by writing

$$\mathbf{S}_i = \eta_i S \hat{\mathbf{n}}(x_i) \sqrt{1 - \left| \frac{\mathbf{M}(x_i)}{S} \right|^2} + \mathbf{M}(x_i),$$

where $\eta_i = e^{i\pi x}$ and we still have $\mathbf{N}(\mathbf{x}) \cdot \mathbf{M}(\mathbf{x}) = 0$. Assuming that $\mathbf{M}(\mathbf{x})$ is small, we can integrate out $\mathbf{M}(\mathbf{x})$ in a power series expansion of $\mathbf{M}(\mathbf{x})$ in the path integral. The NL σ M for $\hat{\mathbf{n}}(\mathbf{x})$ is thus obtained to the leading (Gaussian) order (Auerbach, 1994).

II.3.1. Topological term

We next consider the Berry’s phase contribution to the action. Following Appendix A, the total Berry’s phase contribution is

$$S_T = \sum_i S_B(\hat{r}_i) \sim \hbar S \sum_i (-1)^i \Omega(\hat{n}_i), \quad (14)$$

where $S\Omega(\hat{r}_i) = S \int dt \mathbf{A}_M(\hat{r}_i) \cdot \dot{\hat{r}}_i$ is the Berry’s phase for a single spin and $(-1)^i = 1(-1)$ for sites on even (odd) sublattices. In the last step, we have assumed that the spins are almost anti-parallel. In the continuum limit, we obtain

$$S_T \sim \frac{\hbar S}{2^d} \int d^d x \left(\frac{\partial}{\partial x^1} \cdots \frac{\partial}{\partial x^d} \right) \Omega(\hat{n}(\mathbf{x})). \quad (15)$$

S_T is sensitive to the boundary conditions (see the discussion below), and we assume closed (periodic) boundary

conditions in the following. The case of open boundary conditions is discussed afterward. For periodic boundary conditions, it is easy to see that S_T is zero unless the integrand has a non-trivial topological structure.

To evaluate $\partial_x \Omega$, we recall that $\Omega(\hat{n})$ measures the area on the surface of the sphere bounded by the trajectory $\hat{n}(t)$. Thus, the variation $\delta\Omega(\hat{n})$ due to a small variation in the trajectory $\delta\hat{n}$ is simply

$$\delta\Omega(\hat{n}) = \int dt \delta\hat{n} \cdot (\hat{n} \times \partial_t \hat{n}),$$

and

$$S_T = \frac{\hbar S}{2^d} \int d^d x \int dt \left[\left(\frac{\partial}{\partial x^1} \cdots \frac{\partial}{\partial x^d} \right) \hat{n} \right] \cdot (\hat{n} \times \partial_t \hat{n}). \quad (16)$$

The total effective action describing the quantum antiferromagnet is $S = S_\sigma + S_T$.

The topological term is nonzero in one dimension and is usually written in the form

$$\frac{S_T}{\hbar} = \frac{\theta}{8\pi} \sum_{\mu, \nu=0,1} \int d^2 x \varepsilon_{\mu\nu} \hat{n} \cdot (\partial_\mu \hat{n} \times \partial_\nu \hat{n}), \quad (17a)$$

where $x_0 = t$, $x_1 = x$, $\theta = 2\pi S$ and $\varepsilon_{\mu\nu}$ is the rank-2 Levi-Civita antisymmetric tensor (Affleck, 1986; Haldane, 1985). The Pontryagin index

$$Q = \frac{1}{8\pi} \sum_{\mu, \nu=0,1} \int d^2 x \varepsilon_{\mu\nu} \hat{n} \cdot (\partial_\mu \hat{n} \times \partial_\nu \hat{n}) = \text{integer} \quad (17b)$$

measures how many times the $2[=1(\text{space})+1(\text{time})]$ -dimensional spin configuration \hat{n} has wrapped around the unit sphere. In two dimensions,

$$S_T \rightarrow \frac{\hbar\theta}{2} \int dy \frac{\partial Q(y)}{\partial y} = 0,$$

where $Q(y)$ is the Pontryagin index that arises from summing over all spin configurations in the y^{th} column of the two-dimensional lattice. The sum is zero for smooth spin configurations because Q is an integer and thus cannot “change smoothly” (Dombre and Read, 1988; Fradkin and Stone, 1988; Haldane, 1988b; Wen and Zee, 1988). For the same reason, S_T vanishes for any number of dimensions greater than one. However, one should be cautioned that this conclusion is valid only when we restrict ourselves to smooth spin configurations $\hat{n}(\mathbf{x}, t)$ when computing S_T . The Berry’s phase may have a nonzero contribution if we also allow singular spin configurations in the theory. This is the case in $2+1$ D, where monopole-like spin configurations are allowed in 3D space (Haldane, 1988b; Read and Sachdev, 1990).

II.4. Quantum spin chains and the Haldane conjecture

We now study the predictions of the effective action for quantum spin chains. In one dimension, the quantum

spin chains are described by the path integral

$$\int D[\hat{n}(x, t)] e^{\frac{i}{\hbar} (S_\sigma(\hat{n}) + S_T(\hat{n}))}.$$

We first consider the topological term. We note that $S_T = 2\hbar\pi S Q$ and $e^{\frac{i}{\hbar} S_T} = (-1)^{2SQ}$ ($Q = \text{integer}$). In particular, $e^{\frac{i}{\hbar} S_T} \equiv 1$ for integer spin chains, and the Berry’s phase has no effect on the effective action. However, $e^{\frac{i}{\hbar} S_T} = \pm 1$ for half-odd-integer spin chains, depending on whether Q is even or odd. There is no further distinction between spin chains with different spin values S in S_T . This result leads to the first part of the Haldane conjecture, namely, that fundamental differences exist between integer and half-odd-integer spin chains (Haldane, 1988b). To proceed further, we first consider integer spin chains, where $e^{\frac{i}{\hbar} S_T} \equiv 1$ and the system is described by the “pure” NL σ M S_σ .

II.4.1. Integer spin chains

We start by asking the following question: what are the plausible ground states described by S_σ ? For this purpose, it is more convenient to consider a lattice version of S_σ :

$$S_\sigma \rightarrow \frac{1}{2} \int dt \sum_i \left(\frac{1}{J} \left(\frac{\partial \hat{n}_i}{\partial t} \right)^2 + JS^2 \hat{n}_i \cdot \hat{n}_{i+1} \right), \quad (18)$$

with the corresponding Hamiltonian

$$H_\sigma = \frac{J}{2} \sum_i \left((\mathbf{L}_i)^2 - S^2 \hat{n}_i \cdot \hat{n}_{i+1} \right), \quad (19)$$

where \mathbf{L}_i is the angular momentum operator for the i^{th} rotor. The Hamiltonian contains two competing terms, and we expect that it may describe two plausible phases, a strong coupling phase, in which the kinetic energy (first) term dominates, and a weak coupling phase, in which the potential energy (second) term dominates. A natural control parameter for this analysis is the spin magnitude S , which dictates the magnitude of the potential energy. In the first case (small S), in which the potential energy term is small, we expect that the ground state can be viewed, to a first approximation, as a product of local spin singlets, i.e., $\mathbf{L} = 0$ states,

$$|G\rangle = |0\rangle_1 |0\rangle_2 \cdots |0\rangle_N,$$

where $|0\rangle_i$ represents the $\mathbf{L} = 0$ state for the rotor on site i . The lowest-energy excitations are $\mathbf{L} = 1$ states separated from the ground state by an excitation gap $\sim \hbar^2 J$. This picture is believed to be correct as long as the magnitude of the potential energy term is much smaller than the excitation energy for the $\mathbf{L} = 1$ state. In the second case, in which the potential energy term

dominates (large S), we expect that the ground state is a magnetically ordered (Néel state) with $\hat{n}_i = \hat{n}_0$ at all sites i , where the excitations are Goldstone modes of the ordered state (spin waves).

It turns out that this naive expectation is valid only in dimensions of $d > 1$. In one dimension, the magnetically ordered state is not stable because of quantum fluctuations associated with the Goldstone mode (Mermin-Wigner-Hohenberg Theorem), and the ground state is always quantum disordered (Hohenberg, 1967; Mermin and Wagner, 1966), i.e., a spin liquid state. This result can be shown more rigorously through a renormalization group (RG) analysis of the NL σ M. We do not go through this analysis in detail in this article; instead, we simply assume that this is the case and examine its consequences. Readers interested in the RG analysis can consult, for example, references (Brézin and Zinn-Justin, 1976; Polyakov, 1987, 1975).

Physically, this result means that after some renormalization, the ground state of integer spin chains can always be viewed as a product state of local spin singlets, irrespective of the spin magnitude S . The lowest-energy excitations are gapped spin triplet ($\mathbf{L} = 1$) excitations. This is the Haldane conjecture for integer spin chains.

II.4.2. Half-odd-integer spin chains

The RG analysis cannot be straightforwardly applied to half-odd-integer spin chains because of the appearance of the topological term S_T . To understand why, let us again take the RG to the strong coupling limit and examine what happens in this case.

To zeroth order, the Hamiltonian of the system consists only of the kinetic energy term. However, the rotors are moving under the influence of effective monopole potentials originating from S_T . In particular, all half-odd-integer spin chains have the same S_T with an effective magnetic monopole strength of $1/2$, corresponding to that of a spin- $1/2$ chain. In this case, the ground state of a single rotor has an angular momentum of $\mathbf{L} = 1/2$ and is two-fold degenerate (see the discussion after Eq. (9)). The total degeneracy of the ground state is 2^N , where N =number of lattice sites. This enormous degeneracy implies that the coupling between rotors cannot be neglected when we consider the rotor Hamiltonian given in Eq. (19), and the strong coupling expansion simply tells us that the system behaves like a coupled-spin- $1/2$ chain (Shankar and Read, 1990).

Fortunately, the antiferromagnetic spin- $1/2$ chain can be solved using the exact Bethe ansatz technique (Giamarchi, 2003). The exact Bethe ansatz solution tells us that the antiferromagnetic spin- $1/2$ Heisenberg chain is critical, namely, the ground state has no long-range magnetic order but has a gapless excitation spectrum. Unlike integer spin chains, where the lowest-energy ex-

citations carry spin $S = 1$, the elementary excitation of this system has spin $S = 1/2$. Combining this with the continuum theory leads to the Haldane conjecture for half-odd integer spin chains, namely, that they are all critical with elementary $S = 1/2$ excitations.

II.4.3. Open spin chains and end states

The Haldane conjecture has been checked numerically for quantum spin chains with different spin magnitudes and has been found to be correct in all cases that have been studied thus far. One may wonder whether the difference in spin magnitudes may manifest at all in some low-energy properties of quantum spin chains. The answer is yes, when we consider open spin chains.

Recall that we have always assumed periodic boundary conditions in deriving S_T . In fact, a periodic boundary condition is needed to define the Pontryagin index for the topological term S_T . For an open chain of length L , S_T is replaced by (Affleck, 1990; Haldane, 1983a; Ng, 1994)

$$S_T^{(o)} = \frac{\hbar}{2} \int_0^L d^d x \frac{\partial S_B(\hat{n}(x))}{\partial x} = 2\pi\hbar S Q + \frac{\hbar S}{2} (\Omega(\hat{n}(L)) - \Omega(\hat{n}(0))), \quad (20)$$

where $2\pi S Q = \theta Q$ is the usual topological θ term that we obtain when $\Omega(\hat{n}(0)) = \Omega(\hat{n}(L))$, i.e., when we consider periodic boundary conditions. An open chain differs from a closed chain in the existence of an additional boundary Berry's phase term with an effective spin magnitude of $S/2$.

We now examine the effect of this additional Berry's phase term. First, we consider integer spin chains. Following the previous discussion, we expect the spin chain to be described by the strong coupling limit of the effective Hamiltonian given in Eq. (19), except that the rotors at the two ends of the spin chain are subjected to monopole potentials of strength $S/2$, resulting in effective free spins of magnitude $S/2$ located at the ends of the spin chain. The two spins are coupled by a term $J_{eff} \sim JS^2 e^{-L/\xi}$ when the coupling between rotors is considered, where $\xi \sim E_g^{-1}$ is the correlation length and E_g is the spin gap. These end states can also be understood based on a wavefunction proposed by Affleck, Lieb, Kennedy and Tasaki (the AKLT state) for $S = 1$ spin chains (Affleck *et al.*, 1987) (see section IV) and have been observed experimentally in $S = 1$ spin chain materials (Glarum *et al.*, 1991). In modern terminology, the end states of integer spin chains are a manifestation of symmetry-protected topological (SPT) order (Chen *et al.*, 2012; Gu and Wen, 2009; Pollmann *et al.*, 2012), which manifests itself as a boundary action that

is protected by rotational (SO(3)) symmetry.¹

For half-odd-integer spin chains, the analysis is a bit more complicated. We start by rewriting Eq. (20) for $S_T^{(o)}$ as follows (Ng, 1994):

$$\begin{aligned} S_T^{(o)} &= \frac{\hbar}{2} \left(4\pi \frac{1}{2} Q + S(\Omega(\hat{n}(L)) - \Omega(\hat{n}(0))) \right) \quad (21) \\ &= \frac{\hbar}{2} \left(4\pi \frac{1}{2} Q + \frac{1}{2} (\Omega(\hat{n}(L)) - \Omega(\hat{n}(0))) \right. \\ &\quad \left. + (S - \frac{1}{2})(\Omega(\hat{n}(L)) - \Omega(\hat{n}(0))) \right) \end{aligned}$$

where we have replaced S with $1/2$ in the usual topological (Pontryagin index) term and have divided the boundary Berry's phase term into two parts; the first part, when combined with the Pontryagin index term, is the total Berry's phase contribution for an open $S = 1/2$ spin chain, and the second part is the additional contribution when $S > 1/2$. Performing the strong coupling expansion as before, we find that the system behaves as an open spin-1/2 chain coupled to two end spins with a magnitude of $\frac{1}{2} + \frac{1}{2}(S - \frac{1}{2})$. The problem of impurity end spins coupled to a spin-1/2 chain has been analyzed using the bosonization technique, through which it was found that after the screening induced by the spin-1/2 chain (essentially a Kondo effect), a free spin with a magnitude of $\frac{1}{2}(S - \frac{1}{2})$ is left at each end of the spin chain (Eggert and Affleck, 1992). Note that the existence of end states in half-odd-integer spin chains is rather non-trivial because the bulk spin excitations are *gapless*. As a result, the end spins at the two ends of a half-odd-integer spin chain are coupled by a term $J_{eff} \sim JS^2/(L \ln L)$, where L is the length of the spin chain. The excitation energy of the end state is logarithmically lower than the energy of the bulk spin excitations, which have an energy of $\sim J/L$ (Ng, 1994). These predictions for open chains and end states based on the NL σ M plus topological θ term analysis have been verified numerically by means of density matrix renormalization group (DMRG) calculations (Qin *et al.*, 1995).

II.5. Higher dimensions and frustrated quantum antiferromagnets

The NL σ M approach to quantum antiferromagnets has been extended to higher dimensions and to frustrated quantum antiferromagnets. For simple antiferromagnets, S_T vanishes in dimensions of $d > 1$, and we need only consider the NL σ M, i.e., S_σ . As discussed before, S_σ describes two plausible phases, the weak coupling phase, in which the ground state is antiferromagnetically ordered,

and the strong coupling phase, in which the ground state is gapped. The weak coupling phase is favored for large spin magnitudes S . Various numerical and analytical studies have consistently demonstrated that the ground state is always Néel ordered for simple quantum antiferromagnets on a 2d square lattice, even for the smallest possible spin value of $S = 1/2$ (Manousakis, 1991). For this reason, physicists have turned to frustrated spin models to look for exotic spin liquid states.

The NL σ M approach has generated interesting results when applied to weakly frustrated spin models, where the main effect of frustration is to reduce the effective coupling strength between rotors (for example, $J_1 - J_2$ models, in which a next-nearest neighbor antiferromagnetic coupling is added to the Heisenberg model on a square lattice). In this case, it has been shown that spin-Peierls order can be obtained when discontinuous monopole-like spin configurations are included in the calculation of S_T (Read and Sachdev, 1990). However, the method becomes questionable when applied to strongly frustrated spin systems, in which effective rotors become difficult to define locally, for example, the antiferromagnetic Heisenberg model on a kagome lattice.

Generally speaking, a continuum theory is reliable only if the short-distance physics is captured correctly by the underlying classical or mean-field theory. A continuum theory becomes unreliable if the short-distance physics it assumes is not correct. This seems to be the case for the NL σ M approach when applied to strongly frustrated spin systems. In the following sections, we consider alternative methods of treating quantum spin systems, keeping in mind the physics that we have previously discussed.

III. RESONANT VALENCE BOND (RVB) STATES

The semi-classical approach, which is based on fluctuations around a presumed classical (Néel) order, is difficult to apply in frustrated lattice models. The difficulties arise from two main sources. First, different degenerate or quasi-degenerate classical ground states may exist in a frustrated spin system. It is difficult to include these quasi-degenerate classical ground states in the NL σ M description. Second, the effect of Berry's phases becomes intractable because of the complicated (classical) spin trajectory.

The term geometric frustration (or frustration for short) was introduced by Gerard Toulouse in the context of frustrated magnetic systems (Toulouse, 1977; Vannimenus and Toulouse, 1977). Indeed, frustrated magnetic systems had long been studied prior to that time. Early work included a study conducted by G. H. Wannier (Wannier, 1950) on the classical Ising model on a triangular lattice with antiferromagnetically coupled nearest neighbor spins, which serves as the simplest example of geometric frustration (Diep, 2004). Because of

¹ For $S = 1$ chains, the $S = 1/2$ end states are protected by a weaker $Z_2 \times Z_2$ symmetry (Chen *et al.*, 2011a,b).

the AFM coupling, two nearest neighboring spins A and B tend to be anti-parallel. Then, a third spin C that is a neighbor of both A and B is *frustrated* because its two possible orientations, up and down, both have the same energy. The classical ground state has a high level of degeneracy. As a result, we cannot choose a classical spin order as the starting point for constructing the NL σ M for the quantum $S = 1/2$ XXZ model

$$H = J_z \sum_{\langle i,j \rangle} S_i^{(z)} S_j^{(z)} + J_{\perp} \sum_{\langle i,j \rangle} \left(S_i^{(x)} S_j^{(x)} + S_i^{(y)} S_j^{(y)} \right)$$

with $J_z \gg J_{\perp}$ because there exist infinite spin configurations with the same classical energy. We note that the spin-spin correlation has been found to decay following a power law at zero temperature in the exact solution for the classical Ising model (Stephenson, 1970).

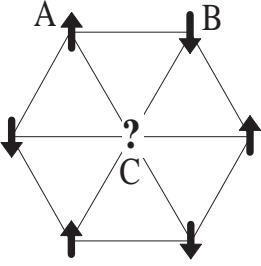


FIG. 2 Geometric frustration. The spin C is frustrated because either the up or down orientation will give rise to the same energy in the AFM Ising limit.

In this case, an alternative approach is a variational wavefunction, in which we essentially must *guess* the ground state wavefunction based on experience or physical intuition. A very important idea related to this approach is the resonating valence bond (RVB) concept for spin-1/2 systems suggested by Anderson. The term RVB was first coined by Pauling (Pauling, 1949) in the context of metallic materials. Anderson revived interest in this concept in 1973 when he constructed a non-degenerate quantum ground state for an $S = 1/2$ AFM system on a triangular lattice (Anderson, 1973). A valence bond is a spin singlet state constructed from two $S = 1/2$ spins at sites i and j , given by

$$(i, j) = \frac{1}{\sqrt{2}} (|\uparrow_i \downarrow_j\rangle - |\downarrow_i \uparrow_j\rangle), \quad (22)$$

and an RVB state is a tensor product of valence bond states, whose wavefunction is given by

$$|\Psi_{RVB}\rangle = \sum_{i_1 j_1 \dots i_n j_n} a_{(i_1 j_1 \dots i_n j_n)} |(i_1, j_1) \dots (i_n, j_n)\rangle, \quad (23)$$

where $(i_1, j_1) \dots (i_n, j_n)$ are dimer configurations covering the entire lattice. The wavefunction is summed over all possible ways in which the lattice can be divided

into pairs of lattice sites (i.e., dimers). The quantities $a_{(i_1 j_1 \dots i_n j_n)}$ are variational parameters determined by minimizing the ground-state energy of a given Hamiltonian. For a quantum disordered antiferromagnet, it has been proposed that the valence bond pairs in the RVB construction are dominated by short-range pairs, resulting in liquid-like states with no long-range spin order. The corresponding spin correlation function $\langle \mathbf{S}_i \cdot \mathbf{S}_j \rangle$ in the RVB state may be short in range, with a finite correlation length (usually called short-range RVB (sRVB)), or may decay with distance following a power law (algebraic spin liquid states). The state is called a valence-bond solid (VBS) state if a single dimer configuration dominates in the ground state. An algebraic spin liquid state is usually invariant under all symmetry operations allowed by the lattice, whereas a VBS state usually breaks the translational or rotational lattice symmetry.

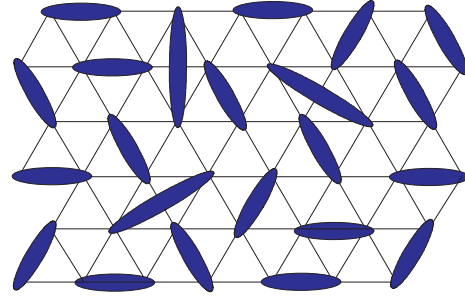


FIG. 3 A spin-singlet dimer configuration covering a lattice. An RVB state is a superposition of such configurations.

The wavefunction given in Eq. (23), which is parameterized by $a_{(i_1 j_1 \dots i_n j_n)}$, has too many variational degrees of freedom even after the translational and rotational symmetries of the wavefunction are considered and must be simplified for practical purposes. A solution has been proposed by Baskaran, Zou and Anderson (Baskaran *et al.*, 1987), who noted that the Bardeen-Cooper-Schrieffer (BCS) states for superconductors are direct product states of spin-singlet Cooper pairs and suggested that good RVB wavefunctions can be constructed from BCS wavefunctions *via* Gutzwiller projection, denoted by P_G :

$$|\Psi_{RVB}\rangle = P_G |\Psi_{BCS}\rangle, \quad (24)$$

$$|\Psi_{BCS}\rangle = \prod_{\mathbf{k}} (u_{\mathbf{k}} + v_{\mathbf{k}} c_{\mathbf{k}\uparrow}^{\dagger} c_{-\mathbf{k}\downarrow}^{\dagger}) |0\rangle,$$

where $c_{\mathbf{k}\uparrow}^{\dagger}$ and $c_{-\mathbf{k}\downarrow}^{\dagger}$ are electron creation operators and the numerical coefficients $u_{\mathbf{k}}$ and $v_{\mathbf{k}}$ are determined from a trial BCS mean-field Hamiltonian H_{BCS} through the Bogoliubov-de Gennes equations, i.e., the RVB wavefunction is fixed by the parameters determining H_{BCS} . The number of electrons at each lattice site may take a value of 0, 1 or 2 in the original BCS wavefunctions. The Gutzwiller projection P_G removes all wavefunction com-

ponents with doubly occupied sites from the BCS state and freezes the charge degrees of freedom. A half-filled Mott insulator state is obtained if the total number of electrons is equal to the number of lattice sites. We note that the technique of Gutzwiller projection is currently being widely applied to other mean-field wavefunctions $|\Psi_{MF}\rangle$ to study Mott insulating states in diverse physical systems. Interesting and energetically favorable wavefunctions are often obtained when $|\Psi_{MF}\rangle$ is chosen properly.

In addition to representing spins by electrons or fermions, one may also use Schwinger bosons to represent spins to construct RVB wavefunctions (see also the discussion after Eq. (27)). It is easy to recognize that in general, almost any mean-field wavefunction $|\Psi_{MF}\rangle$ can be employed to construct a corresponding spin state as follows:

$$|\Psi_{Spin}\rangle = P_G |\Psi_{MF}\rangle, \quad (25)$$

where $|\Psi_{MF}\rangle$ is the ground state of a trial mean-field Hamiltonian $H_{trial}(c, c^\dagger; a_1, \dots, a_N)$, where $c_{i\sigma}^\dagger (c_{i\sigma})$ can represent either fermions or bosons and a_1, \dots, a_N are variational parameters determined by minimizing the energy of the parent spin Hamiltonian.² The invention of Gutzwiller projection techniques enables us to construct a large variety of variational spin wavefunctions, of which the best is the one with the lowest energy.

The most important difference between the fermion and boson constructions is that they lead to very different sign structures in the spin wavefunction $|\Psi_{RVB}\rangle$. In a bosonic wavefunction, when two spins (note that only spin degrees of freedom remain after Gutzwiller projection) at different sites are interchanged, the wavefunction does not change, whereas the wavefunction does change sign when two spins are interchanged in a fermionic wavefunction. These different sign structures represent very different quantum entanglement structures in the corresponding RVB wavefunctions. A famous example is Marshall's sign rule (Marshall, 1955) for the AFM Heisenberg model on a bipartite lattice, where the Heisenberg exchange exists only between bonds linking sites in different sublattices. Marshall's theorem tells us that the ground state for such an AFM system is a spin-singlet state with positive-definite coefficients in the Ising basis $\{(-1)^{N_{A\downarrow}} |\sigma_1 \dots \sigma_N\rangle\}$, where $N_{A\downarrow}$ is the number of

down spins in sublattice A and N is the number of lattice sites. Using this result, Liang, Doucot and Anderson (Liang *et al.*, 1988) proposed the use of the following trial ground-state RVB wavefunction for spin-1/2 Heisenberg antiferromagnets on a square lattice:

$$|\Psi_{LDA}\rangle = \sum_{i_\alpha \in A, j_\beta \in B} h(i_1 - j_1) \dots h(i_n - j_n) \times (-1)^{N_{A\downarrow}} |(i_1, j_1) \dots (i_n, j_n)\rangle, \quad (26)$$

where $h(r)$ represents a positive-definite function of the bond length r . This particular wavefunction can be conveniently represented as a Gutzwiller-projected wavefunction in the Schwinger boson representation, whereas the representation of the same wavefunction in terms of fermions is far from straightforward (Read and Chakraborty, 1989). However, it has been shown that the projected BCS wavefunction given in Eq. (24) will satisfy Marshall's sign rule provided that the spatial Fourier transformation of $u_{\mathbf{k}}$ and $v_{\mathbf{k}}$ ($= u_{ij}$ and v_{ij}) connects only sites in different sublattices in a bipartite lattice (Li and Yang, 2007; Yunoki and Sorella, 2006)

It has been noted by Ma (Ma, 1988) that the sum of states $|(i_1, j_1) \dots (i_n, j_n)\rangle$, with $i_\alpha \in A$ and $j_\beta \in B$, forms an overcomplete set for spin-singlet states in a bipartite lattice. Because h is a positive function, it can be interpreted as a weight factor in a Monte Carlo simulation based on loop gas statistics. Such a calculation has been performed for large lattices by Liang *et al.* (Liang *et al.*, 1988), and a very accurate ground-state wavefunction for the AFM Heisenberg model on a square lattice was obtained. The wavefunction can give rise to either long-range or short-range spin correlations depending on the choice of $h(r)$.

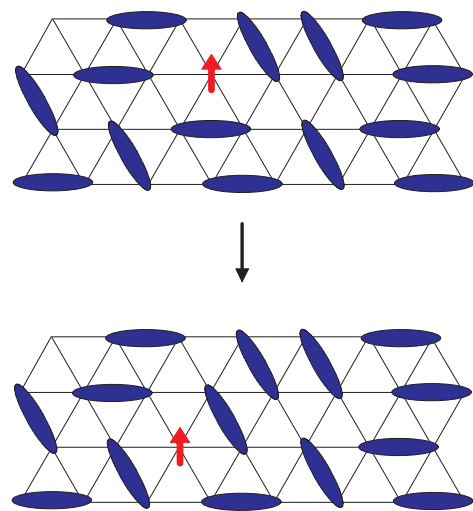


FIG. 4 A spinon excitation on top of an RVB ground state.

Once a proper RVB ground-state wavefunction has

² For historical reasons, the fermion representation is also called the slave-boson representation, and the Schwinger boson representation is also called the slave-fermion representation. In the context of doped Mott insulators, one can decompose the electron annihilation operator as $c_{i\sigma} = h_i^\dagger f_{i\sigma}$, where $f_{i\sigma}$ carries a charge-neutral spin and h_i^\dagger is the (spinless) hole creation operator. If the spinon operator $f_{i\sigma}$ is fermionic, then the charge carrier (h_i^\dagger) is a "slave boson", whereas if the spinon operator is bosonic, then the charge carrier is a "slave fermion".

been constructed, the next natural question is what are the low-energy dynamics, or the elementary excitations on top of the ground states? A natural candidate for excitation is to break a spin-singlet pair in the ground state to form a spin-triplet excited state with two unpaired spins. For a long-range magnetically ordered state, it has been found that the two unpaired spins will bind together closely in space and that the resulting elementary excitations will be localized spin-triplet excitations with well-defined energy and momentum. This is nothing but a spin wave or magnon excitation, as guaranteed by the Goldstone theorem. By contrast, for a QSL state with short-range spin correlation, it has been proposed that the two unpaired spins may interact only weakly with each other and can be regarded as independent spin-1/2 elementary excitations called spinons. The existence of $S = 1/2$ spinon excitations is one of the most important predictions in QSLs and is crucial to the experimental verification of QSLs. The process through which a spin-1 magnon turns into two independent spin-1/2 spinons is an example of *fractionalization*. Whether fractionalization of spin excitations actually occurs in a particular spin system is a highly non-trivial question. A systematic way to examine whether fractionalization may occur in a spin model was first proposed by X.G. Wen (Wen, 1989, 1991) based on the concept of confinement/deconfinement in lattice gauge theory.³ This approach is explained in the following subsection, where the gauge theory for QSLs is introduced.

III.1. RVB theory and gauge Theory

This subsection presents a brief survey of how RVB theory is implemented in practice, especially how low-energy effective field theories for QSL states are constructed, which is crucial for characterizing QSLs. We discuss a few common examples of QSLs and define the $SU(2)$, $U(1)$ and Z_2 spin liquid states. The nature of the $U(1)$ QSL state is then further illuminated by relating it to a Fermi liquid state through a Mott metal-insulator transition. We shall see that analytical approaches have strong limitations and should be complemented by numerical approaches in practice.

One complication associated with the RVB construction is that there exist, in general, different mean-field states $|\Psi_{MF}\rangle$ that correspond to the same RVB spin wavefunction after Gutzwiller projection. This redundancy originates from the enlarged Hilbert space in

the boson/fermion representation for spins and is called *gauge redundancy* or *gauge symmetry*. Gutzwiller projection removes this redundancy, resulting in a unique state in spin Hilbert space. To see how this occurs, we consider the fermion representation of $S = 1/2$ spin operators (Abrikosov, 1965; Baskaran and Anderson, 1988; Baskaran *et al.*, 1987):

$$\vec{S}_i = \frac{1}{2} \sum_{\alpha\beta} f_{i\alpha}^\dagger \vec{\sigma}_{\alpha\beta} f_{i\beta}, \quad (27a)$$

where $\alpha, \beta = \uparrow, \downarrow$ are spin indices, $f_{i\alpha}^\dagger$ ($f_{i\alpha}$) is the fermion creation (annihilation) operator, and $\vec{\sigma} = (\sigma^1, \sigma^2, \sigma^3)$ represents the Pauli matrices. It is easy to confirm that the three components of \vec{S}_i satisfy the $SU(2)$ Lie algebra relation, $[S_i^\lambda, S_j^\mu] = i\epsilon_{\lambda\mu\nu} S_i^\nu \delta_{ij}$, where $\lambda, \mu, \nu = 1, 2, 3$ and $\epsilon_{\lambda\mu\nu}$ is the antisymmetric tensor. Hence, Eq. (27a) is a representation of $SU(2)$ spins. However, the local Hilbert space for two fermions contains four Fock states, $\{|0\rangle, f_\uparrow^\dagger |0\rangle = |\uparrow\rangle, f_\downarrow^\dagger |0\rangle = |\downarrow\rangle, f_\uparrow^\dagger f_\downarrow^\dagger |0\rangle = |\uparrow\downarrow\rangle\}$; this is larger than the physical spin Hilbert space for spin-1/2 = $\{|\uparrow\rangle, |\downarrow\rangle\}$, and we need to impose the single-occupancy constraint

$$\sum_{\alpha} f_{i\alpha}^\dagger f_{i\alpha} = 1 \quad (27b)$$

to remove the unphysical states to obtain a proper spin representation. This is what the Gutzwiller projection does. The construction presented in Eq. (27) is equally applicable for bosons (the Schwinger boson representation) because the $SU(2)$ Lie algebra is independent of the statistics of the represented particles. In the following, we focus on the fermion representation approach because it has been found to be a more fruitful approach for constructing QSLs. Readers who are interested in the Schwinger boson approach may refer to reference (Arovas and Auerbach, 1988) for details.

There are multiple choices of $\{f_{i\alpha}\}$ available to represent spin operators even once the single-occupancy constraint is satisfied and the statistics of the particles have been chosen. For example, a new set of $\{f'_{i\alpha}\}$ can be obtained through an $U(1)$ gauge transformation:

$$f_{i\alpha} \rightarrow f'_{i\alpha} = e^{i\theta(i)} f_{i\alpha}.$$

It is easy to verify that $\{f'_{i\alpha}\}$ forms another representation of spin operators by replacing $f_{i\alpha}$ with $f'_{i\alpha}$ in Eq. (27), independent of whether the f s are fermions or bosons. This multiplicity is called gauge redundancy or gauge symmetry in the literature. We call it gauge redundancy here because symmetry usually refers to situations in which there are multiple physically distinct states with the same properties, e.g., there is a degeneracy in energy. However, the gauge degree of freedom we discuss here is not a “real” symmetry among different physical states. Here, two gauge-equivalent states are the *same* state in

³ This criterion for fractionalization works only in dimensions $d > 1$. In one dimension, gauge fields are always confining, while spinons appear in energy spectrum as the gapless spin-1/2 excitations of the quantum antiferromagnet Heisenberg model (Mudry and Fradkin, 1994a,b).

the spin Hilbert space. They just “look” different when they are represented by particles that live in an enlarged Hilbert space. There is no way to distinguish them physically (Wen, 2002).

The gauge redundancy in the fermion representation of $S = 1/2$ spins extends beyond $U(1)$. There exists an additional $SU(2)$ gauge structure because of the particle-hole symmetry in the fermion representation, which is absent in the Schwinger boson representation. An elegant way of showing this $SU(2)$ gauge structure was suggested by Affleck, Zou, Tsu and Anderson (Affleck *et al.*, 1988b), who introduced the following 2×2 matrix operator:

$$\Psi = \begin{pmatrix} f_\uparrow & f_\downarrow^\dagger \\ f_\downarrow & -f_\uparrow^\dagger \end{pmatrix}. \quad (28)$$

It is straightforward to show that the spin operator can be re-expressed in terms of Ψ as

$$\vec{S}_i = \text{tr} \left(\Psi_i^\dagger \vec{\sigma} \Psi_i \right). \quad (29)$$

The single-occupancy condition given in Eq. (27b) also leads to the identities

$$f_{i\uparrow} f_{i\downarrow} = f_{i\uparrow}^\dagger f_{i\downarrow}^\dagger = 0. \quad (30a)$$

Together with Eq. (30a), Eq. (27b) can be rewritten in the following compact vector form:

$$\text{tr} \left(\Psi_i \vec{\sigma} \Psi_i^\dagger \right) = 0. \quad (30b)$$

We now consider the following $SU(2)$ gauge transformation of Ψ :

$$\Psi_i \rightarrow \Psi'_i = \Psi_i W_i, W_i \in SU(2). \quad (31)$$

The spin operator \vec{S}_i in Eq. (29) remains invariant under this transformation because $W_i W_i^\dagger = 1$. The single-occupancy constraint given in Eq. (30b) is also invariant because $W_i \vec{\sigma} W_i^\dagger$ represents a rotation of vector $\vec{\sigma}$ but all components of $\text{tr} \left(\Psi_i \vec{\sigma} \Psi_i^\dagger \right)$ are zero, i.e., $\Psi_i \rightarrow \Psi'_i = \Psi_i W_i$ is also a valid representation for $S = 1/2$ spins.

We show now how RVB theory is implemented in an analytical fermionic approach. For concreteness, we consider an AFM Heisenberg model on a lattice:

$$H = J \sum_{\langle ij \rangle} \vec{S}_i \cdot \vec{S}_j, \quad (32)$$

where $\langle ij \rangle$ denotes a nearest neighbor bond and $J > 0$. The spin exchange $\vec{S}_i \cdot \vec{S}_j$ can be written in terms of fermionic (spinon) operators:

$$\vec{S}_i \cdot \vec{S}_j = \frac{1}{4} \sum_{\alpha\beta} \left(2f_{i\alpha}^\dagger f_{i\beta} f_{j\beta}^\dagger f_{j\alpha} - f_{i\alpha}^\dagger f_{i\alpha} f_{j\beta}^\dagger f_{j\beta} \right), \quad (33)$$

where we have used the relation $\vec{\sigma}_{\alpha\beta} \cdot \vec{\sigma}_{\alpha'\beta'} = 2\delta_{\alpha\beta}\delta_{\alpha'\beta'} - \delta_{\alpha\beta}\delta_{\alpha'\beta'}$. The constraint given in Eq. (27b) or (30b) can be imposed by inserting delta functions into the imaginary-time path integral. The corresponding partition function is

$$Z = \int D[f, \bar{f}] \exp[-S(f, \bar{f})] \prod_i \delta \left(\sum_\alpha \bar{f}_{i\alpha} f_{i\alpha} - 1 \right) \times \delta \left(\sum_{\alpha\beta} \epsilon_{\alpha\beta} f_{i\alpha} f_{i\beta} \right) \delta \left(\sum_{\alpha\beta} \epsilon_{\alpha\beta} \bar{f}_{i\alpha} \bar{f}_{i\beta} \right), \quad (34)$$

where the action $S(f, \bar{f})$ is given by

$$S(f, \bar{f}) = \int_0^\beta d\tau \left(\sum_{i\alpha} \bar{f}_{i\alpha} \partial_\tau f_{i\alpha} - H \right). \quad (35)$$

The delta functions can be represented by the integration over real auxiliary fields $a_0^l(i)$ on all sites i , $l = 1, 2, 3$. Using the relation $\delta(x) = \int \frac{dk}{2\pi} e^{ikx}$, we obtain

$$Z = \int D[f, \bar{f}; a] \exp[-S(f, \bar{f}; a)], \quad (36)$$

with

$$S(f, \bar{f}; a) = S(f, \bar{f}) - i \left\{ \sum_i a_0^3 \left(\sum_\alpha \bar{f}_{i\alpha} f_{i\alpha} - 1 \right) + \left[(a_0^1 + ia_0^2) \sum_{\alpha\beta} \epsilon_{\alpha\beta} f_{i\alpha} f_{i\beta} + h.c. \right] \right\} \quad (37)$$

It is generally believed (but has not been proven) that the partition function Z will remain invariant under a Wick rotation of the fields a_0^l in the path integral, namely, we can replace ia_0^l with a_0^l . Then, the action becomes

$$S(f, \bar{f}; a) = S(f, \bar{f}) - \left\{ \sum_i a_0^3 \left(\sum_\alpha \bar{f}_{i\alpha} f_{i\alpha} - 1 \right) + \left[(a_0^1 + ia_0^2) \sum_{\alpha\beta} \epsilon_{\alpha\beta} f_{i\alpha} f_{i\beta} + h.c. \right] \right\} \quad (38)$$

The action given in Eq. (38) serves as the starting point for theoretical analysis. The path integral is difficult to solve, and approximate methods are generally needed. We start with a mean-field theory in which we assume that the path integral is dominated by saddle points characterized by equal-time expectation values of the operators $\sum_\alpha f_{i\alpha}^\dagger f_{i\alpha}$, $\sum_{\alpha\beta} \epsilon_{\alpha\beta} f_{i\alpha} f_{i\beta}$ and $a_0^l(i)$:

$$\begin{aligned} \chi_{ij} &= \sum_\alpha \langle f_{i\alpha}^\dagger f_{j\alpha} \rangle, \\ \Delta_{ij} &= \sum_{\alpha\beta} \epsilon_{\alpha\beta} \langle f_{i\alpha} f_{j\beta} \rangle, \\ a_0^l &= \langle a_0^l(i) \rangle, \end{aligned} \quad (39)$$

where $\epsilon_{\alpha\beta}$ is the totally antisymmetric tensor ($\epsilon_{\uparrow\downarrow}=1$), $l = 1, 2, 3$. It is easy to verify that χ_{ij} and Δ_{ij} satisfy the relations $\chi_{ij} = \chi_{ji}^*$ and $\Delta_{ij} = \Delta_{ji}$. Note that any

time-dependent fluctuations in Δ_{ij} , χ_{ij} and $a_0^l(i)$ are ignored in mean-field theory. With these approximations, we arrive at the following mean-field Hamiltonian:

$$H_{MF} = \sum_{\langle ij \rangle} -\frac{3}{8}J \left[(\chi_{ji} \sum_{\alpha} f_{i\alpha}^{\dagger} f_{j\alpha} + \Delta_{ij} \sum_{\alpha\beta} \epsilon_{\alpha\beta} f_{i\alpha}^{\dagger} f_{j\beta}^{\dagger} + h.c.) - |\chi_{ij}|^2 - |\Delta_{ij}|^2 \right] + \sum_i \left\{ a_0^3 \left(\sum_{\alpha} f_{i\alpha}^{\dagger} f_{i\alpha} - 1 \right) + \left[(a_0^1 + ia_0^2) \sum_{\alpha\beta} \epsilon_{\alpha\beta} f_{i\alpha} f_{i\beta} + h.c. \right] \right\}, \quad (40)$$

where χ_{ij} , Δ_{ij} and a_0^l are determined by minimizing the ground-state energy with the exact constraint condition (27b) replaced with the average constraint

$$\sum_{\alpha} \langle f_{i\alpha}^{\dagger} f_{i\alpha} \rangle = 1. \quad (41)$$

The spin exchange term $\vec{S}_i \cdot \vec{S}_j$ in Eq. (33) can be evaluated within the mean-field assumption using the Wick theorem. Maintaining spin rotation invariance in the calculation, we obtain

$$\langle \vec{S}_i \cdot \vec{S}_j \rangle = -\frac{3}{8} (\chi_{ij}^* \chi_{ij} + \Delta_{ij}^* \Delta_{ij}). \quad (42)$$

in mean-field theory.

Physically, the mean-field theory outlined above is equivalent to assuming that the ground state of the spin system is given by a mean-field wavefunction $|\Psi_{MF}\rangle$ without Gutzwiller projection. The spin exchange energy (42) evaluated in this way is usually not a good estimate of the energy of the “real” spin wavefunction. In practice, this mean-field theory provides an effective way to obtain a BCS Hamiltonian to construct a Gutzwiller-projected wavefunction. Whether the spin wavefunction obtained through Gutzwiller projection is a good wavefunction for the spin Hamiltonian can only be tested by evaluating the energy of the wavefunction numerically (see section III.4).

In the following section, we assume that the Gutzwiller-projected wavefunction $P_G |\Psi_{MF}\rangle$ is a sufficiently good starting point to locate the true ground state of the spin Hamiltonian. In this case, we expect that the ground and low-energy states constructed from H_{MF} are adiabatically connected to the corresponding Gutzwiller-projected wavefunctions and that we may construct an effective low-energy Hamiltonian/Lagrangian of the spin system from fluctuations around H_{MF} through the usual path integral technique. The fluctuations in Δ_{ij} , χ_{ij} and $a_0^l(i)$ describe spin-singlet excitations and are usually called *gauge fluctuations*. Before discussing gauge fluctuations, we first discuss the effect of gauge redundancy on the mean-field states.

To illustrate, we consider two mean-field QSL states with different structures of the mean-field parameters

$\{\chi_{ij}, \Delta_{ij}, a_0^l(i)\}$. We place the states on a simple square lattice. The first state is the uniform RVB state with

$$\begin{aligned} \chi_{ij} &= 0, \\ \Delta_{ij} &= \begin{cases} \Delta, & \text{NN bonds,} \\ 0, & \text{others,} \end{cases} \\ a_0^l &= 0 \ (l = 1, 2, 3). \end{aligned} \quad (43a)$$

The second example considered is the zero-flux state given by

$$\begin{aligned} \chi_{ij} &= \begin{cases} \chi, & \text{NN bonds,} \\ 0, & \text{others,} \end{cases} \\ \Delta_{ij} &= 0, \\ a_0^l &= 0 \ (l = 1, 2, 3). \end{aligned} \quad (43b)$$

Δ and χ are real numbers. We show that irrespective of their very different appearances, these two mean-field ansatze actually give rise to the same spin state after Gutzwiller projection. The two states are gauge equivalent because they can be transformed into each other through a proper gauge transformation.

The Hamiltonian given in Eq. (40) retains a local $SU(2)$ structure, which originates from the gauge redundancy in the fermion representation of spin. This local $SU(2)$ symmetry becomes explicit if we introduce a doublet field $\psi = (f_{\uparrow}, f_{\downarrow}^{\dagger})^T$ and a 2×2 matrix

$$u_{ij} = \begin{pmatrix} \chi_{ij} & \Delta_{ji}^* \\ \Delta_{ij} & -\chi_{ji} \end{pmatrix}.$$

The mean-field Hamiltonian (40) can be written in a compact manner as

$$\begin{aligned} H_{MF} &= \sum_{\langle ij \rangle} \frac{3}{8}J \left[\frac{1}{2} \text{Tr}(u_{ij}^{\dagger} u_{ij}) - (\psi_i^{\dagger} u_{ij} \psi_j + h.c.) \right] \\ &+ \sum_{i,l} a_0^l \psi_i^{\dagger} \tau^l \psi_i, \end{aligned} \quad (44)$$

where the τ^l , $l = 1, 2, 3$, are the Pauli matrices. From Eq. (44) we can clearly see that the Hamiltonian H_{MF} is invariant under a local $SU(2)$ transformation W_i :

$$\begin{aligned} \psi_i &\rightarrow W_i \psi_i, \\ u_{ij} &\rightarrow W_i u_{ij} W_j^{\dagger}. \end{aligned} \quad (45)$$

This $SU(2)$ gauge transformation is the same as that in (31), where $\Psi = (\psi, i\sigma_2 \psi^{\dagger})^T$.

Because of this $SU(2)$ gauge structure, if we regard the ansatz $(u_{ij}, a_0^l \tau^l)$ as labeling a physical spin wavefunction $|\Psi_{spin}^{(u_{ij}, a_0^l \tau^l)}\rangle = P_G |\Psi_{MF}^{(u_{ij}, a_0^l \tau^l)}\rangle$, then such a label is not a one-to-one label. Two ansatze related by an $SU(2)$ gauge transformation, $(u_{ij}, a_0^l \tau^l)$ and $(u'_{ij}, a'_0 \tau^l) = (W(u_{ij}), W(a_0^l \tau^l))$, label the same physical spin wavefunction:

$$\begin{aligned} |\Psi_{spin}(\{\alpha_i\})\rangle &= P_G |\Psi_{MF}^{(W(u_{ij}), W(a_0^l \tau^l))}\rangle \\ &= P_G |\Psi_{MF}^{(u'_{ij}, a'_0 \tau^l)}\rangle \end{aligned} \quad (46)$$

where $W(u_{ij}) = W_i u_{ij} W_j^\dagger$ and $W(a_0^l(i)\tau^l) = W_i a_0^l(i)\tau^l W_i^\dagger$, $W_i \in SU(2)$. The uniform RVB state and the zero-flux state discussed above denote the same physical spin state because they are related by a gauge transformation,

$$W_i = \exp\left(i\frac{\pi}{4}\tau^2\right).$$

More generally, the existence of gauge redundancy implies that the low-energy fluctuations in spin systems have a similar redundancy. To measure gauge fluctuations, we introduce the loop variables

$$P(C_i) = u_{ij} u_{jk} \cdots u_{li},$$

where i, j, k, \dots, l denote a loop of lattice sites that passes through site i . $P(C_i)$ measures gauge fluxes and has the general form

$$P(C_i) = A(C_i)\tau^0 + \mathbf{B}(C_i) \cdot \vec{\tau},$$

where τ^0 is the identity matrix and $\vec{\tau} = \{\tau^1, \tau^2, \tau^3\}$ represents the Pauli matrices, $A(C_i)$ and $\mathbf{B}(C_i)$ measure the $U(1)$ and $SU(2)$ components, respectively, of the gauge flux. For a translationally invariant mean-field state, we can find a gauge with $\mathbf{B}(C_i) = \hat{n}B(C_i)$, where $A(C_i)$ and $B(C_i)$ are proportional to the area of the loop. Under a gauge transformation,

$$P(C_i) \rightarrow W_i P(C_i) W_i^\dagger,$$

and the “direction” of \hat{n} changes. The presence of gauge redundancy means that we may perform gauge transformations to change the “local” directions of \hat{n} , but the physical spin state remains unchanged.

For a given mean-field state, it is useful to distinguish between two kinds of gauge transformations: those that change the mean-field ansatz $\{u_{ij}, a_0^l(i)\}$ and those that do not. The latter constitute a subgroup of the original $SU(2)$ symmetry called an invariant gauge group (IGG) (Wen, 2002):

$$IGG \equiv \left\{ W_i | W_i u_{ij} W_j^\dagger = u_{ij}, W_i \in SU(2) \right\}. \quad (47)$$

It can be shown rather generally that for a stable QSL state, physical gapless gauge excitations exist only for those fluctuations belonging to the IGG of the corresponding mean-field ansatz. Therefore, it is important to understand the structure of the IGGs in spin liquid states. Within the fermionic $SU(2)$ formalism, there are only three plausible kinds of IGG: $SU(2)$, $U(1)$ and Z_2 . We call the corresponding spin liquids $SU(2)$, $U(1)$ and Z_2 spin liquids. $SU(2)$ spin liquids have $\mathbf{B}(C_i) = 0$ with $IGG = SU(2)$. They are rather unstable because of the existence of a large amount of gapless $SU(2)$ gauge field fluctuations. $U(1)$ spin liquids have $\mathbf{B}(C_i)$ pointing in only one direction for all loops C_i . The condensation

of fluxes in one “direction” provides an Anderson-Higgs mechanism for $SU(2)$ fluxes in “directions” perpendicular to $\mathbf{B}(C)$ and turns the IGG into $U(1)$. The low-energy fluctuations are $U(1)$ gauge field fluctuations. Z_2 spin liquids have $\mathbf{B}(C_i)$ pointing in different directions for different loops that pass through the same site i . The gauge fluctuations are all gapped because the Anderson-Higgs mechanism now applies to fluxes in all directions. A few examples of mean-field ansatze for these three types of spin liquid states are presented in the following subsections.

III.2. $U(1)$ gauge fluctuations

We briefly discuss the $U(1)$ gauge theory in regard to two examples of spin liquids that are believed to exist in nature (see section V). The first example is the zero-flux state given in Eq. (43b), for which $\Delta_{ij} = a_0^l = 0$ and $\chi_{ij} = \chi$ in the mean-field ansatz.

It is easy to see that $\mathbf{B}(C_i) \equiv \mathbf{0}$ and that the IGG of such a QSL is $SU(2)$, i.e., the zero-flux state describes a $SU(2)$ spin liquid. The low-energy fluctuations are $SU(2)$ gauge fluctuations. Here, we do not consider the full $SU(2)$ gauge fluctuations; we consider only the phase fluctuations of χ_{ij} , i.e., $U(1)$ gauge fluctuations. The consideration of only $U(1)$ gauge fluctuations for the zero-flux state can be justified in a slave-rotor theory for the Hubbard model (Lee and Lee, 2005) or in a phenomenological Landau Fermi-liquid-type approach for spin liquid states *near the metal-insulator transition* (see the next subsection).

Upon writing $\chi_{ij} = \chi e^{ia_{ij}}$, where a_{ij} denotes phase fluctuations, it is straightforward to see that

$$P(C_i) \propto \exp(i\Phi(C_i)\tau^3),$$

where $\Phi(C_i) = (a_{ij} + a_{jk} + \cdots + a_{li})$ is the total $U(1)$ gauge flux enclosed by the loop, i.e., the phase fluctuations of χ_{ij} represent one component of the $SU(2)$ gauge fluctuations.

The effective Lagrangian describing these low-energy phase fluctuations is

$$L^{(0)} = \sum_{i\alpha} \bar{f}_{i\alpha} (\partial_\tau - a_0) f_{i\alpha} + \frac{3}{8} \sum_{\langle ij \rangle} \left(J \chi e^{ia_{ji}} \sum_\alpha \bar{f}_{i\alpha} f_{j\alpha} + h.c. \right), \quad (48)$$

and the corresponding Lagrangian in the continuum limit is

$$L^{(0)} = \int d\vec{r} \sum_\alpha \bar{f}_\alpha(\vec{r}) (\partial_\tau - a_0) f_\alpha(\vec{r}) + \frac{1}{2m^*} \bar{f}_\alpha(\vec{r}) (-i\nabla + \vec{a})^2 f_\alpha(\vec{r}), \quad (49)$$

where m^* is the effective mass for the spinon energy dispersion determined by $J\chi$ and the vector field $\vec{a}(\vec{r})$ is given by the lattice gauge field a_{ij} through

$$a_{ij} = (\vec{r}_i - \vec{r}_j) \cdot \vec{a} \left(\frac{\vec{r}_i + \vec{r}_j}{2} \right). \quad (50)$$

Thus, the low-energy effective field theory describes non-relativistic spin-1/2 fermions (spinons) coupled to the $U(1)$ gauge field $(a_0(\vec{r}), \vec{a}(\vec{r}))$ in the continuum limit.

The other spin liquid state we introduce here is the π -flux state (Affleck and Marston, 1988; Kotliar, 1988) on a square lattice given by $\Delta_{ij} = a_0^l = 0$ and

$$\chi_{i,i+\hat{\mu}} = \begin{cases} \chi, & \mu = x, \\ i\chi(-1)^{i_x}, & \mu = y. \end{cases} \quad (51)$$

It is easy to see that $P(C_i) \propto \exp(i\pi\tau^3)$ per square plaquette in the mean-field ansatz, i.e., the π -flux state has $IGG = U(1)$ and is a $U(1)$ spin liquid.

The zero-flux and π -flux states are physically distinct states because of their different IGGs. Their mean-field spinon dispersions are also qualitatively different. The zero-flux state has a mean-field dispersion of $E_0(\vec{k}) = -J\chi(\cos k_x + \cos k_y)$, whereas the π -flux state has $E_\pi(\vec{k}) = \pm J\chi\sqrt{\cos^2 k_x + \cos^2 k_y}$ with a reduced Brillouin zone. The continuum theory describes non-relativistic fermions with a large Fermi surface in the zero-flux state and describes Dirac fermions with four Fermi points ($\mathbf{k} = (\pm\pi/2, \pm\pi/2)$) in the π -flux state (Affleck and Marston, 1988). The effective continuum theory for the π -flux state has the form

$$L^{(\pi)} = \sum_{\mu\sigma} (\bar{\psi}_{+\sigma}(\partial_\mu - ia_\mu)\tau_\mu\psi_{+\sigma} + \bar{\psi}_{-\sigma}(\partial_\mu - ia_\mu)\tau_\mu\psi_{-\sigma}), \quad (52)$$

where $\mu = 0, 1, 2$. The two-component Dirac spinor fields $\psi_{\pm\sigma}$ describe two inequivalent Dirac nodes in the spinon spectrum (Affleck and Marston, 1988). The two effective low-energy Lagrangians $L^{(0)}$ and $L^{(\pi)}$ describe two different types of spin liquid states that are believed to exist in nature. We discuss these states again in section V.

The continuum action L serves as the starting point for studying the stability and low-energy properties of spin liquid states. Integrating out the fermion fields (at each momentum shell) gives rise to a Maxwellian potential energy term in the gauge field:

$$\frac{1}{2g^2(\Lambda)}(\nabla \times \vec{a})^2,$$

where $g(\Lambda)$ is a running gauge coupling constant in the sense of renormalization group theory, which depends on the energy or momentum scale Λ . If $g(\Lambda) \rightarrow 0$ in the low-energy and long-wavelength limit of $\Lambda \rightarrow 0$, then the gauge fluctuations become increasingly weak. The corresponding interaction between two fermions becomes too

weak to bind them together, and the elementary excitations in the spin system are spin-1/2 fermionic excitations called spinons. This phenomenon is called deconfinement, and the ground state is a filled Fermi sea of spinons. By contrast, if $g(\Lambda) \rightarrow \infty$ as $\Lambda \rightarrow 0$, then two spinons will always be confined together to form a magnon. This phenomenon is called confinement. In this case, the mean-field QSL ground state breaks down into a spin-ordered state because of the strong gauge fluctuations, and magnon excitations are recovered in this ordered state.

It is not exactly clear which kinds of mean-field QSL states are stable against gauge fluctuation. It is generally believed that Z_2 QSL states are stable because Z_2 (Ising) gauge theories are deconfining (Fradkin and Shenker, 1979), whereas $SU(2)$ QSL states are unstable because of the presence of large gauge fluctuations. The case of $U(1)$ QSL states is more nontrivial. The $SU(2)$ gauge group and the corresponding gauge fields are compact in spin liquid states. To reflect the compactness of the $U(1)$ gauge group, one must replace the electromagnetic field tensor $F_{\mu\nu}^2$ with $2(1 - \cos F_{\mu\nu})$. This periodic version of $U(1)$ gauge theory is called compact $U(1)$ gauge theory. A pure compact $U(1)$ gauge theory always gives rise to confinement in two dimensions (Polyakov, 1977, 1975), but whether deconfinement is possible in the presence of a matter field is an open question. Herbut *et al.* have argued that the theory is always confining in the presence of a Fermi surface (Herbut *et al.*, 2003) or nodal fermions (Herbut and Seradjeh, 2003). Their conclusion depends on an approximate effective action for the gauge field obtained by integrating out the fermions to the lowest order. However, this approximation is questionable for gapless fermions. Indeed, Hermele *et al.* (Hermele *et al.*, 2004) proved that when the spin index is generalized to N flavors, deconfinement arises in the case of $2N$ 2-component Dirac fermions coupled to complex $U(1)$ gauge fields for sufficiently large N , thus providing a counter example to confinement. Further renormalization group analysis for compact quantum electrodynamics in 2 + 1D shows that deconfinement occurs when $N > N_c = 36/\pi^3 \simeq 1.161$, where N is the number of fermion replicas. This implies that a $U(1)$ spin liquid is stable at the physical value of $N = 2$ (Nogueira and Kleinert, 2005). Moreover, by mapping the spinon Fermi surface in 2 + 1D to an infinite set of (1+1)-dimensional chiral fermions, Lee (Lee, 2008b) argued that an instanton has an infinite scaling dimension for any $N > 0$. Therefore, the QSL phase is stable against instantons, and the noncompact $U(1)$ gauge theory is a good low-energy description.

We note that mechanisms other than confinement arising from gauge fluctuations may also lead to the instability of $U(1)$ QSLs, such as Amperean pairing (Lee *et al.*, 2007b) and spin-triplet pairing (Galitski and Kim, 2007) between spinons.

A non-trivial prediction of the $U(1)$ gauge theory for

spin liquids is that it leads to charge excitations with a soft gap (Ng and Lee, 2007), which can be detected by means of their AC conductivities $\sigma(\omega)$. It has been predicted that $\sigma(\omega) \sim \omega^\alpha$ in these spin liquid states, with $\alpha \sim 3.33$ in a non-relativistic spin liquid and $\alpha = 2$ in a Dirac fermion spin liquid (Potter *et al.*, 2013). It is expected that this soft gap and the related charge fluctuations will manifest themselves most clearly when the system is near the metal-insulator transition (see the next subsection).

Because charge fluctuations will manifest themselves near the metal-insulator transition, spin liquids in “weak” Mott insulators become an interesting topic (Grover *et al.*, 2010; Podolsky *et al.*, 2009; Senthil, 2008) for investigation. To study the effect of charge fluctuations near the metal-insulator transition, Lee and Lee (Lee and Lee, 2005) began with the Hubbard model and developed a $U(1)$ gauge theory with the help of the slave-rotor representation (Florens and Georges, 2004). A number of physical phenomena, including transport properties (Nave and Lee, 2007) and Kondo effect (Ribeiro and Lee, 2011), have been studied using this framework. Charge fluctuations correspond to higher-order spin ring-exchange terms in terms of the spin Hamiltonian (Misguich *et al.*, 1998; Yang *et al.*, 2010).

III.2.1. Mott transition: relation between Fermi and spin liquids

Zhou and Ng (Zhou and Ng, 2013) proposed a different way to understand $U(1)$ spin liquids near the Mott transition. They proposed that spin liquids near the Mott transition can be regarded as “Fermi liquids” with a constraint imposed on the current operator. For isotropic systems, they observed that the charge current carried by quasi-particles,

$$\mathbf{J} = \frac{m}{m^*} \left(1 + \frac{F_1^s}{d}\right) \mathbf{J}^{(0)}, \quad (53a)$$

is renormalized by the Landau parameter F_1^s in Fermi liquid theory, but the thermal current,

$$\mathbf{J}_\mathbf{Q} = \frac{m}{m^*} \mathbf{J}_\mathbf{Q}^{(0)}, \quad (53b)$$

is not, where $\mathbf{J}^{(0)}$ and $\mathbf{J}_\mathbf{Q}^{(0)}$ are the charge and thermal currents, respectively, carried by the corresponding non-interacting fermions and d is the number of dimensions of the system. For systems with Galilean invariance, the charge current carried by quasi-particles is not renormalized, and $\frac{m^*}{m} = 1 + \frac{F_1^s}{d}$ (Baym and Pethick, 2004). However, this is not valid in general for electrons in crystals, where Galilean invariance is lost. In this case, $\frac{m^*}{m} \neq 1 + \frac{F_1^s}{d}$, and the charge current carried by quasi-particles is renormalized through quasi-particle interaction. In the special case in which $1 + F_1^s/d \rightarrow 0$ while $\frac{m^*}{m}$

remains finite, $\mathbf{J} \rightarrow 0$, suggesting that the fermionic system is in a special state wherein spin-1/2 quasi-particles do not carry charge due to interaction but still carry entropy. This is exactly what one expects for spinons in QSL states.

These authors noted that the limit of $1 + F_1^s/d \rightarrow 0$ is a singular point in Fermi liquid theory and that higher-order q - and ω -dependent terms should be included in the Landau interaction to ensure that finite results are obtained when calculating physical response functions. Expanding at small q and ω , they obtained

$$\frac{1 + F_1^s(q, \omega)/d}{N(0)} \sim \alpha - \beta\omega^2 + \gamma_t q_t^2 + \gamma_l q_l^2, \quad (54)$$

where $q_t \sim \nabla \times$ and $q_l \sim \nabla$ are associated with the transverse (curl) and longitudinal (gradient) parts, respectively, of the small- \vec{q} expansion. In a QSL state, $\alpha = 0$. They found that to ensure that the system is in an incompressible (insulator) state, it is necessary to have $\gamma_l = 0$.

To show that this phenomenology actually describes fermionic spin liquids with $U(1)$ gauge fluctuations, Zhou and Ng (Zhou and Ng, 2013) considered a Landau Fermi liquid with interaction parameters of $F_0^s(q)$ and $F_1^s(q)$ only. The long-wavelength and low-energy dynamics of the Fermi liquid are described by the following effective Lagrangian:

$$L_{\text{eff}} = \sum_{\mathbf{k}, \sigma} \left[c_{\mathbf{k}\sigma}^\dagger \left(i \frac{\partial}{\partial t} - \xi_{\mathbf{k}} \right) c_{\mathbf{k}\sigma} - H'(c^\dagger, c) \right], \quad (55)$$

where $c_{\mathbf{k}\sigma}^\dagger (c_{\mathbf{k}\sigma})$ is the spin- σ fermion creation (annihilation) operator with momentum \mathbf{k} and

$$H'(c^\dagger, c) = \frac{1}{2N(0)} \sum_q \left[\frac{F_1^s(q)}{v_F^2} \mathbf{j}(q) \cdot \mathbf{j}(-q) + F_0^s(q) n(q) n(-q) \right] \quad (56)$$

describes the current-current and density-density interactions between quasi-particles (Larkin, 1964; Leggett, 1965), where $q = (\mathbf{q}, \omega)$ and $v_F = \hbar k_F/m^*$ is the Fermi velocity.

The current and density interactions can be decoupled by introducing fictitious gauge potentials \mathbf{a} and φ (Hubbard-Stratonovich transformation) as follows:

$$H'(c^\dagger, c) \rightarrow \sum_q \left[\mathbf{j} \cdot \mathbf{a} + n\varphi - \frac{1}{2} \left(\frac{n}{m^*} \frac{d}{F_1^s(q)} \mathbf{a}^2 + \frac{N(0)}{F_0^s(q)} \varphi^2 \right) \right], \quad (57)$$

where n is the fermion density. The equality $d(n/m^*) = N(0)v_F^2$ was used in formulating Eq. (57).

The Lagrangian presented in Eq. (55) and (57) can be rewritten in the standard form of $U(1)$ gauge theory by noting that in this representation, the fermion current is given by

$$\mathbf{j} = \frac{-i}{2m^*} \sum_\sigma [\psi_\sigma^\dagger \nabla \psi_\sigma - (\nabla \psi_\sigma^\dagger) \psi_\sigma] - \frac{n}{m^*} \mathbf{a},$$

where $\psi_\sigma(\mathbf{r}) = \int e^{-i\mathbf{k}\cdot\mathbf{r}} c_{\mathbf{k}\sigma}$ is the Fourier transform of $c_{\mathbf{k}\sigma}$. The Lagrangian can be written as

$$L = \sum_\sigma \int d^d \mathbf{r} \left[\psi_\sigma^\dagger (i \frac{\partial}{\partial t} - \varphi) \psi_\sigma - H(\psi_\sigma^\dagger, \psi_\sigma) \right] + L(\varphi, \mathbf{a}), \quad (58a)$$

where

$$H(\psi_\sigma^\dagger, \psi_\sigma) = \frac{1}{2m^*} |(\nabla - i\mathbf{a})\psi_\sigma|^2 \quad (58b)$$

and

$$L(\varphi, \mathbf{a}) = \frac{1}{2} \int d^d \mathbf{r} \left[\frac{n}{m^*} \left(1 + \frac{d}{F_1^s} \right) \mathbf{a}^2 + \frac{N(0)}{F_0^s} \varphi^2 \right]. \quad (58c)$$

Using Eq. (54), they find that in the small- q limit, the transverse part of $L(\varphi, \mathbf{a})$ in the spin liquid state is given by

$$L_t(\varphi, \mathbf{a}) = -\frac{n}{2m^*} \int d^d \mathbf{r} \left[\beta \left(\frac{\partial \mathbf{a}}{\partial t} \right)^2 - \gamma_t (\nabla \times \mathbf{a})^2 \right]. \quad (59)$$

The Lagrangian as expressed in Eq. (58) together with Eq. (59) is the standard Lagrangian used to describe QSLs with $U(1)$ gauge fluctuations. The analysis can be rather straightforwardly generalized to a $U(1)$ spin liquid with Dirac fermion dispersion. The appearance of a soft charge gap in $U(1)$ spin liquids can be understood from the phenomenological form of $F_1^s(q, \omega)$ as expressed in Eq. (54), which suggests that the quasi-particles carry vanishing charges only in the limit of $q, \omega \rightarrow 0$. The appearance of a non-vanishing β in (54) leads to an AC conductivity $\sigma(\omega)$ with a power-law form. This picture is very different from theories of spin liquid states that start from simple spin models in which charge fluctuations are absent at all energy scales and suggests that charge fluctuations are important in regions near the Mott transition. We note that charge fluctuations can be (partially) incorporated into the spin models through ring-exchange terms.

The close relationship between Fermi liquids and spin liquid states suggests an alternative picture of the Mott metal-insulator transition with respect to that put forward by Brinkman and Rice (Brinkman and Rice, 1970), who proposed that a metal-insulator (Mott) transition is characterized by a diverging effective mass $\frac{m^*}{m} \rightarrow \infty$ and an inverse compressibility $\kappa \rightarrow 0$ at the Mott transition point, with a correspondingly vanishing quasi-particle renormalization weight $Z \sim \frac{m}{m^*} \rightarrow 0$. The diverging effective mass and vanishing quasi-particle weight imply that the Fermi liquid state is destroyed at the Mott transition and that the Mott insulator state is distinct from the Fermi liquid state on the metal side.

The phenomenology described here suggests an alternative picture in which the Fermi surface is not destroyed, but the Landau quasi-particles are converted into spinons $(1 + \frac{F_1^s}{d}) \rightarrow 0$ at the Mott transition. In particular,

the effective mass m^*/m may not diverge at the metal-insulator transition, although $Z \rightarrow 0$. A schematic phase diagram for the Mott (metal-QSL) transition is presented in Fig. 5 for a generic Hubbard-type Hamiltonian with a hopping integral t and an on-site Coulomb repulsion U . The system is driven into a Mott insulator state at zero temperature at $U = U_c$, where $1 + F_1^s(U > U_c)/d = 0$. This picture suggests that a $U(1)$ spin liquid state is likely to exist in an insulator close to the Mott transition.

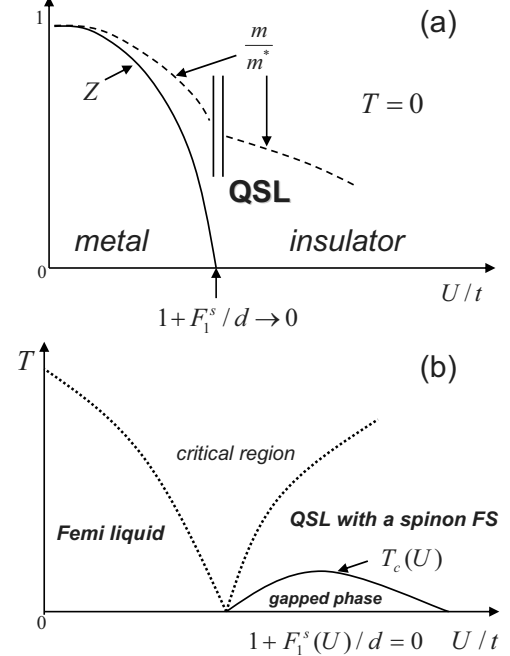


FIG. 5 (Zhou and Ng, 2013) (a) Schematic zero-temperature phase diagram for the Mott transition. U is the strength of the Hubbard interaction, and t is the hopping integral. The electron quasi-particle weight and the quasi-particle charge current $\sim 1 + F_1^s/d$ vanish at the critical point, whereas the effective mass remains finite. (b) Schematic phase diagram showing finite-temperature crossovers and possible instability toward gapped phases at lower temperatures. There exists a (finite-temperature) critical region around U_c where the phenomenology is not applicable.

The point $1 + F_1^s/d = 0$ is a critical point in Fermi liquid theory called the Pomeranchuk point. The Fermi surface is unstable with respect to deformation when $1 + F_1^s/d < 0$. The criticality of this point implies that the QSLs obtained in this way are marginally stable because of large critical fluctuations. A similar conclusion can be drawn from $U(1)$ gauge theory by analyzing the $U(1)$ gauge fluctuations. As a result, QSLs with large Fermi surfaces are, in general, susceptible to the formation of other, more stable QSLs at lower temperatures, such as Z_2 QSLs or valence-bond solid (VBS) states that gap out part of or the entire Fermi surface. This is indicated schematically in the phase diagram shown in Fig. 5(b), where the system is driven into a gapped QSL at low temperatures of $T < T_c(U)$ on the insulating side. The

nature of the low-temperature QSLs depends on the microscopic details of the system and cannot be determined based on the above phenomenological considerations.

III.3. Z_2 spin liquid states

An example of a Z_2 spin liquid state was first constructed by Wen (Wen, 1991) for a $J_1 - J_2$ Heisenberg model on a square lattice, where J_1 and J_2 are the nearest neighbor and next nearest neighbor Heisenberg interactions, respectively. Wen considered the mean-field ansatz

$$u_{i,i+\hat{\mu}} = \begin{pmatrix} \chi & 0 \\ 0 & -\chi \end{pmatrix} \quad (60a)$$

where $\hat{\mu} = \hat{x}, \hat{y}$, and

$$u_{i,i\pm\hat{x}+\hat{y}} = u_{i,i\mp\hat{x}-\hat{y}} = \begin{pmatrix} 0 & \Delta_0 \pm i\Delta_1 \\ \Delta_0 \mp i\Delta_1 & 0 \end{pmatrix}, \quad (60b)$$

where χ , Δ_0 and Δ_1 are nonzero real numbers; $a_0^{2,3} = 0$; and $a_0^1 \neq 0$. It is easy to check $P(C)$ for two loops: $C_1 = i \rightarrow i + \hat{x} \rightarrow i + \hat{x} + \hat{y} \rightarrow i$ and $C_2 = i \rightarrow i + \hat{y} \rightarrow i + \hat{y} - \hat{x} \rightarrow i$. We obtain

$$P(C_1) = \chi^2 (\Delta_0 \tau^1 + \Delta_1 \tau^2) \quad (61a)$$

and

$$P(C_2) = -\chi^2 (\Delta_0 \tau^1 - \Delta_1 \tau^2), \quad (61b)$$

which clearly demonstrates that $\mathbf{B}(C_1) \neq \mathbf{B}(C_2)$ and that the spin liquid state described above is a Z_2 spin liquid state. The mean-field ground state describes a half-filled spinon band with a band dispersion given by $E_{\pm}(\mathbf{k}) = \pm \sqrt{\varepsilon_1(\vec{k})^2 + \varepsilon_2(\vec{k})^2 + \varepsilon_3(\vec{k})^2}$, where

$$\begin{aligned} \varepsilon_1(\vec{k}) &= 2J_1\chi(\cos(k_x) + \cos(k_y)), \\ \varepsilon_2(\vec{k}) &= 2J_2\Delta_0(\cos(k_x + k_y) + \cos(k_x - k_y)) + a_0^1, \\ \varepsilon_3(\vec{k}) &= 2J_2\Delta_1(\cos(k_x + k_y) - \cos(k_x - k_y)). \end{aligned}$$

Note that the spinon spectrum is fully gapped.

Many other examples of Z_2 spin liquid states have been constructed in the literature. For instance, a nodal gapped Z_2 spin liquid state was proposed by Balents, Fisher and Nayak (Balents *et al.*, 1998) and by Senthil and Fisher (Senthil and Fisher, 2000). The corresponding mean-field ansatz includes nearest neighbor and next nearest neighbor hopping as well as d-wave pairing on nearest neighbor bonds on the square lattice:

$$u_{i,i+\hat{x}} = \begin{pmatrix} \chi_1 & \Delta \\ \Delta & -\chi_1 \end{pmatrix}, \quad (62a)$$

$$u_{i,i+\hat{y}} = \begin{pmatrix} \chi_1 & -\Delta \\ -\Delta & -\chi_1 \end{pmatrix}, \quad (62b)$$

and

$$u_{i,i\pm\hat{x}\pm\hat{y}} = \begin{pmatrix} \chi_2 & 0 \\ 0 & -\chi_2 \end{pmatrix}, \quad (62c)$$

where χ_1 , χ_2 , and Δ are nonzero real numbers; $a_0^{1,2} = 0$; and $a_0^3 \neq 0$. The spinon dispersion is given by $E_{\pm}(\mathbf{k}) = \pm \sqrt{\varepsilon(\vec{k})^2 + \Delta(\vec{k})^2}$, where

$$\begin{aligned} \varepsilon(\vec{k}) &= 2J_1\chi_1(\cos(k_x) + \cos(k_y)) \\ &\quad + 2J_2\chi_2(\cos(k_x + k_y) + \cos(k_x - k_y)) + a_0^3, \\ \Delta(\vec{k}) &= 2J_1\Delta(\cos(k_x) - \cos(k_y)) + a_0^3, \end{aligned}$$

and is found to be gapless at four \vec{k} points with a linear dispersion. Thus, this spin liquid is a Z_2 nodal spin liquid. We reiterate that Z_2 spin liquid states are expected to be the most stable because the $SU(2)$ gauge fields are gapped and the fermionic spins are interacting only through short-range interactions.

It has been observed by Wen (Wen, 1991) that in addition to spinons, a soliton-type excitation exists in a Z_2 spin liquid. This excitation is nothing but a π flux in the Z_2 gauge field, called a “ Z_2 vortex”. This Z_2 vortex can be described by a new mean-field ansatz,

$$\tilde{u}_{ij} = u_{ij}\Theta_{ij},$$

where $\Theta_{ij} = \pm 1$ generates a π flux on a lattice. One possible choice of Θ_{ij} is illustrated in Fig. 6, where $\Theta_{ij} = -1$ on the bonds cut by the dashed line and $\Theta_{ij} = 1$ on the other bonds. An interesting consequence of such a Z_2 vortex is that the statistics of a spinon can be changed from bosonic to fermionic and vice versa if it is bound to a vortex. Therefore, Z_2 spin liquids may contain charge-neutral spin-1/2 spinons with both bosonic and fermionic statistics (Ng, 1999). The dynamics of Z_2 vortices can give rise to interesting physical consequences (Ng, 1999; Qi *et al.*, 2009).

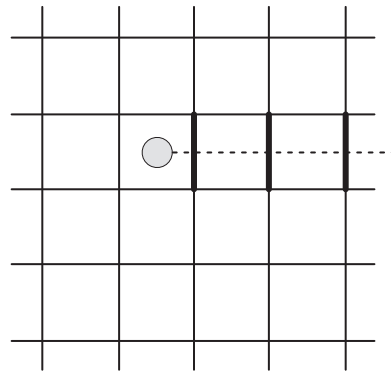


FIG. 6 A Z_2 vortex created by flipping the signs of the u_{ij} on the bonds cut by the dashed line (indicated by thick lines).

It is worth noting that the $J_1 - J_2$ model on a square lattice has been well studied. The lowest-energy

Z_2 spin liquid state is a nodal spin liquid with four Dirac points (Capriotti *et al.*, 2001; Hu *et al.*, 2013), labeled as Z2Azz13 in the projected group symmetry classification scheme (Wen, 2002), which we discuss in section III.5. This nodal Z_2 spin liquid is energetically competitive with calculations performed using the DMRG (Gong *et al.*, 2014b; Jiang *et al.*, 2012b) and PEPS (Wang *et al.*, 2013) approaches.

Relation to superconductivity: RVB theory were developed not only for QSLs but also for high- T_c superconductivity (Anderson, 1987). It is generally believed that Z_2 spin liquid states may become superconductors upon doping (Lee *et al.*, 2006). The superconducting state inherits novel properties from its QSL parent, and new phenomena may also emerge. For instance, it has been proposed that doping a kagome system can give rise to an exotic superconductor with an $hc/4e$ -quantized flux (as opposed to the usual $hc/2e$ quantization) (Ko *et al.*, 2009).

III.4. Numerical realization of Gutzwiller projection: variational Monte Carlo method and some results

The theories of QSL states rely heavily on the reliability of Gutzwiller-projected wavefunctions. In this subsection, we discuss how Gutzwiller projection is performed numerically in practice and how the physical observables can be evaluated using a Monte Carlo method for a given projected wavefunction $|\Psi_{RVB}\rangle = P_G |\Psi_{MF}\rangle$.

Two types of mean-field ansatz are frequently used in constructing QSL states. The first one contains only (fermionic) spinon hopping terms χ , and the mean-field ground state is a half-filled Fermi sea. The second one includes both hopping terms and pairing terms Δ , and the mean-field ground state is a BCS-type state with a fermion energy gap. These two types of wavefunctions describe $U(1)$ and Z_2 spin liquid states, respectively, with the proper choice of hopping and pairing parameters. For a given spin Hamiltonian, we can determine these hopping and pairing parameters by optimizing the ground-state energy. Therefore, this approach is called the variational Monte Carlo (VMC) method.

For a projected Fermi sea state, the mean-field ground-state wavefunction on a lattice with N sites can be constructed by filling the N lowest states in the mean-field band:

$$|\Psi_{FS}\rangle = \prod_{\sigma} \prod_{k=1}^{N/2} \psi_{k\sigma}^{\dagger} |0\rangle,$$

where $\sigma = \uparrow, \downarrow$ is the spin index and the states are sorted in order of ascending energy, $E_1 \leq \dots \leq E_{N/2} < E_F$. $\psi_{k\sigma}^{\dagger}$ creates an eigenstate in the mean-field band and can

be expressed as

$$\psi_{k\sigma}^{\dagger} = \sum_i a_k(i) c_{i\sigma}^{\dagger},$$

where each value of i denotes a site and $c_{i\sigma}^{\dagger}$ is a local fermion creation operator. The eigenstate wavefunction $a_k(i)$ does not depend on the spin index σ for spin-singlet states because of the spin rotational symmetry. More explicitly,

$$|\Psi_{FS}\rangle = \prod_{\sigma} \prod_{i=1}^{N/2} \left(\sum_{j=1}^N a_i(j) c_{j\sigma}^{\dagger} \right) |0\rangle, \quad (63)$$

and the Gutzwiller-projected wavefunction can be written in terms of the product of three factors:

$$\begin{aligned} P_G |\Psi_{FS}\rangle &= \sum_{\{\sigma_i\}} \text{sgn}\{i_1, \dots, i_{N/2}, j_1, \dots, j_{N/2}\} \\ &\times \det [A(i_1, \dots, i_{N/2})] \\ &\times \det [A(j_1, \dots, j_{N/2})] |\sigma_1, \dots, \sigma_N\rangle \end{aligned} \quad (64)$$

where $|\sigma_1, \dots, \sigma_N\rangle$ is a state in the Ising basis with $N/2$ up spins located at sites $i_1, \dots, i_{N/2}$ and $N/2$ down spins located at sites $j_1, \dots, j_{N/2}$; $\text{sgn}\{i_1, \dots, i_{N/2}, j_1, \dots, j_{N/2}\}$ is the sign of the permutation $P = \{i_1, \dots, i_{N/2}, j_1, \dots, j_{N/2}\}$; and $A(i_1, \dots, i_{N/2})$ is an $N/2 \times N/2$ matrix given by

$$A(i_1, \dots, i_{N/2}) = \begin{pmatrix} a_1(i_1) & \dots & a_1(i_{N/2}) \\ \dots & \ddots & \dots \\ a_{N/2}(i_1) & \dots & a_{N/2}(i_{N/2}) \end{pmatrix}. \quad (65)$$

A BCS-type mean-field ground state with spin-singlet pairing can be written as

$$|\Psi_{BCS}\rangle = e^{\frac{1}{2} \sum_{i,j} W_{ij} (c_{i\uparrow}^{\dagger} c_{j\downarrow}^{\dagger} - c_{i\downarrow}^{\dagger} c_{j\uparrow}^{\dagger})} |0\rangle, \quad (66)$$

where i and j are site indices and $W_{ij} = W_{ji}$ for fermionic spin-singlet pairing. For a system with lattice translational symmetry, W_{ij} can be written explicitly as

$$W_{ij} = - \sum_{\mathbf{k}} \frac{v_{\mathbf{k}}}{u_{\mathbf{k}}} e^{-i\mathbf{k} \cdot (\mathbf{R}_i - \mathbf{R}_j)},$$

where $u_{\mathbf{k}}$ and $v_{\mathbf{k}}$ are given in the BCS form. In the more general situation in which lattice translational symmetry is lost, the W_{ij} s are determined from the Bogoliubov-de Gennes equations. Gutzwiller projection retains only states with a number of electrons equal to the number of lattice sites and removes all terms with more than one electron per site, i.e.,

$$|\Psi_{RVB}\rangle = P_G \left(\sum_{i < j} W_{ij} c_{i\uparrow}^{\dagger} c_{j\downarrow}^{\dagger} \right)^{N/2} |0\rangle. \quad (67)$$

In the spin representation, the projected BCS state can be written as

$$\begin{aligned} P_G |\Psi_{BCS}\rangle &= \sum_{\{\sigma_i\}} \text{sgn}(i_1, \dots, i_{N/2}, j_1, \dots, j_{N/2}) \\ &\times \det[w(i_1, \dots, i_{N/2}, j_1, \dots, j_{N/2})] \\ &\times |\sigma_1, \dots, \sigma_N\rangle, \end{aligned} \quad (68)$$

where $|\sigma_1, \dots, \sigma_N\rangle$ is a state in the Ising basis with $N/2$ up spins located at sites $i_1, \dots, i_{N/2}$ and $N/2$ down spins located at sites $j_1, \dots, j_{N/2}$ and $w(i_1, \dots, i_{N/2}, j_1, \dots, j_{N/2})$ is an $N/2 \times N/2$ matrix given by

$$w(i_1, \dots, i_{N/2}, j_1, \dots, j_{N/2}) = \begin{pmatrix} W_{i_1 j_1} & \cdots & W_{i_1 j_{N/2}} \\ \cdots & \ddots & \cdots \\ W_{i_{N/2} j_1} & \cdots & W_{i_{N/2} j_{N/2}} \end{pmatrix}. \quad (69)$$

A key observation regarding these two projected wavefunctions, Eqs.(64) and (68), is that both of them can be written as a determinant or as a product of two determinants. This allows us to evaluate a projected wavefunction numerically. For a large system, the number of degrees of freedom increases exponentially with the system size. In this case, the Monte Carlo method is applied to evaluate the energy, magnetization and spin correlation for these projected wavefunctions (Gros, 1989; Horsch and Kaplan, 1983). Below, we briefly describe how the MC method works. Those who are interested in the details may refer to Gros(Gros, 1989).

The expectation value of an operator Θ in a system with the spin wavefunction $|\Psi\rangle$ can be written as

$$\langle \Theta \rangle = \frac{\langle \Psi | \Theta | \Psi \rangle}{\langle \Psi | \Psi \rangle} = \sum_{\alpha, \beta} \langle \alpha | \Theta | \beta \rangle \frac{\langle \Psi | \alpha \rangle \langle \beta | \Psi \rangle}{\langle \Psi | \Psi \rangle}, \quad (70)$$

where the spin configurations $|\alpha\rangle$ and $|\beta\rangle$ are states in the Ising basis with $N/2$ up spins and $N/2$ down spins. This sort of expectation value is recognized to be amenable to a Monte Carlo (MC) evaluation (Horsch and Kaplan, 1983). The expectation value expression given in Eq. (70) can be rewritten as

$$\begin{aligned} \langle \Theta \rangle &= \sum_{\alpha} \left(\sum_{\beta} \frac{\langle \alpha | \Theta | \beta \rangle \langle \beta | \Psi \rangle}{\langle \alpha | \Psi \rangle} \right) \frac{|\langle \alpha | \Psi \rangle|^2}{\langle \Psi | \Psi \rangle} \\ &= \sum_{\alpha} f(\alpha) \rho(\alpha), \end{aligned} \quad (71)$$

with

$$\begin{aligned} f(\alpha) &= \sum_{\beta} \frac{\langle \alpha | \Theta | \beta \rangle \langle \beta | \Psi \rangle}{\langle \alpha | \Psi \rangle}, \\ \rho(\alpha) &= \frac{|\langle \alpha | \Psi \rangle|^2}{\langle \Psi | \Psi \rangle}. \end{aligned}$$

It follows that

$$\rho(\alpha) \geq 0, \sum_{\alpha} \rho(\alpha) = 1.$$

Note that for a “local operator” Θ (e.g., $\Theta = \vec{S}_i \cdot \vec{S}_j$) and a given spin configuration $|\alpha\rangle$, only a limited number of “neighbor” configurations $|\beta\rangle$ give rise to a non-vanishing $\langle \alpha | \Theta | \beta \rangle$. As noted by Horsch and Kaplan (Horsch and Kaplan, 1983), the computation time for the ratio $\frac{\langle \beta | \Psi \rangle}{\langle \alpha | \Psi \rangle}$ is of $O(N^2)$. Therefore, $\langle \Theta \rangle$ can be evaluated by means of a random walk through spin configuration space with weight $\rho(\alpha)$. As in the standard MC method, the probability $T(\alpha \rightarrow \alpha')$ of transitioning from one configuration α to another configuration α' can be chosen as follows:

$$T(\alpha \rightarrow \alpha') = \begin{cases} 1, & \rho(\alpha') \geq \rho(\alpha), \\ \frac{\rho(\alpha')}{\rho(\alpha)}, & \rho(\alpha') < \rho(\alpha). \end{cases}$$

The new configuration α' is accepted with probability $T(\alpha \rightarrow \alpha')$.

Because $\langle \alpha | \Psi \rangle$ is either a determinant or a product of two determinants, the computation time for $\langle \alpha | \Psi \rangle$ is of $O(N^3)$. The computational resource consumption for the MC weight factor $T(\alpha \rightarrow \alpha')$ is not too high, and consequently, this MC method is feasible for Gutzwiller projection. Moreover, the computation time of the ratio $T(\alpha \rightarrow \alpha')$ can be reduced to $O(N^2)$ if the corresponding matrix $A(\alpha')$ or $w(\alpha')$ in Eq. (65) or (69) differs from $A(\alpha)$ or $w(\alpha)$ by only one row or column. This can be achieved by properly choosing the spin update procedure, e.g., the interchange of two opposite spins. This algorithm was first introduced by Ceperley *et al.* for the MC evaluation of a fermionic trial wavefunction (Ceperley *et al.*, 1977).

As a variational method, the VMC method not only yields an upper bound on the ground-state energy for a spin Hamiltonian but also provides detailed information on the trial ground state. This information is useful for understanding the nature of the ground-state wavefunction. In the remainder of this subsection, we discuss some numerical results regarding Gutzwiller-projected wavefunctions on one- and two-dimensional frustrated lattices.

III.4.1. One-dimensional lattice

One-dimensional systems usually serve as benchmarks for comparison because exact solutions are often available. It turns out that $P_G |\Psi_{FS}\rangle$, which is gauge equivalent to $P_G |\Psi_{BCS}\rangle$ in one dimension, is an excellent trial wavefunction for the ground state of the one-dimensional Heisenberg model. The energy for $P_G |\Psi_{FS}\rangle$ is higher than that of the exact ground state by only 0.2% (Gebhard and Vollhardt, 1987; Gros *et al.*,

1987; Yokoyama and Shiba, 1987). The spin-spin correlation decays following a power law at large distances, $\langle \vec{S}_i \cdot \vec{S}_{i+r} \rangle \sim \frac{(-1)^r}{|r|}$, consistent with the results obtained through bosonization (Luther and Peschel, 1975). Indeed, it has been shown that this Gutzwiller-projected wavefunction is the exact ground state of the Haldane-Shastry model (Haldane, 1988a; Shastry, 1988),

$$H_{H-S} = \frac{J}{2} \sum_{i=1}^N \sum_{r=1}^{N-1} \frac{1}{\sin^2(\pi r/N)} \vec{S}_i \cdot \vec{S}_{i+r},$$

which describes an AFM Heisenberg chain with long-range coupling (a periodic version of $1/r^2$ exchange).

Excited states with $S_z = m = (N_\uparrow - N_\downarrow)/2$ can also be constructed, where N_\uparrow and N_\downarrow are the numbers of up and down spins, respectively, in the wavefunction. The lowest-energy state in the subspace with $S_z = m$ is given by

$$P_G |\Psi_m\rangle = P_G \prod_{|k| \leq k_F \uparrow} \psi_{k\uparrow}^\dagger \prod_{|k| \leq k_F \downarrow} \psi_{k\uparrow}^\dagger |0\rangle, \quad (72)$$

where $k_{F\sigma} = \pi(N_\sigma - 1)/N = \pi(N_\sigma - 1)/(N_\uparrow + N_\downarrow)$. With the help of this trial wavefunction, the spin susceptibility χ can be calculated (Gros *et al.*, 1987). It is found that χ is close to the value obtained from the exact solution (Griffiths, 1964). The numerical results are summarized in Table I.

TABLE I (Gros, 1989) Comparison of ground-state energy and spin susceptibility in one dimension. The first row shows the results for the projected Fermi sea. The second row shows the results for the exact ground state of the Heisenberg model.

	$\langle \vec{S}_i \cdot \vec{S}_{i+1} \rangle$	χ
Gutzwiller	-0.442118 (Gebhard and Vollhardt, 1987)	0.058 ± 0.008 (Gros <i>et al.</i> , 1987)
Exact	-0.443147 (Lieb and Wu, 1968)	0.0506 (Griffiths, 1964)

III.4.2. Triangular lattice

Historically, the AFM spin-1/2 Heisenberg Hamiltonian on a triangular lattice was the first model to be proposed for the microscopic realization of a spin liquid ground state (Fazekas and Anderson, 1974). However, the minimum-energy configuration for the classical Heisenberg model on a triangular lattice is well known to be the 120° Néel state. There has been a long-standing debate regarding whether the frustration together with quantum fluctuations could destroy the long-range 120° Néel order, leading to a spin liquid state. Many trial wavefunctions have been proposed as the ground state of the nearest neighbor Heisenberg model on a triangular lattice, including a chiral spin liquid state (Kalmeyer and Laughlin, 1987) and 120° -Néel-order states with quantum mechanical corrections (Huse and Elser, 1988; Sindzingre *et al.*, 1994). In 1999, Capriotti *et al.* (Capriotti *et al.*, 1999) utilized the Green's function Monte Carlo (GFMC) method with the stochastic reconfiguration technique to obtain the state of the model with the lowest energy (to our knowledge; the ground state energy per site is 0.5458 ± 0.0001), which exhibits 120° long-range Néel order. More recently, the three-sublattice 120° -Néel-order has been further confirmed by DMRG (White and Chernyshev, 2007).

It thus seemed that for a triangular lattice, the possibility of a spin liquid state had been ruled out. However, the story continues. It was found that a four-spin ring ex-

change stabilizes the projected Fermi sea state against a long-range AFM state (Motrunich, 2005). Because multi-spin ring exchange reflects the charge fluctuations in the vicinity of the Mott transition, this result provides theoretical support for the search for spin liquid states in a Mott insulating state close to the metal-insulator transition.

The model Hamiltonian that contains both nearest neighbor Heisenberg exchange and four-spin ring exchange is

$$H_{\text{ring}} = J \sum_{\bullet\bullet} P_{12} + J_{\text{ring}} \sum_{\bullet\bullet\bullet\bullet} \left(P_{1234} + P_{1234}^\dagger \right), \quad (73)$$

where $P_{12} = 2\vec{S}_1 \cdot \vec{S}_2 + \frac{1}{2}$ interchanges the two spins at site 1 and site 2 and the four-spin exchange operators satisfy the following relations: $P_{1234}^\dagger = P_{4321}$ and $P_{1234} + P_{4321} = P_{12}P_{34} + P_{14}P_{23} - P_{13}P_{24} + P_{13} + P_{24} - 1$.

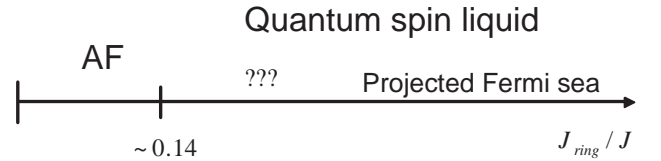


FIG. 7 (Motrunich, 2005) Variational phase diagram for the Hamiltonian presented in (73).

By comparing the trial energies of the AF-ordered

states proposed by Huse and Elser (Huse and Elser, 1988) with those of various fermionic spin liquid states, Motrunich found that the ring-exchange term favors a spin liquid ground state over the AFM-ordered state (Motrunich, 2005). The results are summarized in Fig. 7. For small ring exchange, i.e., $J_{ring}/J \lesssim 0.14$, the ordered states are of lower energy. However, for $J_{ring}/J \gtrsim 0.14$, spin liquid states are energetically favored. For larger values of $J_{ring}/J \gtrsim 0.3 - 0.35$, the optimal spin liquid state is the projected Fermi sea state. In the intermediate regime, optimized wavefunctions with extended anisotropic s -wave, $d_{x^2-y^2}$, and $d_{x^2-y^2}+id_{xy}$ spinon pairings have similar energies.

Recently, a novel Z_2 spin liquid state on a triangular lattice was proposed, where the paired fermionic spinons preserve all symmetries of the system and the system has a gapless excitation spectrum with quadratic bands that touch at $q = 0$. It was shown through the VMC method that this Z_2 spin liquid state has a highly competitive energy when J_{ring}/J is realistically large (Mishmash *et al.*, 2013).

III.4.3. Kagome lattice

Unlike the case of a triangular lattice, the classical Heisenberg model on a kagome lattice has an infinite number of degenerate ground states that are connected to one another by continuous “local” distortions of the spin configuration (Villain, J. *et al.*, 1980). This property holds on any lattice with corner-sharing units, such as checkerboard, kagome, and pyrochlore lattices (Moessner and Chalker, 1998). For instance, on a kagome lattice formed by corner-sharing triangles, the nearest neighbor Heisenberg Hamiltonian can be written as the sum of the squares of the total spins $\vec{S}_\Delta = \vec{S}_1 + \vec{S}_2 + \vec{S}_3$ of individual triangles that share only one vertex:

$$H = J \sum_{\Delta} (\vec{S}_\Delta)^2.$$

Classical ground states are obtained whenever $\vec{S}_\Delta = 0$. This triangle rule fixes the relative orientations of the three classical spins of a triangle at 120° from each other in a plane, but it does not fix the relative orientation of the plane of one triad with respect to the planes of the triads on neighboring triangles. These degrees of freedom lead to a continuous local degeneracy of the ground states. Note that this degeneracy exists even if we restrict ourselves to coplanar spin states. Two of the simplest examples (Sachdev, 1992) are the three sublattice planar states shown in Fig. 8 for the $q = 0$ and $\sqrt{3} \times \sqrt{3}$ ordered states.

The large classical ground-state degeneracy must be lifted by quantum fluctuations. The nature of the ground state for the quantum model is highly speculative because

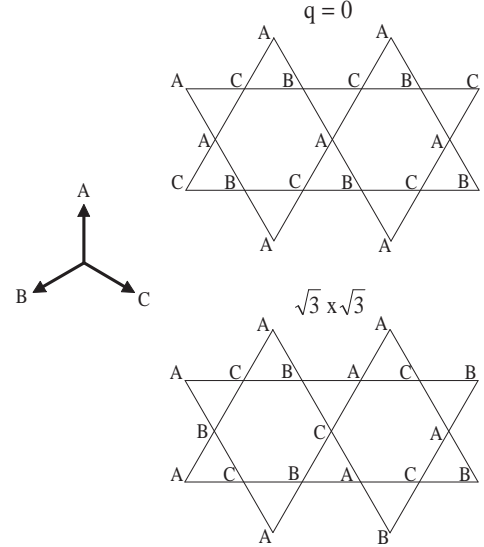


FIG. 8 Two classical planar Néel states ($q = 0$ and $\sqrt{3} \times \sqrt{3}$) on a kagome lattice. A, B and C specify three coplanar spin orientations with intersection angles of 120° .

of the enormous degeneracy in the classical model. Many arguments have been presented in the literature regarding what kind of ground state is favored, and this issue is still under debate (Diep, 2004). In the following, we discuss the $U(1)$ QSL state, which is one of the promising candidates for the ground state of a spin-1/2 Heisenberg antiferromagnet on a kagome lattice.

Inspired by neutron scattering experiments on herbertsmithite, $\text{ZnCu}_3(\text{OH})_6\text{Cl}_2$, Ran *et al.* constructed a series of variational wavefunctions of $U(1)$ spin liquids on a kagome lattice (Ran *et al.*, 2007). The corresponding mean-field ansatz involves only fermionic spinon hopping on nearest neighbor bonds:

$$H_{MF} = J \sum_{\langle ij \rangle \sigma} (\chi_{ij} f_{j\sigma}^\dagger f_{i\sigma} + h.c.),$$

where the complex field χ_{ij} lives on the links between two neighboring sites. For a kagome lattice, the mean-field states are characterized by the $U(1)$ gauge fluxes through the triangles and hexagons. Large- N expansion suggests several candidate mean-field states (Hastings, 2000; Marston and Zeng, 1991): (i) VBS states, which break translation symmetry; (ii) a spin liquid state (SL- $[\frac{\pi}{2}, 0]$) with a flux of $+\pi/2$ through each triangle on the kagome lattice and zero flux through the hexagons, which is a chiral spin liquid state that breaks time-reversal symmetry; (iii) a spin liquid state (SL- $[\pm \frac{\pi}{2}, 0]$) with staggered $\pi/2$ fluxes through the triangles ($+\pi/2$ through up triangles and $-\pi/2$ through down triangles) and zero flux through the hexagons; (iv) a spin liquid state (SL- $[\frac{\pi}{2}, \pi]$) with a flux of $+\pi/2$ flux through each triangle and a flux of π through each hexagon; (v) a uniform RVB spin liquid state (SL- $[0, 0]$) with zero flux through both triangles

and hexagons, which has a spinon Fermi surface; and (vi) a $U(1)$ -Dirac spin liquid state (SL-[0, π]) with zero flux through the triangles and a flux of π through each hexagon, which has four flavors of two-component Dirac fermions.

By performing VMC calculations on $8 \times 8 \times 3$ and $12 \times 12 \times 3$ lattices, Ran *et al.* (Ran *et al.*, 2007) found that the $U(1)$ -Dirac spin liquid state (SL-[0, π]) has the lowest energy among states (i)-(vi) listed above after Gutzwiller projection, with a ground-state energy of $-0.429J$ per site. Note that there is no tunable parameter in this $U(1)$ -Dirac spin liquid state. This energy is remarkably favorable because the value is very close to the exact diagonalization result when extrapolated to the thermodynamic limit. A comparison among the ground-state energies determined using this VMC method and other numerical methods is presented in Table II. The authors also found that the $U(1)$ -Dirac spin liquid state is stable against VBS ordering and chiral spin liquid states with fluxes of θ through the triangles and $(\pi-2\theta)$ through the hexagons. The spin correlation functions exhibit algebraic decay with distance because of the Dirac nodes in the spinon spectrum.

TABLE II Comparison of the ground-state energies (in units of J) determined using different methods for the nearest neighbor Heisenberg model on a kagome lattice. In the VMC method, the $U(1)$ -Dirac spin liquid state (SL-[0, π]) is used.

Method	Energy per site
Exact diagonalization	-0.43 (Waldtmann <i>et al.</i> , 1998)
Coupled cluster method	-0.4252 (Farnell <i>et al.</i> , 2001)
Spin-wave variational method	-0.419 (Arrachea <i>et al.</i> , 2004)
VMC method	-0.429 (Ran <i>et al.</i> , 2007)

We note that exact diagonalization (Lecheminant *et al.*, 1997; Leung and Elser, 1993; Mila, 1998; Waldtmann *et al.*, 1998) and DMRG calculations (Depenbrock *et al.*, 2012; Jiang *et al.*, 2012a, 2008; Yan *et al.*, 2011) strongly indicate the existence of a spin gap and seem to rule out the $U(1)$ -Dirac spin liquid scenario. However, this disagreement may be a finite-size effect. The applicability of exact diagonalization is limited to very small lattices of up to 36 sites, and the maximum cylinder circumference used in the DMRG approach is only 17 lattice spacings. Very recently, through the combination of the Lanczos algorithm for projected fermionic wavefunctions with the Green's function Monte Carlo technique, Iqbal, Becca, Sorella, and Poilblanc (Iqbal *et al.*, 2013, 2014) found that the gapless $U(1)$ -Dirac spin liquid is competitive with gapped Z_2 spin liquids. By performing a finite-size extrapolation of the ground-state energy, these authors obtained an energy per site of $E/J = -0.4365(2)$, which is within three error bars of the estimates obtained

using the DMRG method. In summary, the $U(1)$ -Dirac spin liquid state has proven to be a good candidate for describing a critical phase on a kagome lattice.

III.5. Classification of spin liquid states: quantum orders and projective symmetry groups

The use of Gutzwiller-projected wavefunctions can be made more systematic by using a powerful approach based on classifying spin liquid states according to their symmetry properties. For classical systems, it was observed by Landau that symmetry is a universal property shared by all macroscopic states within the same phase, irrespective of microscopic details. Consequently, the symmetry (or broken symmetry) associated with classical order parameters serves as a powerful tool for characterizing different classical phases. This approach can be generalized to quantum spin systems described by Gutzwiller-projected wavefunctions, with additional constraints.

For spin liquid states described by Gutzwiller-projected wavefunctions, one might expect that the quantum phases could be classified according to the symmetry properties of the mean-field ansatz $(u_{ij}, a_0^l \tau^l)$. However, the usual classical symmetry group (SG) is insufficient for classifying these states for two reasons: (i) Because of the gauge redundancy, different mean-field descriptions exist for the same QSL state. For instance, the uniform RVB state and the zero-flux state correspond to the same spin state, and the d -wave RVB state on a square lattice is also the π -flux state. (ii) QSL states may have inherent (phase) structures contained in the mean-field ansatz $(u_{ij}, a_0^l \tau^l)$ that cannot be fully distinguished based on the SG constructed for classical systems. To address this issue, X.G. Wen proposed a new mathematical object called a projective symmetry group (PSG) (Wen, 2002), which generalizes Landau's approach and has now become an important tool in studying QSLs and the quantum phase transitions between different QSL states.

Wen proposed that the symmetry of the mean-field ansatz $(u_{ij}, a_0^l \tau^l)$ is a universal property and serves as a kind of "quantum number" that can be used to characterize quantum orders in QSLs. The macroscopic properties of the ansatz are characterized by its projective symmetry group (PSG). An element of a PSG is a combined operation consisting of a symmetry transformation U followed by a local gauge transformation $G_U(i)$. The PSG of a given mean-field ansatz consists of all combined operations that leave the ansatz unchanged, i.e.,

$$PSG \equiv \{G_U | G_U U(u_{ij}) = u_{ij}, G_U(i) \in SU(2)\}, \quad (74)$$

where $U(u_{ij}) = \tilde{u}_{ij} \equiv u_{U(i), U(j)}$, $G_U U(u_{ij}) \equiv G_U(i) \tilde{u}_{ij} G_U^\dagger(j)$, U generates the symmetry transformation (SG), and G_U is the associated gauge transforma-

tion. From this definition, it is easy to see that

$$SG \equiv \frac{PSG}{IGG}.$$

The PSGs of two mean-field ansatze related by a gauge transformation W are obviously also related. From $WG_UU(u_{ij}) = W(u_{ij})$, where $W(u_{ij}) \equiv W_i u_{ij} W_j^\dagger$, we obtain $WG_UUW^{-1}W(u_{ij}) = W(u_{ij})$. Therefore, if G_{UU} belongs to the PSG of the mean-field ansatz u_{ij} , then WG_UUW^{-1} belongs to the PSG of the gauge-transformed ansatz $W(u_{ij})$. We see that the gauge transformation G_U associated with the transformation U changes in the following way under an $SU(2)$ gauge transformation W :

$$G_U(i) \rightarrow W(i)G_U(i)W(U(i))^\dagger. \quad (75)$$

Wen proposed that mean-field ansatze with different PSGs belong to different classes of QSL states, just as classical states with different SGs belong to different classical phases.

As examples, we consider the PSGs of the zero-flux state given in Eq. (43b) and the π -flux state given in Eq. (51) on a square lattice. For illustration, let us consider the PSG associated with translational symmetry. First, we consider the zero-flux state. The mean-field ansatz given in Eq. (43b) is invariant under the translation transformations $T_x(i \rightarrow i + \hat{x})$ and $T_y(i \rightarrow i + \hat{y})$ and the gauge transformation $G(\theta) = e^{i\theta\tau^3}$. The elements of the PSG have the form G_UU ; $G_U = \pm G(\theta)$, and $U = (T_x)^n(T_y)^m$, where n and m are arbitrary integers. The π -flux state is different. The mean-field ansatz given in Eq. (51) breaks translational symmetry in the x direction because of the odd number of lattice sites. Thus, we naively expect that the PSG should consist of elements G_UU with $G_U = \pm G(\theta)$ and $U = (T_x)^{2n}(T_y)^m$. However, this is incorrect because the two mean-field ansatze

$$\chi_{i,i+\hat{\mu}} = \begin{cases} \chi, & \mu = x \\ i\chi(-1)^{i_x}, & \mu = y \end{cases}$$

and

$$\chi_{i,i+\hat{\mu}} = \begin{cases} \chi, & \mu = x \\ i\chi(-1)^{i_x+1}, & \mu = y \end{cases}$$

are actually related by a gauge transformation $W_i = (-1)^{i_y}\tau^0$ and correspond to the same physical spin state. As a result, the transformations $G_{U'}U'$ with $G_{U'} = \pm G(\theta)(-1)^{i_y}\tau^0$ and $U' = (T_x)^{2n+1}(T_y)^m$ are also elements of the PSG for the π -flux state. The zero-flux state and the π -flux state have different PSGs and therefore belong to different classes of $U(1)$ QSL states.

More generally, other lattice symmetry operations (reflections and rotations), such as the parity transformations $P_{xy}((i_x, i_y) \rightarrow (i_y, i_x))$ and $P_{x\bar{y}}((i_x, i_y) \rightarrow (-i_y, -i_x))$ on a square lattice, the

spin rotation transformation and the time-reversal transformation, are also considered when constructing PSGs, in addition to translations. The spin rotational symmetry of spin liquid states requires the mean-field ansatz to take the form:

$$\begin{aligned} u_{ij} &= i\rho_{ij}W_{ij}, \\ \rho_{ij} &= \text{real number}, \\ W_{ij} &\in SU(2). \end{aligned} \quad (76)$$

We end with a brief discussion of an issue related to techniques for the classification of PSGs. For any two given symmetry transformations, their corresponding PSG elements must satisfy certain algebraic relations determined by the symmetry transformations. Solving these equations allows us to construct a PSG of a type called an *algebraic PSG*. The name algebraic PSG is introduced to distinguish such PSGs from the invariant PSGs defined above. Any invariant PSG is an algebraic PSG; however, an algebraic PSG is not necessarily an invariant PSG unless there exists an ansatz such that the algebraic PSG is the total symmetry group of that ansatz.

To provide an example, we again consider translations. The two translation elements T_x and T_y satisfy the following relation:

$$T_x T_y T_x^{-1} T_y^{-1} = 1. \quad (77)$$

From the definition of a PSG, we find that the two PSG elements $G_x T_x$ and $G_y T_y$ must satisfy the algebraic relation

$$\begin{aligned} &G_x T_x G_y T_y (G_x T_x)^{-1} (G_y T_y)^{-1} \\ &= G_x T_x G_y T_y T_x^{-1} G_x^{-1} T_y^{-1} G_y^{-1} \\ &= G_x(i) G_y(i - \hat{x}) G_x^{-1}(i - \hat{y}) G_y^{-1}(i) \in \mathcal{G}, \end{aligned} \quad (78)$$

where we denote the IGG by \mathcal{G} . Each solution $(G_x T_x, G_y T_y)$ of equation (78) is an algebraic PSG for T_x and T_y . By adding other symmetry transformations, we can find and classify all algebraic PSGs associated with a given symmetry group. Because an invariant PSG is always an algebraic PSG, we can check whether an algebraic PSG is an invariant PSG by constructing an explicit ansatz u_{ij} . If an algebraic PSG supports an ansatz u_{ij} with no additional symmetries, then it is an invariant PSG. Through this method, we can classify symmetric spin liquids in terms of PSGs.

In reference (Wen, 2002), Wen utilized PSGs to classify QSL states with spin rotational symmetry, time-reversal symmetry and all lattice symmetries on a square lattice. Later, the PSG classification approach for symmetric QSLs was applied to triangular (Zhou and Wen, 2002), star (Choy and Kim, 2009), and kagome (Lu *et al.*, 2011) lattices. The PSG classification scheme can also be generalized to bosonic QSL states (Wang, 2010b; Wang and Vishwanath, 2006) and to QSL states that

break spin rotational symmetry and/or time-reversal symmetry (Bieri *et al.*, 2016; Kou and Wen, 2009).

IV. BEYOND RVB APPROACHES

There are many reasons to go beyond the simple RVB approach for $S = 1/2$ spin systems, for example, the discovery of a plausible spin liquid state in a spin $S = 1$ system (Zhou *et al.*, 2011) and the rise in interest in Mott insulators in systems with strong spin-orbit coupling where rotational symmetry is broken and the ground state cannot be a pure spin singlet (Jackeli and Khaliullin, 2009). What is the nature of the spin liquid states in these systems? More importantly, we are interested in the possibility of exotic spin liquid states beyond the RVB description, where the elementary excitations may possess exotic properties beyond the simple spinon picture.

We introduce some of these developments in this section. We start by introducing the generalization of the RVB approach to spin systems with strong spin-orbit coupling and to $S > 1/2$ spin systems in sections IV.1 and IV.2, followed by the introduction of matrix product states and projected entangled pair states in section IV.3, which are completely different ways of constructing spin wavefunctions compared with the RVB approach. We end this section with an introduction to the Kitaev honeycomb model, which represents yet another different approach to constructing spin wavefunctions in a system with strong spin-orbit coupling with exotic properties beyond the simple spinon picture.

IV.1. RVB and its generalization to spin systems with strong spin-orbit coupling

Strong spin-orbit coupling may cause interesting experimental consequences that are absent in systems with spin rotational symmetry. An example suggested by Zhou *et al.* (Zhou *et al.*, 2008) is presented here, in which strong spin-orbit coupling in Ir atoms is used to explain the anomalous behavior of the Wilson ratio observed in $\text{Na}_4\text{Ir}_3\text{O}_8$, which was experimentally proposed (Okamoto *et al.*, 2007) as the first candidate for a 3D QSL on a hyperkagome lattice with fermionic spinons.

Although the Curie-Weiss constant is estimated to be as large as $\theta_W \sim 650$ K in $\text{Na}_4\text{Ir}_3\text{O}_8$, indicating strong AFM coupling, there is no observed thermodynamic and magnetic anomaly indicative of long-range spin ordering down to 2 K. The specific heat ratio $\gamma = C_V/T$ shows a rather sharp peak at a temperature of $T_c \sim 20$ K, indicating the existence of a phase transition or crossover at T_c . By contrast, the spin susceptibility $\chi(T)$ is nearly independent of temperature for all temperatures $T \ll \theta_W$. Using the experimental values of the spin susceptibility χ and the specific heat ratio γ at the specific heat peak at

~ 20 K, for $T > T_c$, the Wilson ratio $R_W = \pi^2 k_B^2 \chi / 3\mu_B^2 \gamma$ of the material is 0.88, which is very close to that of a Fermi gas where R_W is unity. Therefore, for a wide range of temperatures $T_c < T < \theta_W$, the system seems to behave as a Fermi liquid of spinons. Below T_c , the specific heat decreases to zero as $C_V \sim T^2$, suggesting a line nodal gap in the low-lying quasi-particle spectrum. However, this picture needs to be reconciled with the observation that the spin susceptibility χ remains almost constant, resulting in an anomalously large Wilson ratio of $R_W \gg 1$ at temperatures of $T < T_c$.

The spins in $\text{Na}_4\text{Ir}_3\text{O}_8$ originate from the low-spin $5d^5 \text{Ir}^{4+}$ ions, which form a 3D network in the form of a corner-sharing hyperkagome lattice. Chen and Balents (Chen and Balents, 2008) suggested that because of the large atomic number, the spin-orbit coupling in Ir atoms is expected to be strong. In the following section, we explain the anomalous Wilson ratio based on a modified RVB spin liquid picture in which both spin-singlet and spin-triplet pairings exist in the spin-pairing wavefunction.

Based on the experimental observations discussed above, Zhou *et al.* (Zhou *et al.*, 2008) proposed that a simple spinon hopping Hamiltonian H_0 determines the physics of the spin liquid state at $T > T_c$, where there exists a finite spinon Fermi surface, and that a spinon pairing gap characterized by H_{pair} opens up at $T < T_c$. The power-law behavior $C_V \propto T^2$ that is observed at low temperatures of $T < T_c$ indicates that the gap has line nodes on the Fermi surfaces. To determine the pairing symmetry, Zhou *et al.* noted that a group theoretical analysis indicates that a spin-triplet pairing state on a cubic lattice can create only full or point nodal gaps (Sigrist and Ueda, 1991), which seems to imply singlet pairing. However, because of the broken inversion symmetry on a hyperkagome lattice (Hahn, 1996), the spin-singlet and spin-triplet pairing states are, in general, mixed together in the presence of spin-orbit coupling (Frigeri *et al.*, 2004; Gor'kov and Rashba, 2001).⁴

In terms of the d -vector, the gap function $\Delta_{\alpha\beta}(\mathbf{k})$ ($\alpha, \beta = \uparrow, \downarrow$) has the general matrix form (Leggett, 1975),

$$\Delta(\mathbf{k}) = i(d_0(\mathbf{k})\sigma_0 + \mathbf{d}(\mathbf{k}) \cdot \boldsymbol{\sigma})\sigma_y, \quad (79)$$

and the spinon pairing must be singlet or a singlet-with-triplet admixture because of spin-orbit coupling in order to have line nodes (Zhou *et al.*, 2008).

⁴ In general, for a many-spin system in which spin rotational symmetry is broken, the spin $S = 0$ state(s) will mix with spin $S \geq 1$ states even in the presence of spatial inversion symmetry. The only exception is the two-spin system, in which inversion symmetry provides a good quantum number that separates the spin-singlet state from the spin-triplet states. Because the RVB approach begins from mean-field spin wavefunctions that are superpositions of two-spin pairing states, broken inversion symmetry is needed for the construction of mixed spin-singlet and spin-triplet states.

We now consider the spin susceptibility of such mixed states. Zhou et al. showed that if both singlet and triplet pairings are present and the spin-orbit scattering is much weaker than the pairing gap Δ , then the k -dependent electronic contribution to the spin susceptibility is given by

$$\frac{\chi_{ii}(\mathbf{k})}{\chi_N(\mathbf{k})} = 1 - \frac{d_0 d_0^* + d_i^* d_i}{d_0 d_0^* + \mathbf{d} \cdot \mathbf{d}^*} + \frac{d_0 d_0^* + d_i^* d_i}{d_0 d_0^* + \mathbf{d} \cdot \mathbf{d}^*} Y(\mathbf{k}; T),$$

where $i = x, y, z$; χ_N is the normal state contribution at $\Delta = 0$; and $Y(\mathbf{k}; T)$ is the k -dependent Yosida function (Leggett, 1975). Under the assumption that the d -vector is pinned by the lattice, for a polycrystalline sample, one must average over all spatial directions, resulting in

$$\frac{\chi_s}{\chi_N} = \frac{2}{3} - \frac{2}{3} \frac{|d_0|^2}{|d_0|^2 + |\mathbf{d}|^2} + \left(\frac{1}{3} + \frac{2}{3} \frac{|d_0|^2}{|d_0|^2 + |\mathbf{d}|^2} \right) Y(T), \quad (80)$$

where $Y(T)$ is the (spatially averaged) Yosida function, which vanishes at zero temperature; χ_s is the spin susceptibility below T_c ; and χ_N is the Pauli spin susceptibility in the normal state. Therefore, χ_s/χ_N reduces to $\frac{2}{3} - \frac{2}{3} \frac{|d_0|^2}{|d_0|^2 + |\mathbf{d}|^2}$ at zero temperature. If the spin-triplet pairing dominates, then $\chi_s/\chi_N \rightarrow \frac{2}{3}$, whereas if the spin-singlet pairing dominates, then $\chi_s/\chi_N \rightarrow 0$. However, neither of these cases is observed in experiments; instead, χ changes only negligibly below T_c (Okamoto *et al.*, 2007). This suggests that strong spin-orbit coupling is needed to explain the absence of a marked change in χ below $T_c \sim 20$ K.

It is well known that in conventional BCS singlet superconductors, the Knight shift, which is proportional to the Pauli paramagnetic susceptibility, changes very little below T_c for heavy elements such as Sn and Hg (Androes and Knight, 1959). It is understood that this is caused by the destruction of spin conservation due to the spin-orbit coupling. A clear explanation was presented by Anderson (Anderson, 1959) using the notion of time-reversed pairing states. We first consider the imaginary part of the spin response function $\chi''(q, \omega)$. If the total spin is conserved, then the dynamics are diffusive and $\chi''(q, \omega)$ will have a central peak in ω space with a width of Dq^2 , which goes to zero as $q \rightarrow 0$. Superconductivity gaps out all low-frequency excitations, thus removing this central peak. By the Kramers-Kronig relation, the real part $\chi'(q = 0, \omega = 0)$ vanishes in the superconducting ground state. In the presence of spin-orbit coupling, the total spin is not conserved but rather decays with a lifetime τ_s . In this case, $\chi''(q = 0, \omega)$ has a central peak with a width of $\frac{1}{\tau_s}$. The superconducting gap (formed by a pair of time-reversal states) Δ cuts a hole in $\chi''(\omega)$ for $\omega < \Delta$ but leaves the $\omega \gg \Delta$ region intact, consistent with the physical expectation that the high-frequency region should be unaffected by pairing. By the Kramers-Kronig relation, χ' will be reduced, but if the spin-orbit

coupling is sufficiently strong that

$$\frac{1}{\tau_s} \gg \Delta, \quad (81)$$

then the reduction will be small, i.e.,

$$\frac{\chi_s}{\chi_N} = 1 - \mathcal{O}(\Delta\tau_s).$$

Eq. (81) is the strong spin-orbit coupling condition that is required to have very little change in the spin susceptibility below T_c . We emphasize that the criterion for discriminating strong from weak spin-orbit coupling that is given by Eq. (81) is completely different from the usual criterion, which compares the spin-orbit energy, λ , with the splitting of the t_{2g} levels, E_3 (Chen and Balents, 2008). Another way to explain the large Wilson ratio observed in $\text{Na}_4\text{Ir}_3\text{O}_8$ was provided by Chen and Kim (Chen and Kim, 2013), in which strong spin-orbit coupling is still essential.

From a theoretical perspective, the PSG classification scheme has been applied to classify the spin liquid states on a kagome lattice with the Dzyaloshinskii-Moriya (DM) interaction (Dodds *et al.*, 2013). More recently, to test the validity of the RVB approach in constructing wavefunctions for spin systems with strong spin-orbit coupling, Sze, Zhou and Ng (Sze *et al.*, 2016) applied the Gutzwiller-projected wavefunction of fermion pairing states to study the $S = 1/2$ anisotropic Heisenberg (XXZ) chain

$$H = J_z \sum_i S_i^z S_{i+1}^z + J_\perp \sum_i (S_i^x S_{i+1}^x + S_i^y S_{i+1}^y), \quad (82)$$

where $J_\perp, J_z > 0$. This model can be mapped to the isotropic (XXX) Heisenberg model with the Dzyaloshinskii-Moriya (DM) interaction,

$$\sum_i \mathbf{D} \cdot (\mathbf{S}_i \times \mathbf{S}_{i+1}),$$

in one dimension with open boundary conditions through the transformation $U = \exp(-i \sum_n \frac{n\theta}{2} S_n^z)$ with $\cos \theta = J_z/J_\perp$ and $D = J_\perp \sin \theta$, where $U^\dagger H_{XXZ} U = H_{J+DM}$, with H_J denoting the isotropic Heisenberg model with interaction J .

Trial mean-field wavefunctions with the general pairing

$$\Delta(\mathbf{k}) = i (d_0(\mathbf{k}) \sigma_0 + \mathbf{d}(\mathbf{k}) \cdot \boldsymbol{\sigma}) \sigma_y$$

are being considered for the construction of the corresponding Gutzwiller-projected wavefunctions. The trial ground-state wavefunctions have the best energy when the d -vector has the form $d_0 = 0$ and $\mathbf{d}(k) = d_z \hat{z} = i\Delta \sin k$ for $J_z > J_\perp$ (Ising regime), whereas the preferred form is $d_0 = 0$ and $\mathbf{d}(k) = d_y \hat{y} = \Delta \sin k$ for $J_z < J_\perp$ (planar regime). The overlap between the trial ground-state wavefunction and the exact ground-state

wavefunction obtained through exact diagonalization is better than 95% in all cases that have been considered. Notably, the pairing state with $\mathbf{d}(k) = d_y \hat{y} = \Delta \sin k$ does not conserve S_z^{tot} and is not considered in the classification scheme used in reference (Dodds *et al.*, 2013).

IV.2. RVB approach to $S > 1/2$ systems

Historically, the search for spin liquid states has been focused on spin 1/2 systems because such systems have the strongest quantum mechanical fluctuation effects (see section II) when the unfrustrated Heisenberg model is considered. The situation is different when we consider spin systems with frustrated interactions (Chandra and Doucot, 1988). In this case, it is not obvious whether a spin liquid state is more likely to exist in systems of lower spin. In fact, it has recently been found that gapless spin liquid states may exist in a two-dimensional spin-1 compound $\text{Ba}_3\text{NiSb}_2\text{O}_9$ under high pressure (Cheng *et al.*, 2011). In this subsection, we examine how we can construct spin liquid states for $S > 1/2$ systems by generalizing the RVB approach developed for $S = 1/2$ systems. It should be noted that there are multiple possible methods of generalization. For example, Greiter and Thomale (Greiter and Thomale, 2009) constructed a chiral spin liquid state using a fractional quantum Hall wavefunction, whereas Xu *et al.* (Xu *et al.*, 2012) constructed a spin liquid state for an $S = 1$ system by representing a spin of 1 as the sum of two $S = 1/2$ spins. Liu, Zhou, and Ng (Liu *et al.*, 2010a,b) have developed an alternative approach in which a spin S is represented by $2S + 1$ fermions. In the following section, we consider this last approach, and we demonstrate the existence of fundamental differences between half-odd-integer spin and integer spin systems in this approach.

We begin with the fermion representation of general spins. To generalize the fermion representation of $S = 1/2$ spins to an arbitrary spin S , Liu, Zhou and Ng (Liu *et al.*, 2010a,b) introduce $2S + 1$ species of fermionic operators c_m that satisfy anti-commutation relations,

$$\{c_m, c_n^\dagger\} = \delta_{mn}, \quad (83)$$

where $m, n = S, S - 1, \dots, -S$. The spin operator can be expressed in terms of these operators as follows:

$$\hat{\mathbf{S}} = C^\dagger \mathbf{I} C,$$

where $C = (c_S, c_{S-1}, \dots, c_{-S})^T$ and I^a ($a = x, y, z$) is a $(2S + 1) \times (2S + 1)$ matrix whose matrix elements are given by

$$I_{mn}^a = \langle S, m | S^a | S, n \rangle.$$

It is straightforward to show that the resulting spin operator $\hat{\mathbf{S}}$ satisfies the $SU(2)$ angular momentum algebra. Under a rotational operation, C is a spin- S “spinor” transforming as $C_m \rightarrow D_{mn}^S C_n$ and $\hat{\mathbf{S}}$ is

a vector transforming as $S^a \rightarrow R_{ab} S^b$; here, D^S is the $2S + 1$ -dimensional irreducible representation of the $SU(2)$ group generated by \mathbf{I} , and R is the adjoint representation.

As in the $S = 1/2$ case, a constraint that there must be only one fermion per site is needed to project the fermionic system into the proper Hilbert space representing spins, i.e.,

$$(\hat{N}_i - N_f) |\text{phy}\rangle = 0, \quad (84)$$

where i is the site index and $N_f = 1$ (the particle picture, one fermion per site). Alternatively, it is straightforward to show that the constraint $N_f = 2S$ (the hole picture, one hole per site) equivalently represents a spin. The $N_f = 1$ representation can be mapped to the $N_f = 2S$ representation *via a particle-hole transformation*. For $S = 1/2$, the particle picture and the hole picture are identical, reflecting an intrinsic particle-hole symmetry of the underlying Hilbert space, which is absent for $S \geq 1$.

Following Affleck, Zou, Hsu and Anderson (Affleck *et al.*, 1988b), Liu, Zhou and Ng (Liu *et al.*, 2010a) introduce another “spinor” $\bar{C} = (c_{-S}^\dagger, -c_{-S+1}^\dagger, c_{-S+2}^\dagger, \dots, (-1)^{2S} c_S^\dagger)^T$, whose components can be written as $\bar{C}_m = (-1)^{S-m} c_{-m}^\dagger$, where the index m runs from S to $-S$ as for C . Upon combining C and \bar{C} into a $(2S + 1) \times 2$ matrix $\psi = (C, \bar{C})$, it is straightforward to see that the spin operators can be re-expressed as

$$\hat{\mathbf{S}} = \frac{1}{2} \text{Tr}(\psi^\dagger \mathbf{I} \psi) \quad (85)$$

and that the constraint can be expressed as

$$\text{Tr}(\psi \sigma_z \psi^\dagger) = 2S + 1 - 2N_f = \pm(2S - 1), \quad (86)$$

where the + sign implies $N_f = 1$ and the - sign implies $N_f = 2S$.

We now examine the internal symmetry group associated with the redundancy in the fermion representation. The internal symmetry group is different for integer and half-odd-integer spins; it is $U(1) \bar{\otimes} Z_2 = \{e^{i\sigma_z \theta}, \sigma_x e^{i\sigma_z \theta} = e^{-i\sigma_z \theta} \sigma_x; \theta \in \mathbb{R}\}$ for the former and $SU(2)$ for the latter. The reason for this difference can be qualitatively understood as follows: Note that C and \bar{C} are not independent. The operators in the internal symmetry group “mix” the two fermion operators in the same row of C and \bar{C} , i.e., c_S and c_{-S}^\dagger . For integer spins, c_0 and $(-1)^S c_0^\dagger$ will be “mixed”. For the relation $\{c_0, c_0^\dagger\} = 1$ to remain invariant, there are only two possible methods of “mixing”: one is a $U(1)$ transformation, and the other is interchanging the two operators. These operations form the $U(1) \bar{\otimes} Z_2$ group. For half-odd-integer spins, the pair $(c_0, (-1)^S c_0^\dagger)$ does not exist, and the symmetry group is the maximum $SU(2)$ group. Thus, the difference between integer and half-odd-integer spins is a fundamental property of the fermion representation.

Now let us see how the constraint expressed in Eq. (86) transforms under the symmetry groups. For $S = 1/2$, constraint given in Eq. (86) is invariant under the transformation $\psi \rightarrow \psi W$ because the right-hand side vanishes (as a result of the particle-hole symmetry of the Hilbert space). For integer spins, if $W = e^{i\sigma_z\theta}$, then $W\sigma_z W^\dagger = \sigma_z$, and Eq. (86) is invariant. If $W = \sigma_x e^{i\sigma_z\theta}$, then $W\sigma_z W^\dagger = -\sigma_z$, meaning that the “particle” picture (+ sign in Eq. (86)) and the “hole” picture (− sign in Eq. (86)) are transformed into each other.

For a half-odd-integer spin with $S \geq 3/2$, $W \in SU(2)$ is a rotation, and we may extend the constraint into a vector form in a manner similar to the $S = 1/2$ case, such that Eq. (86) becomes

$$\text{Tr}(\psi \vec{\sigma} \psi^\dagger) = (0, 0, \pm(2S - 1))^T. \quad (87)$$

Under the group transformation $\psi \rightarrow \psi W$,

$$\text{Tr}(\psi \vec{\sigma} \psi^\dagger) \rightarrow (R^{-1})(0, 0, \pm(2S - 1))^T, \quad (88)$$

where $W\sigma^a W^\dagger = R_{ab}\sigma^b$, $a, b = x, y, z$, i.e., R is a 3 by 3 matrix representing a 3D rotation. The transformed constraint represents a new Hilbert subspace, which is still a $(2N + 1)$ -dimensional irreducible representation of the spin $SU(2)$ algebra. Any measurable physical quantity, such as the spin \mathbf{S} , remains unchanged in this new Hilbert space. Therefore, for half-odd-integer spins ($S \geq 3/2$), there exist infinitely many ways of imposing the constraint that gives rise to a Hilbert subspace representing a spin. However, for integer spins, there exist only two possible constraint representations.

The fermion representation can be used to construct mean-field Hamiltonians for spin models with arbitrary spins after the spin-spin interaction is written down in terms of fermion operators. For the spin-1/2 case, the Heisenberg interaction can be written as (see section III)

$$\begin{aligned} \hat{\mathbf{S}}_i \cdot \hat{\mathbf{S}}_j &= -\frac{1}{8} \text{Tr} : (\psi_i^\dagger \psi_j \psi_j^\dagger \psi_i) : \\ &= -\frac{1}{4} : (\chi_{ij}^\dagger \chi_{ij} + \Delta_{ij}^\dagger \Delta_{ij}) : \end{aligned} \quad (89)$$

where

$$\chi_{ij} = C_i^\dagger C_j, \quad \Delta_{ij} = \bar{C}_i^\dagger C_j. \quad (90)$$

The definitions of χ_{ij} and Δ_{ij} in the above form can be extended to arbitrary spins. The only difference is that for an integer spin, $\chi_{ji} = \chi_{ij}^\dagger$ and $\Delta_{ji} = -\Delta_{ij}$, whereas for a half-odd-integer spin, $\chi_{ji} = \chi_{ij}^\dagger$ and $\Delta_{ji} = \Delta_{ij}$. The parity of the pairing term Δ_{ij} differs for integer and half-odd-integer spins (Liu *et al.*, 2010a). For $S = 1$, it can be shown, after some straightforward algebra, that the Hamiltonian can be written as (Liu *et al.*, 2010a)

$$\begin{aligned} \hat{\mathbf{S}}_i \cdot \hat{\mathbf{S}}_j &= -\frac{1}{2} \text{Tr} : (\psi_i^\dagger \psi_j \psi_j^\dagger \psi_i) : \\ &= - : (\chi_{ij}^\dagger \chi_{ij} + \Delta_{ij}^\dagger \Delta_{ij}) :. \end{aligned} \quad (91)$$

However, for $S > 1$, we cannot write the spin-spin interaction $\hat{\mathbf{S}}_i \cdot \hat{\mathbf{S}}_j$ in terms of χ_{ij} and Δ_{ij} alone. In the case of $S = 3/2$, triplet hopping and pairing terms must be introduced to represent the Heisenberg interaction. Generally speaking, quintet and higher multipolar hopping and pairing operators are needed to represent the Heisenberg Hamiltonian when S becomes larger (Liu *et al.*, 2010a). In the following, we restrict ourselves to $S = 1$ systems.

In this case, the mean-field Hamiltonians are BCS-type Hamiltonians, as in the case of $S = 1/2$ spins. The physical spin wavefunction can be obtained by applying Gutzwiller projection to the mean-field ground state. There are two major differences between $S = 1$ and $S = 1/2$ spin systems: (1) Because of the different internal symmetry group ($U(1) \bar{\otimes} Z_2$), $S = 1$ spin liquid states are of either the $U(1)$ or Z_2 type. There are no $SU(2)$ spin liquid states for integer spin systems in the fermionic construction. Therefore, we expect that in general, spin liquid states for integer spin systems, if they exist, are more stable against gauge fluctuations. (2) The difference in parity of the pairing terms leads to interesting possibilities for obtaining topological spin liquid states in $S = 1$ systems that are not easy to realize in $S = 1/2$ systems (Bieri *et al.*, 2012; Liu *et al.*, 2010b). This difference leads to the existence of a Haldane phase in the bilinear-biquadratic Heisenberg spin chain in the fermionic description (Liu *et al.*, 2012).

Finally, we note the existence of a fundamental difference in the excitation spectrum of an $S = 1$ spin system compared with that of an $S = 1/2$ system, under the assumption that the ground states are spin singlets. For an integer spin system, we can form spin-singlet states in a lattice with either an even or an odd number of lattice sites N , as long as $N > 1$, whereas for a half-odd-integer spin system, spin-singlet states can be formed only in a lattice with an even number of sites. In the RVB approach, angular momentum $L = 1$ excitations of the system are formed by Gutzwiller projecting the excited states in BCS theory, i.e., by breaking a pair of spin singlets in the BCS ground state. The resulting excited state consists of two excited spinons, which are $S = 1/2$ objects for spin 1/2 systems but are $S = 1$ objects for spin 1 systems. In an $S = 1$ spin liquid, these two $S = 1$ spinons together form an $L = 1$ excitation.

There is, however another method of forming an $L = 1$ excitation in a spin-1 spin liquid. Beginning from a lattice system with N sites, we may form an $L = 1$ excitation by rearranging the spins such that the system is a product of spin-singlet ground states for $N - 1$ of the sites plus a single spin-1 spinon. This excitation is a non-perturbative, topological excitation that cannot be achieved by simply Gutzwiller projecting a BCS excited state in the RVB construction. It has been demonstrated in reference (Liu *et al.*, 2014) that the construction of these two kinds of excitations gives rise to the so-called one-magnon and two-magnon excitation spectra in the

Haldane phase of the $S = 1$ bilinear-biquadratic Heisenberg model. Similar construction approaches are not possible for $S = 1/2$ systems.

IV.3. Matrix product state (MPS) and projected entangled pair state (PEPS)

In this subsection, we discuss two approaches to spin liquid states that have completely different starting points from those of the RVB, or Gutzwiller-projected mean-field theory, approach we discussed in section III. We begin with matrix product states (MPSs) and projected entangled pair states (PEPSs), which represent another popular class of variational wavefunctions that are currently being applied to spin systems. Translationally invariant MPSs in spin chains were first constructed and studied by Fannes, Nachtergael and Werner (Fannes *et al.*, 1992) as an extension of the AKLT state (Affleck *et al.*, 1987); in this context, the authors called them *finitely correlated states*. The term MPS was coined by Klümper, Schadschneider and Zittartz (Klümper *et al.*, 1993), who extended the AKLT state in a different way. Later, Östlund and Rommer (Östlund and Rommer, 1995) realized that the state resulting from DMRG (White, 1992) can be written as an MPS. This approach is very successful for one-dimensional systems and can be generalized to systems of two (or more) dimensions.

First, let us consider the quantum wavefunction of a one-dimensional spin system that is translationally invariant with a local Hamiltonian H . The wavefunction can be generally expressed as

$$|\Psi\rangle = \sum_{s_1, s_2, \dots, s_N} \phi(s_1, s_2, \dots, s_N) |s_1, s_2, \dots, s_N\rangle, \quad (92)$$

where $|s_1, s_2, \dots, s_N\rangle$ represents a spin configuration with spins s_i on sites $i = 1, 2, \dots, N$ and $\phi(s_1, s_2, \dots, s_N)$ is the amplitude of the spin configuration in the quantum state $|\Psi\rangle$. Because of the spin-spin interaction, spin configurations at far away sites are generally correlated, and we cannot write $\phi(s_1, s_2, \dots, s_N) = \phi_0(s_1)\phi_0(s_2)\dots\phi_0(s_N)$ in general. The MPS approach is a powerful method of constructing wavefunctions with non-local quantum correlations. The trick is to extend the direct-product wavefunction $\phi(s_1, s_2, \dots, s_N) = \phi_0(s_1)\phi_0(s_2)\dots\phi_0(s_N)$ to matrix products.

More explicitly, we associate a matrix A^s with each spin state s ; then, the wavefunction amplitude $\phi(s_1, s_2, \dots, s_N)$ can be written as

$$\phi(s_1, s_2, \dots, s_N) = \text{Tr}\{A^{s_1}[1]A^{s_2}[2]\dots A^{s_N}[N]\}, \quad (93)$$

where the trace is used to impose the periodic boundary condition. As an example, we consider an $S = 1/2$ two-spin system and choose $A^\uparrow = \sigma_z$ and $A^\downarrow = \sigma_x$, where

the σ s are Pauli matrices. It is easy to see that in this case, $\phi(\uparrow, \uparrow) = \phi(\downarrow, \downarrow) \neq 0$ and $\phi(\uparrow, \downarrow) = \phi(\downarrow, \uparrow) = 0$. A different choice of $A^\uparrow = \sigma_+$ and $A^\downarrow = \sigma_-$ yields $\phi(\uparrow, \downarrow) = \phi(\downarrow, \uparrow) \neq 0$ and $\phi(\uparrow, \uparrow) = \phi(\downarrow, \downarrow) = 0$. The correlation between the different spin states on the two sites is determined by the matrix A^s that is chosen to link the sites. Extending the construction to more than two sites, one sees that the choice of the matrices A^s determines the quantum entanglement structure of the wavefunction.

When the MPSs are treated as variational wavefunctions, one may determine the number of variational parameters in the wavefunctions by means of a simple counting argument. The number of parameters P appearing in an MPS wavefunction in the form of Eq. (93) depends on the size of the matrix A and the number of available states S per site. In general, $P \sim S \times M^2$ for an $M \times M$ matrix as long as $P < S^N$, where N is the number of sites in the system. Thus, MPS wavefunctions are generally variational wavefunctions with a large number of built-in variational parameters. As the dimension $M \rightarrow \infty$, MPSs can represent any quantum state of the many-body Hilbert space with arbitrary accuracy. In practice, the low-energy states of gapped local Hamiltonians in one dimension can be efficiently represented by MPSs with a finite value of M (Hastings, 2007; Verstraete and Cirac, 2006). The DMRG method (White, 1992) and its generalizations (Schollwöck, 2005) can be viewed as systematic approaches for constructing MPS variational wavefunctions as the size of the system gradually increases.

The MPS construction can be extended in several ways. First, it can be extended to higher dimensions by replacing the matrices A (= rank 2 tensors) with higher-rank tensors T . These wavefunctions are presently known as projected entangled pair states (PEPSs) (Verstraete and Cirac, 2004a,b). Second, the local correlation or entanglement between a pair of sites in a PEPS can be generalized to a cluster (or simplex), resulting in states called projected entangled simplex states (PESSs) (Xie *et al.*, 2014). A representative example of a PEPS is the simplex solid state proposed by Arovas (Arovas, 2008).

IV.3.1. Valence-bond solids and MPSs in one dimension

The physics of an MPS or PEPS wavefunction is encoded in the tensors linking neighboring spin states. In general, these link tensors can be optimally constructed using the DMRG approach or tensor-based renormalization methods (Cirac and Verstraete, 2009). In this subsection, we discuss a simple example of tensors that represent a particular class of spin states called valence-bond solid (VBS) states. To begin, we introduce a well-known example of a valence-bond solid

state - the Affleck-Kennedy-Lieb-Tasaki (AKLT) state (Affleck *et al.*, 1987).

The AKLT state is an example of a VBS state in which only one spin-singlet configuration is allowed in the wavefunction given in Eq. (23). It is a one-dimensional VBS state constructed for a $S = 1$ spin chain, represented pictorially in Fig. 9, where each gray bond represents a spin singlet formed by two $S = 1/2$ spins, i.e., Eq. (22). Each lattice site is connected to two other sites by two valence bonds and is occupied by two $S = 1/2$ spins. The AKLT wavefunction is formed by projecting the spin- $1/2 \otimes 1/2 = 1 \oplus 0$ quartet states into the spin $S = 1$ triplet states. This is represented graphically in Fig. 9 by the circles, which represent projection operators tying together two $S = 1/2$ spins, projecting out the spin $S = 0$ or singlet state and preserving only the spin $S = 1$ or triplet states.

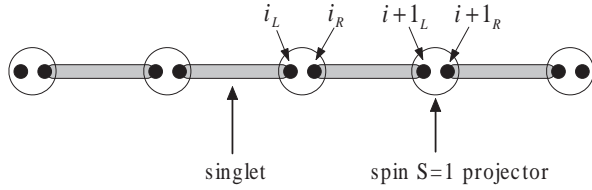


FIG. 9 A valence-bond solid construction of the AKLT state.

For every adjacent pair of $S = 1$ spins, two of the four constituent $S = 1/2$ spins are projected into a state with a total spin of zero by the valence bond. Therefore, the pair of $S = 1$ spins is forbidden from existing in a combined spin $S = 2$ state. This condition can be realized by considering a Hamiltonian that is a sum of projectors $P_{i,i+1}$ that project the pairs of $S = 1$ spins from the $1 \otimes 1 = 2 \oplus 1 \oplus 0$ space into the spin $S = 2$ subspace,

$$H_{\text{AKLT}} = \sum_i P_{i,i+1}. \quad (94a)$$

Because the projection operators $P_{i,i+1}$ are positive semi-definite, the ground state satisfies $H_{\text{AKLT}}|\Psi_G\rangle = 0$ and is simply the AKLT state. The projection operator $P_{i,i+1}$ can be written in terms of spin-1 operators as follows (Affleck *et al.*, 1987):

$$P_{i,i+1} = \frac{1}{3} + \frac{1}{2}(\mathbf{S}_i \cdot \mathbf{S}_{i+1}) + \frac{1}{6}(\mathbf{S}_i \cdot \mathbf{S}_{i+1})^2. \quad (94b)$$

The AKLT state is important because it is an explicit spin wavefunction that realizes the Haldane phase for integer spins (see section II). In particular, it is easy to see from Fig. 9 that an unpaired $S = 1/2$ spin will be left at each end of the spin chain, which is a realization of the end state discussed in section II for $S = 1$ Heisenberg spin chains. In the following, we show how the AKLT state can be written as an MPS state.

The AKLT state can be constructed in two steps. First, we split each site i in the spin-1 chain into two sites i_L and i_R , thereby forming a spin-1/2 chain with $2N$ sites, as in Fig. 9 (where N is the number of sites in the parent spin-1 chain) and construct a dimerized chain in which the spins at sites i_R and $i+1_L$ ($i = 1, 2, \dots, N$) are joined by a valence bond (see Eq. (22)). The singlet bond between sites i_R and $i+1_L$ can be written as

$$(i, i+1) = \sum_{\sigma_{i_R}, \sigma_{i+1_L}} R_{\sigma_{i_R}, \sigma_{i+1_L}} |\sigma_{i_R}\rangle |\sigma_{i+1_L}\rangle, \quad (95)$$

where $\sigma = \uparrow, \downarrow$ and the $R_{\sigma\sigma'}$ are the components of a 2×2 matrix:

$$\mathbf{R} = \begin{pmatrix} 0 & \frac{1}{\sqrt{2}} \\ -\frac{1}{\sqrt{2}} & 0 \end{pmatrix}. \quad (96)$$

In this representation, the wavefunction of the dimerized spin-1/2 chain can be written as

$$|\Psi\rangle = \sum_{\sigma_{1_R}, \dots, \sigma_{N_L}} R_{\sigma_{1_R} \sigma_{2_L}} \dots R_{\sigma_{N-1_R} \sigma_{N_L}} |\sigma_{1_R}, \dots, \sigma_{N_L}\rangle. \quad (97)$$

Note that this state is a direct product state of $S = 1/2$ RVB singlet pairs with the two end spins (σ_{1_L} and σ_{N_R}) unspecified.

Next, we project the two $S = 1/2$ spins at sites i_L and i_R to the spin-1 states $|1, m\rangle$ ($m = 0, \pm 1$) with

$$\begin{aligned} |1, 1\rangle &= |\uparrow\uparrow\rangle, \\ |1, 0\rangle &= \frac{1}{\sqrt{2}} (|\uparrow\downarrow\rangle + |\downarrow\uparrow\rangle), \\ |1, -1\rangle &= |\downarrow\downarrow\rangle. \end{aligned} \quad (98)$$

This projection can be expressed in terms of three matrices, $\mathbf{M}^{0, \pm 1}$, where

$$|1, m\rangle = \sum_{\sigma, \sigma'} M_{\sigma\sigma'}^m |\sigma\rangle |\sigma'\rangle \quad (99)$$

with

$$\mathbf{M}^1 = \begin{pmatrix} 1 & 0 \\ 0 & 0 \end{pmatrix}, \quad (100a)$$

$$\mathbf{M}^{-1} = \begin{pmatrix} 0 & 0 \\ 0 & 1 \end{pmatrix}, \quad (100b)$$

and

$$\mathbf{M}^0 = \begin{pmatrix} 0 & \frac{1}{\sqrt{2}} \\ \frac{1}{\sqrt{2}} & 0 \end{pmatrix}. \quad (100c)$$

Thus, the AKLT state can be written as

$$|\Psi_{\text{AKLT}}\rangle = \sum_{s_1, s_2, \dots, s_N} \phi_{\text{AKLT}}(s_1, \dots, s_N) |s_1, s_2, \dots, s_N\rangle, \quad (101)$$

where $s_i = 0, \pm 1$ and

$$\begin{aligned} \phi_{\text{AKLT}}(s_1, \dots, s_N) &= \sum_{\sigma_{1L}, \dots, \sigma_{N_L}} [M_{\sigma_{1L} \sigma_{1R}}^{s_1} R_{\sigma_{1L} \sigma_{2L}} \\ &\quad \times M_{\sigma_{2L} \sigma_{2R}}^{s_2} \dots R_{\sigma_{N-1L} \sigma_{NL}}] \\ &= [\mathbf{A}^{s_1} \mathbf{A}^{s_2} \dots \mathbf{A}^{s_N}]_{\sigma_{1L} \sigma_{N_R}}. \end{aligned} \quad (102\text{a})$$

Here, $\mathbf{A}^s = \mathbf{M}^s \mathbf{R}$, and $\sigma_{1L}, \sigma_{N_R} = \uparrow, \downarrow$ correspond to four degenerate ground states on an open chain. Imposing the periodic boundary condition gives rise to a non-degenerate ground state with

$$\phi_{\text{AKLT}}(s_1, \dots, s_N) = \text{Tr}[\mathbf{A}^{s_1} \mathbf{A}^{s_2} \dots \mathbf{A}^{s_N}]. \quad (102\text{b})$$

IV.3.2. PEPSs in higher dimensions and beyond

The AKLT construction can be extended to construct other types of VBS states and states in higher dimensions. Straightforward examples include $S = 2$ VBS states on a square lattice and $S = 3/2$ VBS states on a honeycomb lattice (Affleck *et al.*, 1988a). These states can be written as PEPSs in their respective lattices.

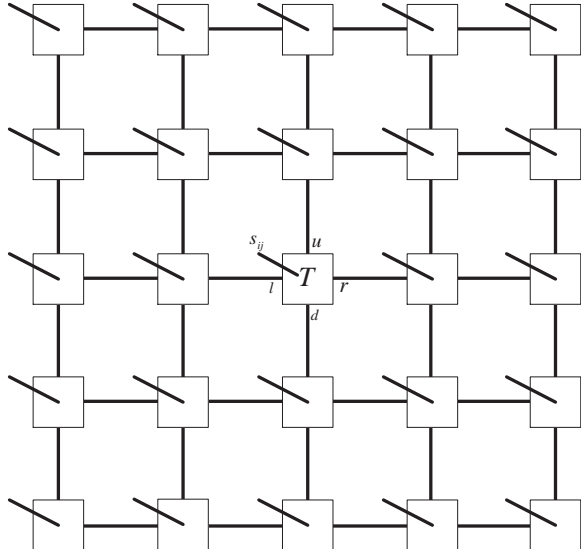


FIG. 10 Graphical representation of a PEPS in terms of contracted tensors (tensor network). Each box denotes a tensor T with components $T_{lru}^{s_{ij}}$ at site ij , where l, u, r , and d are tensor indices related to left, right, up and down bonds, respectively, linking to their neighbors; the open lines represent the physical spin states s_{ij} ; and the connected lines represent the contraction of the tensors.

For instance, on a square lattice with a coordination number of 4, a generic PEPS wavefunction can be written in terms of rank 4 tensors as follows:

$$|\Psi\rangle = \sum_{[s_{ij}]} \phi([s_{ij}]) |[s_{ij}]\rangle, \quad (103\text{a})$$

where $i, j = 1, \dots, N$ for an $N \times N$ system, $[s_{ij}] = (s_{11}, \dots, s_{1N}, s_{21}, \dots, s_{2N}, \dots, s_{N1}, \dots, s_{NN})$ denotes a spin configuration, and

$$\phi([s_{ij}]) = \text{Tr}[T^{s_{11}} \dots T^{s_{1N}} T^{s_{21}} \dots T^{s_{NN}}]. \quad (103\text{b})$$

where, the T^s s are rank 4 tensors with components

$$T_{lru}^{s_{ij}},$$

where s_{ij} is the physical spin index; l, r, u , and d represent links connected to the tensors at the left, right, up and down neighboring sites $(i-1, j)$, $(i+1, j)$, $(i, j-1)$, and $(i, j+1)$, respectively; and “Tr” means tensor contraction. The above mathematical expression of tensor contraction is usually represented by diagrams such as that shown in Fig. 10 for a square lattice, where connected lines represent the contraction of tensors with the same index and open lines represent the physical spin states $s_{ij} = -S, \dots, S$.

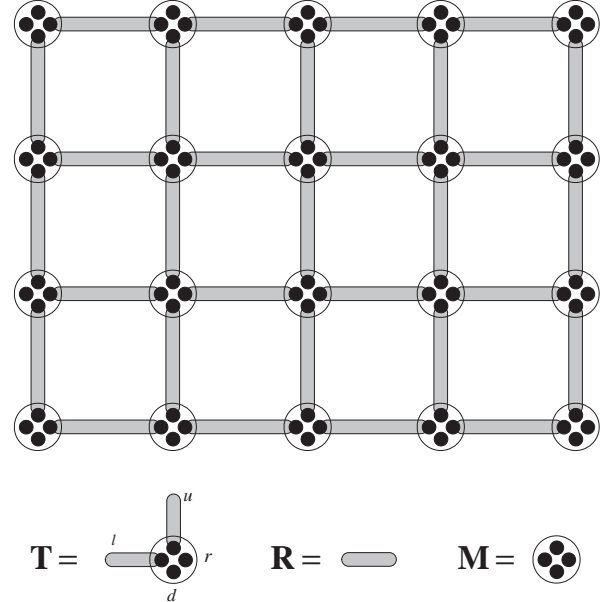


FIG. 11 (Affleck *et al.*, 1988a) The VBS construction of an $S = 2$ AKLT state on a square lattice and the corresponding tensors.

As an example, a spin $S = 2$ AKLT state on a square lattice can be written in PEPS form as shown in Fig. 11. The tensors T^s can be obtained using the VBS construction with the tensors \mathbf{R} and \mathbf{M}^s , as in one dimension. The tensor \mathbf{R} is still defined by Eq. (96). The tensors \mathbf{M}^s , $s = 0, \pm 1, \pm 2$, project a state consisting of four $S = 1/2$ spins in the auxiliary Hilbert space $\frac{1}{2} \otimes \frac{1}{2} \otimes \frac{1}{2} \otimes \frac{1}{2} = 2 \oplus 1 \oplus 0$ into the physical $S = 2$ spin space, whose components are given by

$$M_{\sigma_l \sigma_r \sigma_u \sigma_d}^s = \langle s | \sigma_l \sigma_r \sigma_u \sigma_d \rangle, \quad (104)$$

where $\sigma_l, \sigma_r, \sigma_u, \sigma_d = \uparrow, \downarrow$. The tensor \mathbf{T} is given by

$$T_{\sigma_l \sigma_r \sigma_u \sigma_d}^s = \sum_{\sigma_{l'}, \sigma_{u'}} M_{\sigma_l' \sigma_r \sigma_{u'} \sigma_d}^s R_{\sigma_l \sigma_{l'}} R_{\sigma_u \sigma_{u'}}, \quad (105)$$

The tensor product state constructed from the above T^s s give rise to the $S = 2$ AKLT state on a square lattice.

The VBS construction can be further extended by “fractionalizing” the spins in more exotic ways (for example, using the Majorana fermion representation of spins). In this way, we can write the toric code model (Kitaev, 2003) in the PEPS form as well as the Kitaev honeycomb model (Kitaev, 2006) (with a residual fermionic degree of freedom at each site; see section IV.4). The relation between RVB states and PEPSs has also been exploited to show that some RVB states can be written as PEPSs (Poilblanc and Schuch, 2013; Schuch *et al.*, 2012; Verstraete *et al.*, 2006; Wang *et al.*, 2013). However, the general relation between RVB states and PEPSs remains unclear.

The PEPS construction provides a way to describe entanglement among local spins based on the construction of local pairs, and its application to geometrically frustrated lattices is limited. To overcome this limitation, researchers have extended the pair construction procedure to consider entanglement between more than two sites, say, a cluster or a simplex, to construct projected states. These projected entangled simplex states form the basis for more elaborate numerical approaches (Xie *et al.*, 2014). Combined with numerical techniques (tensor-based renormalization), these tensor-network methods now provide an alternative means of constructing variational wavefunctions. Readers can refer to references (Cirac and Verstraete, 2009; Orus, 2014; Verstraete *et al.*, 2008) for details.

IV.4. Kitaev honeycomb model and related issues

It was previously believed that spin rotational symmetry is essential for a QSL state that supports fractional spinon excitations. If the spin rotational symmetry is broken, the system tends to approach an ordered state. Kitaev (Kitaev, 2006) provided a counterexample to this belief through an unusual, exactly solvable model in two dimensions with strong spin-orbit coupling, which destroys the spin rotational symmetry, but in which deconfined spinons nevertheless exist on top of the QSL ground states. This famous model is now called the Kitaev honeycomb model. In this section, we briefly review the Kitaev honeycomb model to see how exotic ground states and low-energy excitations emerge from this model with broken rotational symmetry. The possibility of the realization of Kitaev-like models in realistic materials is also discussed.

Kitaev considered a spin-1/2 model on a honeycomb lattice with spin-orbit coupling (Kitaev, 2006). He di-

vided all nearest neighbor bonds in the honeycomb lattice into three types, called “ x -links”, “ y -links” and “ z -links” as shown in Fig. 12. The Hamiltonian is given as follows:

$$H = -J_x \sum_{x\text{-link}} K_{ij} - J_y \sum_{y\text{-link}} K_{ij} - J_z \sum_{z\text{-link}} K_{ij}, \quad (106)$$

where K_{ij} is defined as

$$K_{ij} = \begin{cases} \sigma_i^x \sigma_j^x, & \text{if } (i, j) \text{ is a } x\text{-link,} \\ \sigma_i^y \sigma_j^y, & \text{if } (i, j) \text{ is a } y\text{-link,} \\ \sigma_i^z \sigma_j^z, & \text{if } (i, j) \text{ is a } z\text{-link.} \end{cases} \quad (107)$$

Note the strong anisotropy in the spin-spin couplings K_{ij} .

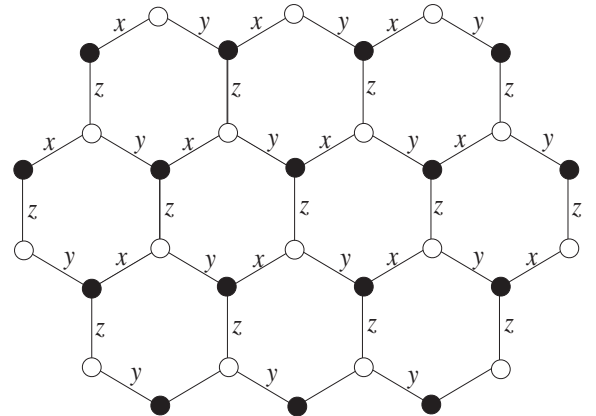


FIG. 12 (Kitaev, 2006) Kitaev honeycomb model. x , y and z denote three types of links in the honeycomb lattice.

We first consider the following loop operators W_p defined for a hexagonal loop:

$$W_p \equiv \sigma_1^x \sigma_2^y \sigma_3^z \sigma_4^x \sigma_5^y \sigma_6^z = K_{12} K_{23} K_{34} K_{45} K_{56} K_{61}, \quad (108)$$

where p is used to label the lattice plaquettes (hexagons), as shown in Fig. 13. It is easy to verify that $[W_p, K_{ij}] = 0$; therefore, $[H, W_p] = 0$. Hence, the W_p s serve as good quantum numbers for the Hamiltonian given in Eq. (106), and the total Hilbert space for spins can be divided into a direct product of sectors that are eigenspaces of $\{W_p\}$. However, the eigenvalue problem cannot be completely solved by determining the eigenspaces of $\{W_p\}$. Each W_p has only two eigenvalues, $w_p = \pm 1$. Each plaquette contains six sites, and each site is shared by three plaquettes. Therefore, the number of plaquettes is given by $m = N/2$, where N is the number of sites. It follows that the dimension of each eigenspace of $\{W_p\}$ is $2^N/2^m = 2^{N/2}$, i.e., splitting the Hilbert space into eigenspaces of $\{W_p\}$ cannot solve the eigenvalue problem completely.

Kitaev realized that to solve the model Hamiltonian given in Eq. (106), spins can be written in terms of four Majorana fermions, because a Majorana fermion can be viewed as the real or imaginary part of a complex

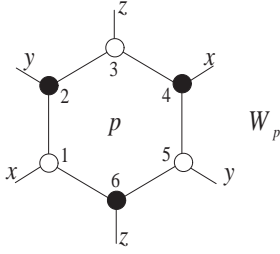


FIG. 13 (Kitaev, 2006) Loop operator $W_p = \sigma_1^x \sigma_2^y \sigma_3^z \sigma_4^x \sigma_5^y \sigma_6^z$ on a lattice plaquette (hexagon).

fermion. To illustrate this approach, we rewrite the complex fermions f_\uparrow and f_\downarrow in Eq. (27) in terms of four Majorana fermions c_1, c_2, c_3 and c_4 :

$$\begin{aligned} f_\uparrow &= \frac{1}{2}(c_1 + ic_2), & f_\uparrow^\dagger &= \frac{1}{2}(c_1 - ic_2), \\ f_\downarrow &= \frac{1}{2}(c_3 + ic_4), & f_\downarrow^\dagger &= \frac{1}{2}(c_3 - ic_4), \end{aligned} \quad (109a)$$

where the operators c_α ($\alpha = 1, 2, 3, 4$) are Hermitian and satisfy

$$c_\alpha c_\beta + c_\beta c_\alpha = 2\delta_{\alpha\beta}. \quad (109b)$$

Thus, the three spin components read $\sigma^x = \frac{i}{2}(c_1 c_4 - c_2 c_3)$, $\sigma^y = \frac{i}{2}(c_3 c_1 - c_2 c_4)$, and $\sigma^z = \frac{i}{2}(c_1 c_2 - c_3 c_4)$. The single-occupancy condition $f_\uparrow^\dagger f_\uparrow + f_\downarrow^\dagger f_\downarrow = 1$ (and $f_\uparrow^\dagger f_\downarrow^\dagger = f_\uparrow f_\downarrow = 0$) becomes

$$c_1 c_2 + c_3 c_4 = c_1 c_3 + c_2 c_4 = c_1 c_4 + c_3 c_2 = 0, \quad (110)$$

which can be simplified to the single equation $c_1 c_2 c_3 c_4 = 1$. Using these constraints, the spin operators can be written as $\sigma^x = ic_1 c_4$, $\sigma^y = -ic_2 c_4$, and $\sigma^z = -ic_3 c_4$. Rewriting $b_x = c_1$, $b_y = -c_2$, $b_z = -c_3$ and $c = c_4$, we arrive at the Kitaev representation

$$\begin{aligned} \sigma^x &= ib^x c, \\ \sigma^y &= ib^y c, \\ \sigma^z &= ib^z c, \end{aligned} \quad (111)$$

with the constraint

$$D \equiv b^x b^y b^z c = 1. \quad (112)$$

The Majorana representation without constraints is redundant and enlarges the physical spin Hilbert space. Note that $D^2 = 1$ and that D has two eigenvalues, $D = \pm 1$, thereby splitting the local Hilbert space into two sectors. The physical spin Hilbert space corresponds to the sector with all $D_j = 1$. Therefore, the physical spin wavefunction $|\Psi_{\text{spin}}\rangle$ can be obtained from the Majorana fermion wavefunction $|\Psi_{\text{Majorana}}\rangle$ through the projection

$$|\Psi_{\text{spin}}\rangle = \prod_j \frac{1+D_j}{2} |\Psi_{\text{Majorana}}\rangle, \quad (113)$$

which retains the $D_j \equiv 1$ sector and removes all other sectors in the enlarged Hilbert space. Note that $\frac{1+D_j}{2} = n_{j\uparrow} + n_{j\downarrow} - 2n_{j\uparrow}n_{j\downarrow}$ and that Eq. (113) is nothing but the Gutzwiller projection. In addition, note that D_j serves as a Z_2 gauge transformation in the enlarged Hilbert space ($D_j b_j^\alpha D_j = -b_j^\alpha$, $D_j c_j D_j = -c_j$) and commutes with the spin operators ($[D_j, \sigma_j^\alpha] = 0$, $\alpha = x, y, z$) and thus with the Hamiltonian. As a result, the Gutzwiller projection is “trivial” in the sense that $\prod_j \frac{1+D_j}{2} |\Psi_{\text{Majorana}}\rangle$ is an eigenstate of H in the projected Hilbert space as long as $|\Psi_{\text{Majorana}}\rangle$ is an eigenstate of H in the “unprojected” Hilbert space and $\prod_j \frac{1+D_j}{2} |\Psi_{\text{Majorana}}\rangle \neq 0$.

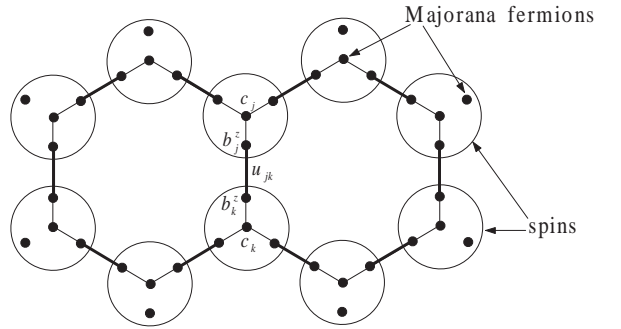


FIG. 14 (Kitaev, 2006) Graphic representation of the four-Majorana-fermion decomposition of the Hamiltonian expressed in Eq. (106).

In the Majorana fermion representation, K_{ij} in Eq. (107) becomes

$$K_{ij} = -i(ib_i^\alpha b_j^\alpha)c_i c_j, \quad (114)$$

where $\alpha = x, y, z$ depends on the type of link (ij) . The operator $ib_i^\alpha b_j^\alpha$ is Hermitian, and we denote it by $\hat{u}_{jk} = ib_i^\alpha b_j^\alpha$. Thus, we may write

$$H = \frac{i}{4} \sum_{\langle j, k \rangle} \hat{A}_{jk} c_j c_k, \quad (115a)$$

with

$$\hat{A}_{jk} = 2J_{\alpha(jk)} \hat{u}_{jk}, \quad \hat{u}_{jk} = ib_k^\alpha b_k^\alpha, \quad (115b)$$

where $\langle j, k \rangle$ denotes nearest neighbor links on the honeycomb lattice and, by definition, $\hat{u}_{jk} = -\hat{u}_{kj}$ and $\hat{A}_{jk} = -\hat{A}_{kj}$. The Hamiltonian structure in this Majorana fermion representation is shown schematically in Fig. 14. Note that $[H, \hat{u}_{jk}] = 0$ and $[\hat{u}_{jk}, \hat{u}_{j'k'}] = 0$. The enlarged Hilbert space of Majorana fermions can be decomposed into common eigenspaces of $\{\hat{u}_{jk}\}$ indexed by the corresponding eigenvalues $u_{jk} = \pm 1$. Thus, the Hamiltonian in the invariant subspace indexed by $u = \{u_{jk}\}$ becomes

$$H_u = \frac{i}{4} \sum_{\langle j, k \rangle} A_{jk} c_j c_k, \quad A_{jk} = 2J_{\alpha(jk)} u_{jk}, \quad (116)$$

where we have replaced \hat{A}_{jk} and \hat{u}_{jk} with their eigenvalues. Note that $u_{jk} \rightarrow -u_{jk}$ upon the Z_2 gauge transformation $u_{jk} \rightarrow D_j u_{jk} D_j$, and it is more convenient to classify the eigenstates of H in terms of the gauge-invariant loop operator $W(j_0, \dots, j_n) = K_{j_n j_{n-1}} \dots K_{j_1 j_0}$, which can be written as

$$W(j_0, \dots, j_n) = \left(\prod_{s=1}^n -i\hat{u}_{j_s j_{s-1}} \right) c_n c_0. \quad (117)$$

The closed-loop operator W_p (see Eq. (108)) is gauge invariant under the Z_2 transformation because $c_n = c_0$, and the gauge-invariant quantities $w = \{w_p\}$ can be used instead of $u = \{u_{jk}\}$ to parameterize the eigenstates, i.e.,

$$H_w = \frac{i}{4} \sum_{\langle j, k \rangle} A_{jk} c_j c_k. \quad (118)$$

For a given set of A_{ij} fixed by $\{w_p\}$, the quadratic Hamiltonian as expressed in Eq. (116) and Eq. (118) can be diagonalized into the following canonical form:

$$H_{\text{canonical}} = \frac{i}{2} \sum_m \epsilon_m c'_m c''_m = \sum_m \epsilon_m \left(f_m^\dagger f_m - \frac{1}{2} \right), \quad (119)$$

where $\epsilon_m \geq 0$, c'_m and c''_m are normal Majorana modes, and $f_m^\dagger = \frac{1}{2}(c'_m - i c''_m)$ and $f_m = \frac{1}{2}(c'_m + i c''_m)$ are the corresponding complex fermion operators. The ground state of the Majorana system has an energy of

$$E = -\frac{1}{2} \sum_m \epsilon_m. \quad (120)$$

We now discuss the system of Majorana fermions on the honeycomb lattice. First, we note that the global ground-state energy does not depend on the signs of the exchange constants J_x , J_y , and J_z . For instance, if J_z is replaced with $-J_z$, we can compensate for this sign change by changing the signs of the variables u_{jk} for all z -links using the gauge operator D_j , leaving the values of A_{jk} and w_p unchanged. Therefore, as far as solving for the ground-state energy and the excitation spectrum is concerned, the signs of the exchange constants J do not matter. However, such a sign change does affect other measurable physical quantities.

Second, it was proven by Lieb (Lieb, 1994) and numerically investigated by Kitaev himself that the ground state of the Majorana system is achieved when the system is in the vortex-free configuration, namely, $w_p = 1$ for all plaquettes p . In this vortex-free configuration, one can solve for the (fermionic) energy spectrum of the Hamiltonian by directly Fourier transforming Eq. (118) to obtain

$$\epsilon_{\mathbf{q}} = \pm |J_x e^{i\mathbf{q} \cdot \mathbf{a}} + J_y e^{i\mathbf{q} \cdot \mathbf{b}} + J_z|, \quad (121)$$

where $\mathbf{a} = (\frac{1}{2}, \frac{\sqrt{3}}{2})$ and $\mathbf{b} = (-\frac{1}{2}, \frac{\sqrt{3}}{2})$ are two basis vectors in the xy coordinates. The fermionic spectrum may

or may not be gapped, depending on whether a solution to the equation $\epsilon_{\mathbf{q}} = 0$ exists. $\epsilon_{\mathbf{q}} = 0$ has a solution if and only if $|J_x|$, $|J_y|$, and $|J_z|$ satisfy the triangle inequalities:

$$|J_x| \leq |J_y| + |J_z|, |J_y| \leq |J_z| + |J_x|, |J_z| \leq |J_x| + |J_y|. \quad (122)$$

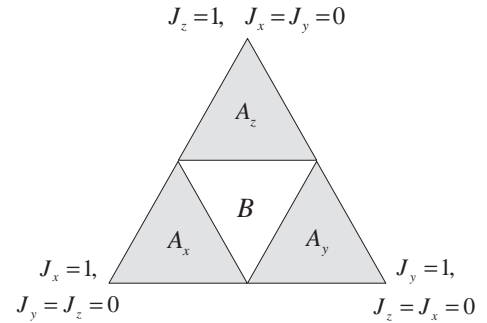


FIG. 15 (Kitaev, 2006) Phase diagram of the Kitaev honeycomb model. The triangle is the section of the positive octant ($J_x, J_y, J_z \geq 0$) that lies in the plane $J_x + J_y + J_z = 1$. The A phase contains three gapped subphases. The B phase is gapless.

As a result, two phases exist in the system of Majorana fermions on the honeycomb lattice, with the phase diagram shown in Fig. 15. The first phase, called the A phase, is gapped and contains three subphases (A_x , A_y , and A_z) in the phase diagram. The second, called the B phase, is gapless. In the A phase, for example, in the A_z subphase, the Hamiltonian expressed in Eq. (106)) can be mapped to the Kitaev toric code model in the limit $|J_x|, |J_y| \ll |J_z|$, and the phase hosts Abelian anyonic excitations. The B phase acquires an energy gap in the presence of a magnetic field. Very interestingly, it hosts stable non-Abelian anyons when the energy gap is opened up by a magnetic field. The B phase is a very attractive state in the context of topological quantum computation. Readers can refer to the recent review article (Nayak *et al.*, 2008) for details.

In addition to the elegant Majorana decomposition method pioneered by Kitaev, other insightful approaches to the Kitaev honeycomb model also exist. For instance, Feng, Zhang and Xiang (Feng *et al.*, 2007) and Chen and Nussinov (Chen and Nussinov, 2008) found that the original Kitaev honeycomb model can be exactly solved with the help of the Jordan-Wigner transformation. This approach provides a topological characterization of the quantum phase transition from the A phase to the B phase. A nonlocal string order parameter can be defined in one of these two phases (Chen and Nussinov, 2008; Feng *et al.*, 2007). In the appropriate dual representations, these string order parameters become local order parameters *after some singular transformation*, and a description of the phase transition in terms of Landau's theory of continuous phase transitions becomes applicable

(Feng *et al.*, 2007). The Jordan-Wigner transformation also enables a fermionization of the Kitaev honeycomb model, allowing it to be mapped to a *p*-wave-type BCS pairing problem. The spin wavefunction can be obtained from the fermion model, and the anyonic character of the vortex excitations in the gapped phase also has an explicit fermionic construction (Chen and Nussinov, 2008).

The Kitaev honeycomb model can also be understood within the framework of fermionic RVB theory. Both confinement-deconfinement transitions from spin liquids to AFM or stripy AF/FM phases and topological quantum phase transitions between gapped and gapless spin liquid phases can be described within the framework of Z_2 gauge theory (Baskaran *et al.*, 2007; Mandal *et al.*, 2011, 2012).

Exact diagonalization has been applied to study the Kitaev honeycomb model on small lattices (Chen *et al.*, 2010). Perturbative expansion methods have been developed to study the gapped phases of the Kitaev honeycomb model and its generalization (Dusuel *et al.*, 2008; Schmidt *et al.*, 2008; Vidal *et al.*, 2008). Several papers (Kells *et al.*, 2009; Lee *et al.*, 2007a; Yu, 2008; Yu and Wang, 2008) have noted the existence of an analogy between the Z_2 vortices in the Kitaev honeycomb model and the vortices in $p + ip$ superconductors.

Enormous efforts have been devoted to searching for exactly solvable generalizations of the Kitaev honeycomb model. It has been proposed that the exact solvability will not be spoiled when the fermion gap is opened for the non-Abelian phase (Lee *et al.*, 2007a; Yu and Wang, 2008). Generalizations to other lattice models and even to three dimensions have also been developed (Baskaran *et al.*, 2009; Lai and Motrunich, 2011; Nussinov and Ortiz, 2009; Ryu, 2009; Tikhonov and Feigel'man, 2010; Wu *et al.*, 2009; Yang *et al.*, 2007; Yao and Kivelson, 2007; Yao and Lee, 2011; Yao *et al.*, 2009). Non-trivial emergent particles, such as chiral fermions (Yao and Kivelson, 2007), have been constructed in these exactly solvable lattice models. These developments have significantly advanced our understanding of emergent phenomena based on solvable models in dimensions greater than one.

The exotic properties of the Kitaev honeycomb model have motivated researchers to search for realizations of this model in realistic materials. It has been demonstrated by Jackeli and Khaliullin (Jackeli and Khaliullin, 2009) and by Chaloupka, Jackeli and Khaliullin (Chaloupka *et al.*, 2010) that a generalization of the Kitaev honeycomb model may indeed arise in layered honeycomb lattice materials in the presence of strong spin-orbit coupling. These authors showed that in certain iridate magnetic insulators (A_2IrO_3 , $A=Li, Na$), the effective low-energy Hamiltonian for the effective $J_{eff} = 1/2$ iridium moments is given by a linear combination of the AFM Heisenberg model (H_H) and

the Kitaev honeycomb model (H_K),

$$H = (1 - \alpha)H_H + 2\alpha H_K, \quad (123)$$

where α , expressed in terms of the microscopic parameters, determines the relative strength of the Heisenberg and Kitaev interactions. Interestingly, the Kitaev honeycomb model can also be realized as the exact low-energy effective Hamiltonian of a spin-1/2 model with spin rotational and time-reversal symmetries (Wang, 2010a). The Heisenberg-Kitaev model (123) exhibits a rich phase diagram. Readers who are interested in these developments may refer to, for example, references (Chaloupka *et al.*, 2010; Jiang *et al.*, 2011; Kimchi and Vishwanath, 2014; Kimchi and You, 2011; Lee *et al.*, 2014; Price and Perkins, 2012; Reuther *et al.*, 2011; Schaffer *et al.*, 2012; Singh *et al.*, 2012; Yu *et al.*, 2013) for details. A comprehensive review on this topic has also been published by Nussinov and van den Brink (Nussinov and van den Brink, 2013).

V. QSL STATES IN REAL MATERIALS

Experimental studies of interacting spins in geometrically frustrated lattices aim at identifying non-trivial and exotic ground states. Among these ground states, spin liquid states have been sought ever since the proposal of the RVB state (Anderson, 1973). This issue has been intensively debated in the context of the spin states behind the high-T_c superconductivity of cuprates. However, before this century, there was no direct observation of spin liquid states. The situation changed in 2003, when an organic Mott insulator with a quasi-triangular lattice was found to exhibit no magnetic ordering even at tens of mK, four orders of magnitude lower than the energy scale of the exchange interactions (Shimizu *et al.*, 2003). The low-temperature state is most likely a form of the sought-after spin liquids. Since then, what can be called spin liquids have been successively reported for quasi-triangular, kagome and hyperkagome lattices. In this section, we review the experimental studies mainly with respect to the magnetic and thermodynamic properties of the materials for which sound experimental data have been accumulated in discussing the presence of spin liquids.

V.1. Anisotropic triangular lattice systems: κ -(ET)₂Cu₂(CN)₃ and EtMe₃Sb[(Pd(dmit)₂)₂]

Both are half-filled band systems with anisotropic triangular lattices, which are isosceles for κ -(ET)₂Cu₂(CN)₃ and three different laterals for EtMe₃Sb[(Pd(dmit)₂)₂] (Kanoda, 2006; Kanoda and Kato, 2011; Kato, 2014). At ambient pressure, they are Mott insulators; however, the spins

are not ordered at low temperatures on the order of tens of mK. A noticeable feature of both systems is that they undergo Mott transitions at moderate pressures 0.4 GPa for κ -(ET)₂Cu₂(CN)₃ (Furukawa *et al.*, 2015a; Komatsu *et al.*, 1996; Kurosaki *et al.*, 2005) and 0.5 GPa for EtMe₃Sb[Pd(dmit)₂]₂ (Kato *et al.*, 2007). (Note that these pressure values indicate pressures applied at room temperature and are reduced by approximately 0.2 GPa at low temperatures.) The temperature-pressure phase diagram of κ -(ET)₂Cu₂(CN)₃ is depicted in Fig. 16. A spin liquid phase resides in proximity to the Mott transition; this feature appears to be a key to the stability of spin liquids and can be closely linked to the metal-insulator transition (Senthil, 2008; Zhou and Ng, 2013). According to the numerical studies of the anisotropic triangular-lattice Hubbard model, the ground states near to the Mott transition are controversial (Kyung and Tremblay, 2006; Laubach *et al.*, 2015; Morita *et al.*, 2002; Tocchio *et al.*, 2013; Watanabe *et al.*, 2008), implying that spin-liquid and magnetic phases are competing very closely and can be easily imbalanced by a tiny perturbation.

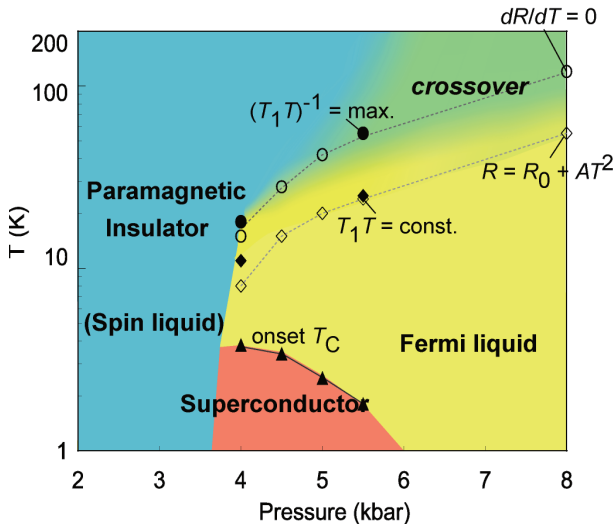


FIG. 16 (Kurosaki *et al.*, 2005) Temperature-pressure phase diagram of the spin-liquid compound with a quasi-triangular lattice, κ -(ET)₂Cu₂(CN)₃, which undergoes a Mott transition at moderate pressure.

i) κ -(ET)₂Cu₂(CN)₃

κ -(ET)₂Cu₂(CN)₃ is a layered compound, where κ -(ET)₂X has a variety of anions X and ET is bis(ethylenedithio)tetrathiafulvalene (Komatsu *et al.*, 1996). κ -(ET)₂X is composed of the ET layers with 1/2 hole per ET and the layers of monovalent anions X⁻, which have no contribution to the electronic conduction or magnetism. In the ET layer, strong ET dimers are formed (ET)₂, each of which accommodates a hole in an anti-bonding orbital of the highest occupied molecular orbital (HOMO) of the ET. As the

anti-bonding band is half-filled and the Coulomb repulsive energy is comparable to the band width, the family of κ -(ET)₂X is good model system to study Mott physics (Kanoda, 1997a,b; Kino and Fukuyama, 1995; Powell and McKenzie, 2011; Shimizu *et al.*, 2006). The estimates of the transfer integrals between the adjacent anti-bonding orbitals on the isosceles triangular lattices, t and t' , are in a range of 50 meV, depending on the method of calculation, e.g., either the molecular orbital (MO)-based tight-binding calculation (Komatsu *et al.*, 1996; Mori *et al.*, 1984, 1999) or the first principles calculation (Kandpal *et al.*, 2009; Koretsune and Hotta, 2014; Nakamura *et al.*, 2009). Nevertheless, one can see that the values have clear systematic variation in terms of anion X, as shown in Fig. 17, where the values of t and t' are calculated via the latter method: the t'/t value of κ -(ET)₂Cu[N(CN)₂]Cl is 0.75 (the MO-based calculations) and 0.44-0.52 (first principles calculations), while that of κ -(ET)₂Cu₂(CN)₃ is 1.06 and 0.80-0.99, respectively, suggestive of high geometrical frustration.

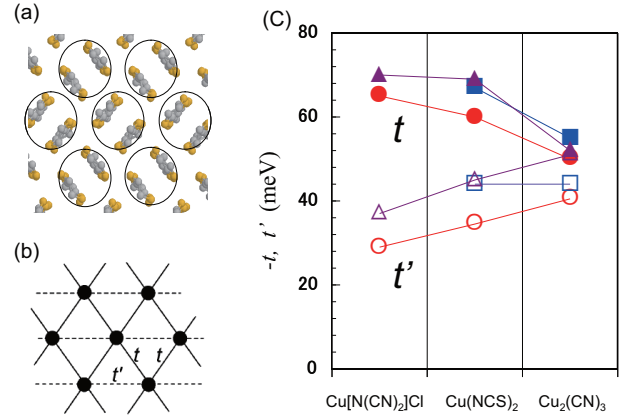


FIG. 17 (a) In-plane structure of the ET layer in κ -(ET)₂X. It is modelled to (b) an anisotropic triangular lattice. (c) First principles calculations of transfer integrals in κ -(ET)₂X for X=Cu[N(CN)₂]Cl, Cu(NCS)₂ and Cu₂(CN)₃ ; squares (Nakamura *et al.*, 2009), circles (Kandpal *et al.*, 2009), and triangles (Koretsune and Hotta, 2014).

The temperature dependence of the spin susceptibility, χ , of κ -(ET)₂Cu₂(CN)₃ differs from that of the less frustrated compound κ -(ET)₂Cu[N(CN)₂]Cl, as seen in Fig. 18 (Shimizu *et al.*, 2003). An abrupt upturn at 27 K in the latter is a manifestation of the antiferromagnetic transition, with a slight spin canting of approximately 0.3 degree (Miyagawa *et al.*, 1995). However, κ -(ET)₂Cu₂(CN)₃ has no anomaly in $\chi(T)$. Its overall behavior features a broad peak, which is reconciled by the triangular-lattice Heisenberg model with an exchange interaction of $J \sim 250$ K. In contrast to κ -(ET)₂Cu[N(CN)₂]Cl, the magnetic susceptibility of κ -(ET)₂Cu₂(CN)₃ may be described by the Heisenberg model because it is situated further from the Mott boundary, while κ -(ET)₂Cu[N(CN)₂]Cl undergoes a Mott tran-

sition at a low pressure (25 MPa) as it is about to enter a metallic state (Kagawa *et al.*, 2005; Lefebvre *et al.*, 2000). There is no indication of magnetic ordering in the susceptibility of κ -(ET)₂Cu₂(CN)₃, at least down to 2 K, the lowest temperature measured. Furthermore, no Curie-like upturn can be identified; the concentration of Cu²⁺ impurity spins detected by ESR is estimated to be less than 0.01 % for κ -(ET)₂Cu₂(CN)₃ (Shimizu *et al.*, 2006).

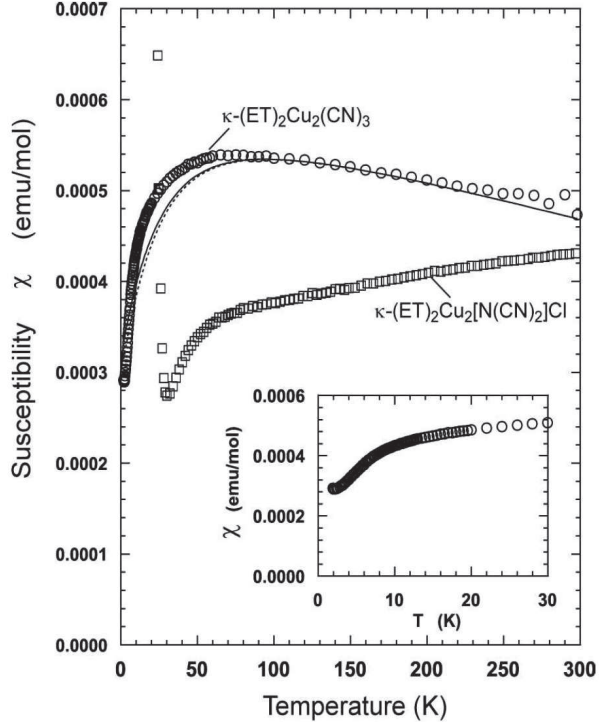


FIG. 18 (Shimizu *et al.*, 2003) Magnetic susceptibility of poly-crystalline κ -(ET)₂Cu₂(CN)₃ and κ -(ET)₂Cu[N(CN)₂]Cl. The core diamagnetic susceptibility has already been subtracted. The solid and dotted lines represent the result of the series expansion of the triangular-lattice Heisenberg model using [6/6] and [7/7] Padé approximations with $J = 250$ K. The susceptibility of κ -(ET)₂Cu₂(CN)₃ below 30 K is expanded in the inset.

The detailed spin states can be examined by performing NMR measurements, which probe the static and dynamical hyperfine fields at the nuclear sites. Fig. 19 shows the single-crystal ¹H NMR spectra for the two compounds (Shimizu *et al.*, 2003). A clear line splitting in κ -(ET)₂Cu[N(CN)₂]Cl at 27 K is evidence for commensurate antiferromagnetic ordering, with the moment estimated to be 0.45 μ B per ET dimer in separate ¹³C NMR studies (Miyagawa *et al.*, 2004). However, the spectra for κ -(ET)₂Cu₂(CN)₃ shows neither a distinct broadening nor splitting down to 32 mK, which is four orders of magnitude lower than the J value of 250 K. This indicates the absence of long-range magnetic ordering. The absence of ordering is also cor-

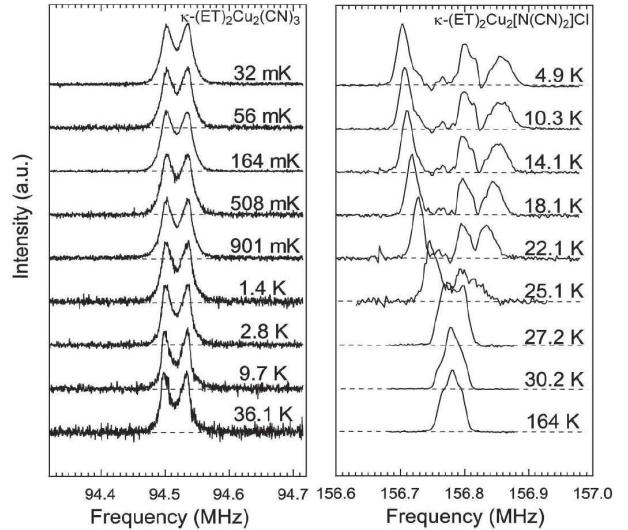


FIG. 19 (Shimizu *et al.*, 2003) ¹H NMR spectra for single crystals of κ -(ET)₂Cu₂(CN)₃ and κ -(ET)₂Cu[N(CN)₂]Cl.

roborated by zero field μ SR experiments (Pratt *et al.*, 2011). The nuclear spin lattice relaxation rate, $1/T_1$, which probes the spin dynamics, behaves similarly at the ¹H and ¹³C sites. Fig. 20 shows $1/T_1$ at the ¹³C sites, which decreases monotonically with a square-root temperature dependence down to 10 K and exhibits a dip-like anomaly at approximately 6 K (Shimizu *et al.*, 2006). Below 6 K, $1/T_1$ levels off down to 1 K or lower, followed by a steep decrease approximated by $T^{3/2}$ at even lower temperatures. The two anomalies at 6 K and 1.0 K are obvious. However, they are not so sharp as to be considered as phase transitions. Due to the large hyperfine coupling of the ¹³C sites located in the central part of ET, an electronic inhomogeneity gradually developing on cooling is captured by spectral broadening, which is enhanced at approximately 6 K and saturates below 1 K (Kawamoto *et al.*, 2006; Shimizu *et al.*, 2006). The detailed NMR (Shimizu *et al.*, 2006) and μ SR (Pratt *et al.*, 2011) measurements point to the field-induced emergence of staggered-like moments, which is distinct from the conventional magnetic order. A separate μ SR study (Nakajima *et al.*, 2012) suggests a phase separation. The degree of inhomogeneity in the ¹³C relaxation curve, which is characterized by the deviation of the exponent in the stretched exponential fitting of the relaxation curve (see Inset of Fig. 20), increases below 5-6 K (Shimizu *et al.*, 2006). The ¹H relaxation curve also starts to bend at the much lower temperatures, e.g., below 0.4 K, and fits to a roughly equally weighed sum of two exponential functions, the $1/T_1$'s of which are proportional to T and T^2 . No appreciable field dependence of the ¹³C relaxation rate is observed between 2 T and 8 T. There is no experimental indication of a finite excitation gap in any of the magnetic measurements.

Thermodynamic investigations were conducted by

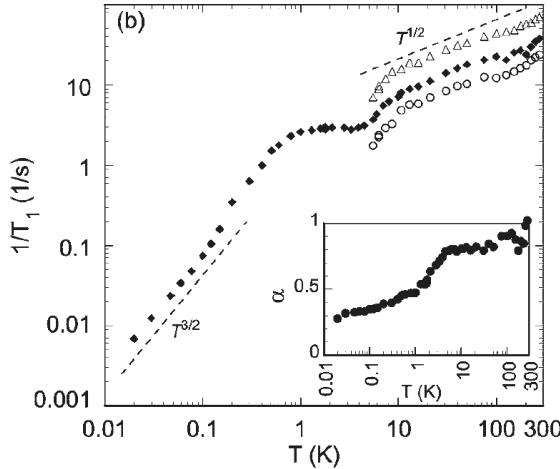


FIG. 20 (Shimizu *et al.*, 2006) ^{13}C nuclear spin-lattice relaxation rate for a single crystal of κ -(ET) $_2$ Cu $_2$ (CN) $_3$. The open triangles and circles represent the relaxation rates of two separated lines coming from two non-equivalent carbon sites in an ET. At low temperatures below 5 K, the two lines merge and are not distinguished. The inset shows the exponent in the stretched exponential fitting to the relaxation curves of the whole spectra, whose relaxation rates are plotted using closed diamonds.

means of the specific heat and thermal conductivity measurements. Fig. 21 shows the specific heat for κ -(ET) $_2$ Cu $_2$ (CN) $_3$ and several Mott insulators with antiferromagnetic spin ordering (Yamashita *et al.*, 2008b). For all of the antiferromagnetic materials, the electronic specific heat coefficient, γ , is vanishing, as expected for insulators. For the κ -(ET) $_2$ Cu $_2$ (CN) $_3$ spin liquid system, however, the extrapolation of the C/T vs. T^2 line to absolute zero yields $\gamma=12\sim15$ mJ/K 2 mol. The linearity holds down to 0.3 K, below which a nuclear Schottky contribution overwhelms the electronic contribution to C . The finite value despite the Mott insulating state is a marked feature of spin liquids and suggests fermionic excitations in the spin degrees of freedom. Interestingly, the low-temperature susceptibility and the γ value give the Wilson ratio on the order of unity. A spinon Fermi sea is an intriguing model for this phenomenon (Motrunich, 2005). However, neither the $U(1)$ spin liquid, where C follows $T^{2/3}$ scaling, nor the Z_2 spin liquid, where C is gapped, reconciles the observed features in their original forms. Randomness may be an optional parameter to modify the temperature dependence. Another interesting feature is the field-insensitivity up to 8 T, which appears incompatible with the $U(1)$ spin liquid states with Dirac cones.

Thermal transport measurements result in somewhat controversial consequences (Yamashita *et al.*, 2008a). The thermal conductivity divided by the temperature tends to vanish with decreasing temperature, as shown in Fig. 22. The gap, if one is present, is estimated to be

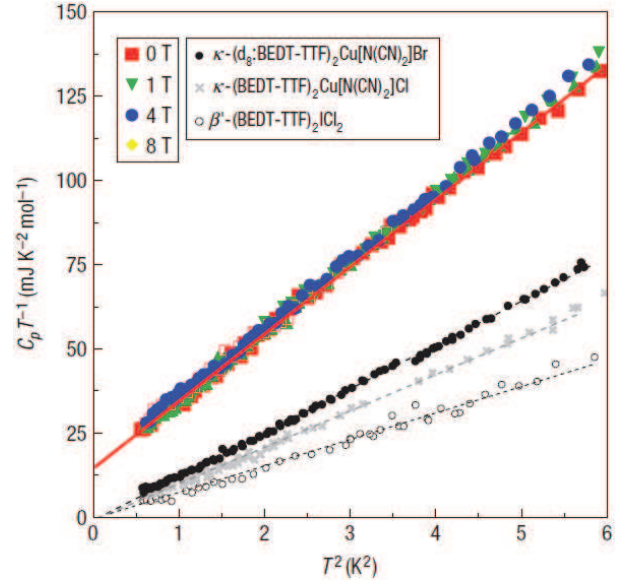


FIG. 21 (Yamashita *et al.*, 2008b) Low-temperature specific heat C_p of κ -(ET) $_2$ Cu $_2$ (CN) $_3$ for several magnetic fields up to 8 T in C_p/T versus T^2 plots. Those of antiferromagnetic insulators κ -(ET) $_2$ Cu[N(CN) $_2$]Cl, deuterated κ -(ET) $_2$ Cu[N(CN) $_2$]Br and β -(ET) $_2$ ICl $_2$ are also plotted for comparison.

0.43 K, which is quite small compared with the exchange energy of 250 K. The extremely small gap may indicate a gapped Z_2 spin liquid located near a quantum critical point. The discrepancy between the thermal transport and NMR and specific heat data remains an open issue. It may be attributed to the Anderson localization of spinons.

The 6-K anomaly in the NMR spectrum and relaxation rate also manifests itself in the specific heat (Yamashita *et al.*, 2008b) and thermal conductivity (Yamashita *et al.*, 2008a) as a hump and a shoulder, respectively, indicating that the anomaly is thermodynamic, as well as magnetic. However, the thermal expansion coefficient shows a cusp (Manna *et al.*, 2010) and the ultrasonic velocity shows a dip-like minimum, signifying lattice softening at approximately 6 K (Poirier *et al.*, 2014). In view of these results, this anomaly is likely associated with spin-lattice coupling. Instabilities of the spinon Fermi surfaces (e.g., (Galitski and Kim, 2007; Grover *et al.*, 2010; Lee and Lee, 2005; Zhou and Lee, 2011)) are among the possible origins of the anomaly.

Although the spin liquid is insulating, anomalous charge dynamics are suggested for the low-energy optical and dielectric responses. The optical gap for κ -(ET) $_2$ Cu $_2$ (CN) $_3$ is much smaller than that for κ -(ET) $_2$ Cu[N(CN) $_2$]Cl, although the former system is situated further from the Mott transition than the latter (Kézsmárki *et al.*, 2006). It is proposed that gapless spinons are responsible for low-energy optical absorption inside the Mott gap (Ng and Lee, 2007).

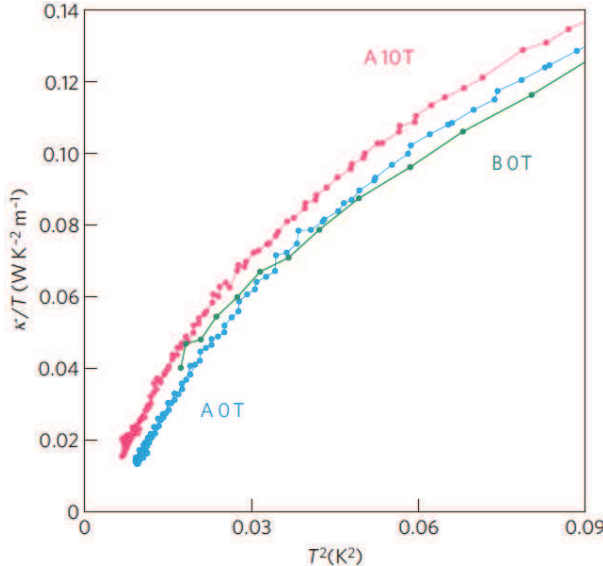


FIG. 22 (Yamashita *et al.*, 2008a) Low-temperature thermal conductivity κ of κ -(ET)₂Cu₂(CN)₃ (samples A and B) in κ/T versus T^2 plots. Sample A was investigated at 10 T applied perpendicular to the basal plane, as well as at 0 T.

The dielectric (Abdel-Jawad *et al.*, 2010), microwave (Poirier *et al.*, 2012) and terahertz (Itoh *et al.*, 2013) responses are enhanced at low temperatures. The possible charge-imbalance excitations within the dimer are theoretically proposed (Dayal *et al.*, 2011; Hotta, 2010; Naka and Ishihara, 2010).

ii) EtMe₃Sb[(Pd(dmit)₂)₂]

This compound is a member of the A[(Pd(dmit)₂)₂] family of materials, which contain a variety of monovalent cations such as $A^+ = Et_xMe_{4-x}Z^+$ (Et = C₂H₅, Me = CH₃, Z = N, P, As, Sb, and $x = 0, 1, 2$), where dmit is 1,3-dithiole-2-thione-4,5-dithiolate (Kato, 2014). A[(Pd(dmit)₂)₂] is a layered system composed of conducting Pd(dmit)₂ layers and insulating A layers. In the conducting layers, Pd(dmit)₂ is strongly dimerized as in κ -(ET)₂X, whereas the [Pd(dmit)₂]₂ dimer accepts an electron from cation A^+ instead of the hole in ET₂⁺. A prominent feature of the A[(Pd(dmit)₂)₂] family is that the transfer integrals of the three laterals in the triangular lattice can be finely tuned via chemical substitution of $A^+ = Et_xMe_{4-x}Z^+$ (Kato, 2014). Their first principles calculations are shown in Fig. 23 (Tsumuraya *et al.*, 2013). The spin liquid material EtMe₃Sb[(Pd(dmit)₂)₂] is in a region where the three transfer integrals are equalized. As expected, the materials situated outside of this region have antiferromagnetic ground states. The alloying of the boundary materials offers the chance to study possible critical regions between spin liquids and ordered states (Kato, 2014). There is a charge-ordered material near the spin liquid, suggesting that the charge cannot always be assumed to be separate degrees of freedom from the spin physics.

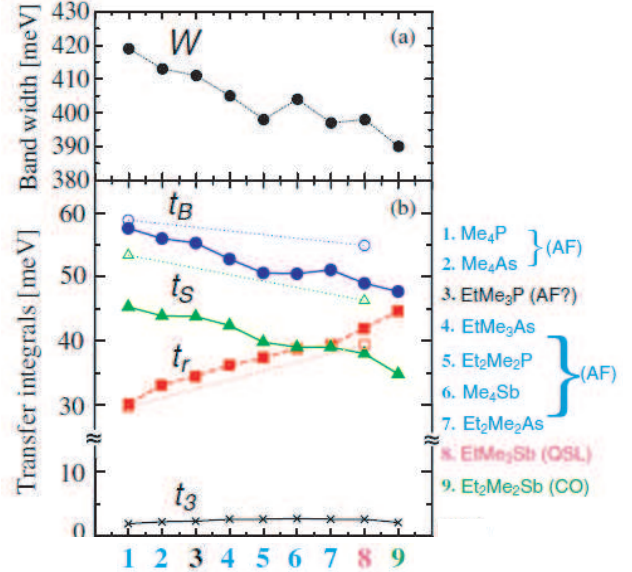


FIG. 23 (Tsumuraya *et al.*, 2013) First principles calculations of band width W (a) and transfer integrals (b) in A[(Pd(dmit)₂)₂] for various cations, A. The Pd(dmit)₂ layers are modeled to triangular lattices characterized by transfer integrals, t_B , t_S and t_r . t_3 is the interlayer transfer integral. AF, QSL and CO stand for antiferromagnet, quantum spin liquid and charge-ordered insulator.

Below, we review the properties of EtMe₃Sb[(Pd(dmit)₂)₂] and other related materials.

The magnetic susceptibility of EtMe₃Sb[(Pd(dmit)₂)₂] shows a broad peak at approximately 50 K and points to a finite value in the low-temperature limit without any anomaly down to 2 K, as shown in Fig. 24 (Kanoda and Kato, 2011; Kato, 2014), which is reminiscent of κ -(ET)₂Cu₂(CN)₃. The fitting of the triangular lattice Heisenberg model to the data yields an exchange interaction of 220 K to 280 K, which is nearly the same as for κ -(ET)₂Cu₂(CN)₃. Also shown are the susceptibilities of antiferromagnetic and charge-ordered insulators, which exhibit small kink signaling of magnetic ordering and a sudden decrease indicative of a spin gapful state, respectively, despite their similar behaviors at high temperatures (Tamura and Kato, 2002). This indicates that the diversity in the ground states is an outcome of low-energy physics, while the same diversity is not distinguished at high energy scales.

The ¹³C NMR captures no signature of magnetic ordering down to 20 mK, although a slight broadening equivalent to the broadening for κ -(ET)₂Cu₂(CN)₃ is observed at low temperatures (Itou *et al.*, 2010). The temperature dependence of the ¹³C nuclear spin-lattice relaxation rate is shown in Fig. 25 (Itou *et al.*, 2010). It exhibits a non-monotonic temperature dependence. At low temperatures below 1 K, it follows a T^2 dependence, suggesting no finite gap. However, the power of 2 implies a complicated nodal gap, which is not obviously consistent with

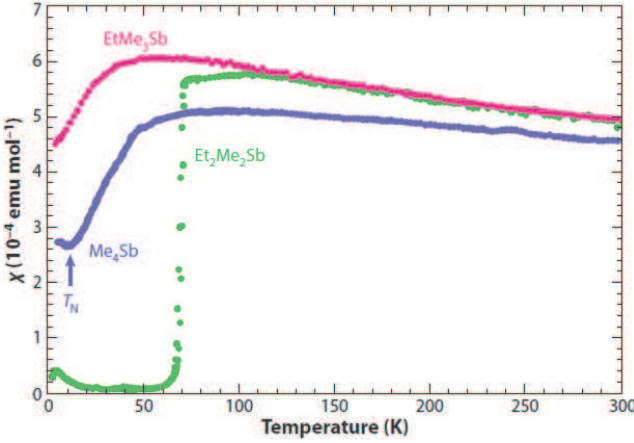


FIG. 24 (Kato, 2014) Magnetic susceptibility of an antiferromagnet $\text{Me}_4\text{Sb}[(\text{Pd}(\text{dmit})_2)_2]$, a spin liquid $\text{EtMe}_3\text{Sb}[(\text{Pd}(\text{dmit})_2)_2]$ and a charge-ordered insulator $\text{Et}_2\text{Me}_2\text{Sb}[(\text{Pd}(\text{dmit})_2)_2]$. The core diamagnetic susceptibility has already been subtracted.

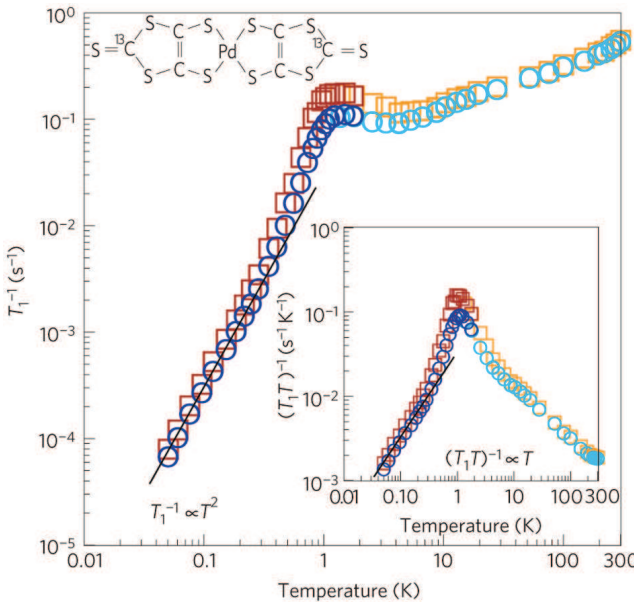


FIG. 25 (Itou *et al.*, 2010) ^{13}C nuclear spin-lattice relaxation rate $1/T_1$ of $\text{EtMe}_3\text{Sb}[\text{Pd}(\text{dmit})_2]_2$. Inset shows the $1/T_1T$ versus T plots. The circles indicate the values determined from the stretched-exponential fitting to the relaxation curves and the squares denote the values determined from the initial decay slopes of the relaxation curves.

the finite susceptibility value and the thermodynamic measurements described below. Furthermore, $1/T_1$ forms a shoulder or a kink at approximately 1 K and becomes moderate in temperature dependence above 1 K. The kink temperature increases for higher magnetic fields or frequencies. The relaxation curve becomes a non-single exponential curve below 10 K but reverses below 1 K, indicating that the inhomogeneity increases below 10 K (Itou *et al.*, 2010, 2011). The reversal at 1 K can be an

indication of either a recovery in the homogeneity below 1 K or the microscopic nature of the inhomogeneity, which is subject to spin-diffusion averaging of the heterogeneous relaxation time that is longer at lower temperatures. The 1-K relaxation-rate anomaly in $\text{Et}_2\text{Me}_2\text{Sb}[(\text{Pd}(\text{dmit})_2)_2]$ may be compared to the broad anomaly around nearly the same temperature for $\kappa-(\text{ET})_2\text{Cu}_2(\text{CN})_3$. However, they appear different with respect to field (or frequency) dependence and spatial scale of inhomogeneity.

The thermodynamic measurements are indicative of fermionic low-energy excitations. Fig. 26 shows the temperature dependence of the specific heat (*Yamashita et al.*, 2011). The linearity of C/T versus T^2 in $\text{EtMe}_3\text{Sb}[(\text{Pd}(\text{dmit})_2)_2]$ is extrapolated to a zero Kelvin to give a finite value of γ , whereas other Mott insulators appear to have vanishing γ , as expected for conventional insulators. There is no field dependence in C/T in $\text{EtMe}_3\text{Sb}[(\text{Pd}(\text{dmit})_2)_2]$ up to 8 T, as in $\kappa-(\text{ET})_2\text{Cu}_2(\text{CN})_3$. The thermal conductivity results are consistent with the specific heat results, as seen in Fig. 27, where the low-temperature κ/T value for $\text{EtMe}_3\text{Sb}[(\text{Pd}(\text{dmit})_2)_2]$ is as high as 0.2 $\text{W K}^{-2}\text{m}$ in the zero-Kelvin limit, implying the presence of gapless thermal transporters with fermionic statistics (*Yamashita et al.*, 2010). The mean free path for thermal transport is estimated to be of the order of 1 μm . κ is enhanced by the application of a magnetic field above a threshold value, suggesting that the gapped excitations coexist with the gapless excitations (*Yamashita et al.*, 2010).

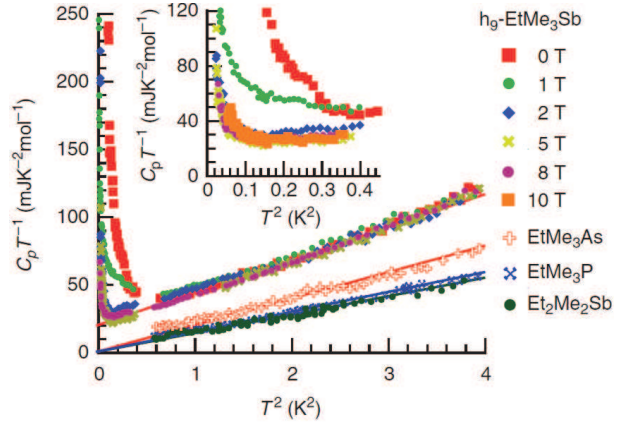


FIG. 26 (Yamashita *et al.*, 2011) Low-temperature specific heat C_p of $\text{EtMe}_3\text{Sb}[\text{Pd}(\text{dmit})_2]_2$ for several magnetic fields up to 10 T in C_p/T versus T^2 plots. The data of other insulating systems, i.e., $\text{Et}_2\text{Me}_2\text{As}[(\text{Pd}(\text{dmit})_2)_2]$, $\text{EtMe}_3\text{As}[(\text{Pd}(\text{dmit})_2)_2]$ and $\text{EtMe}_3\text{P}[(\text{Pd}(\text{dmit})_2)_2]$, are also plotted for comparison. A large upturn below 1 K is probably attributable to the rotational tunneling of Me groups. The low-temperature data are expanded in the inset.

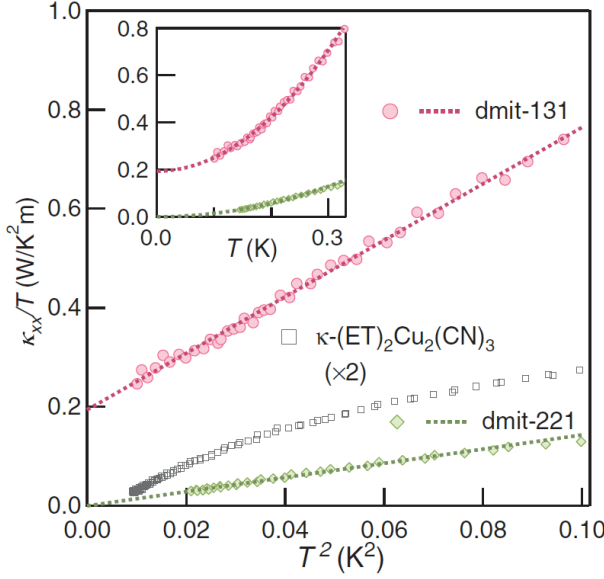


FIG. 27 (Yamashita *et al.*, 2010) Low-temperature thermal conductivity κ of $\text{EtMe}_3\text{Sb}[\text{Pd}(\text{dmit})_2]_2$ (dmit-131) in κ/T versus T^2 and κ/T versus T (inset) plots. The data of other insulators, i.e., $\text{Et}_2\text{Me}_2\text{Sb}[\text{Pd}(\text{dmit})_2]_2$ (dmit-221, non-magnetic) and $\kappa-(\text{ET})_2\text{Cu}_2(\text{CN})_3$, are also plotted for comparison.

V.2. Kagome-lattice system: $\text{ZnCu}_3(\text{OH})_6\text{Cl}_2$

The kagome lattice is constructed by using corner-sharing triangles in contrast to the edge-sharing in the triangular lattices, as shown in Fig. 8. Thus, the spin states in the kagome lattice have larger degeneracy than those in the triangular lattices, leading to high potential for hosting a spin liquid. Actually, the theoretical perspective of seeking a spin liquid is more promising for the kagome-lattice Heisenberg model than for the triangular lattice (Lecheminant *et al.*, 1997; Mila, 1998; Misguich and Lhuillier, 2004; Sachdev, 1992). Among several candidates for the kagome spin systems, we select a spin-1/2 system, $\text{ZnCu}_3(\text{OH})_6\text{Cl}_2$, which is known as herbertsmithite, whose magnetism has been extensively investigated. This is a member of a family of materials with variable compositions, i.e., $\text{Zn}_x\text{Cu}_{4-x}(\text{OH})_6\text{Cl}_2$ ($0 < x < 1$). As an end material, $\text{Cu}_4(\text{OH})_6\text{Cl}_2$ has a distorted pyrochlore lattice of $S = 1/2$ Cu^{2+} spins, whereas the other end material, $\text{ZnCu}_3(\text{OH})_6\text{Cl}_2$, has a two-dimensional ($a - b$ plane) perfect kagome-lattice of Cu^{2+} spins separated by different crystallographic sites occupied by Zn^{2+} (Shores *et al.*, 2005). The structural symmetry changes across $x = 0.33$, above which Cu^{2+} partially occupies the Zn sites in addition to the kagome lattice. There is an argument for the mixture of Zn in the kagome sites in $\text{ZnCu}_3(\text{OH})_6\text{Cl}_2$. Magnetic susceptibility (Bert *et al.*, 2007) and specific heat (de Vries *et al.*, 2008) suggest that approximately 6% of the kagome sites are replaced by non-magnetic Zn. The same amount of

Cu is assumed to invade the nominal Zn sites. Thus, significant efforts have been made to extract the intrinsic properties of the kagome lattice from the experimental data.

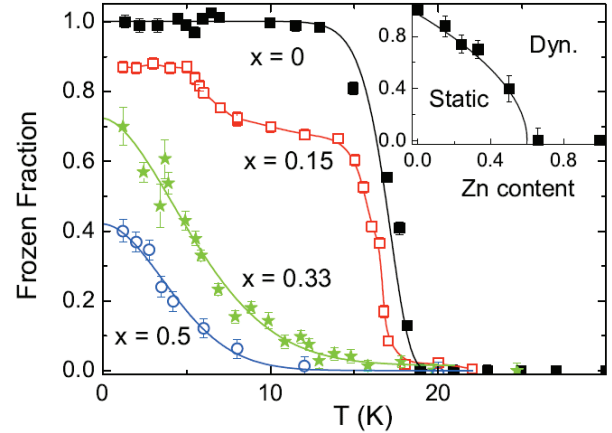


FIG. 28 (Mendels *et al.*, 2007) Temperature variation of the spin-frozen fraction determined by muon spin rotation experiments for $\text{Zn}_x\text{Cu}_{4-x}(\text{OH})_6\text{Cl}_2$. Inset shows the x -dependence of the spin-frozen fraction at a low temperature.

Experimental evidence for the absence of magnetic ordering in $\text{ZnCu}_3(\text{OH})_6\text{Cl}_2$ can be obtained from μSR experiments (Mendels *et al.*, 2007). The relaxation profile shows no internal field down to 50 mK. The experiments for a wide range of x found that the absence of an internal field was persistent in a certain range below $x = 1$ (see Fig. 28) (Mendels *et al.*, 2007). The magnetic susceptibility exhibits a Curie-Weiss behavior at high temperatures above 100 K, as shown in Fig. 29 (Helton *et al.*, 2007). The Weiss temperature is ~ 300 K, which implies an antiferromagnetic exchange interaction of $J = 17$ meV. The dc and ac magnetic susceptibility indicates no magnetic ordering down to 0.1 K and 0.05 K, respectively, which is four orders of magnitude lower than J (Helton *et al.*, 2007). The susceptibility increases progressively at lower temperatures. Two mechanisms are possible. First, impurities from Cu/Zn inter-site mixing can give a Curie-like upturn. Second, Dzyaloshinsky-Moriya interactions may be present between the adjacent sites with broken inversion symmetry, as in the kagome lattice (Rigol and Singh, 2007). The high-field magnetization measurements suggest that the former is mainly responsible for the increasing susceptibility (Bert *et al.*, 2007).

NMR, which probes magnetism in a site-selective manner, was informative particularly for this material because the analysis of spectra allows one to distinguish the intrinsic magnetism from the extrinsic one. The NMR spectra at ^{35}Cl and ^{17}O sites are broad (Imai *et al.*, 2008; Olariu *et al.*, 2008), reflecting the inhomogeneous local fields, supposedly due to the Zn/Cu mixture. However, the smallest shift value in the broad ^{35}Cl spec-

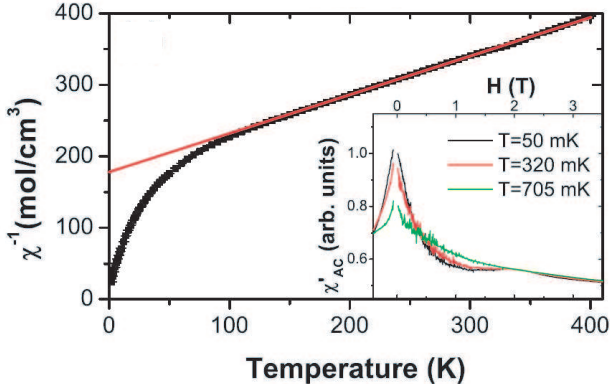


FIG. 29 (Helton *et al.*, 2007) Temperature dependence of the inverse magnetic susceptibility χ^{-1} of $\text{ZnCu}_3(\text{OH})_6\text{Cl}_2$. The line denotes a Curie-Weiss fit. Inset: ac susceptibility (at 654 Hz) at low temperatures.

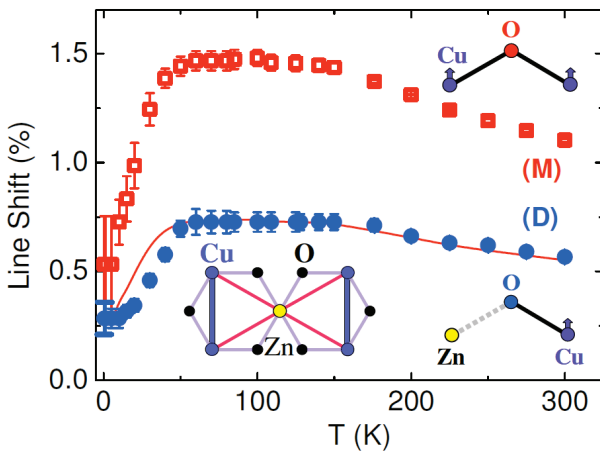


FIG. 30 (Olariu *et al.*, 2008) ^{17}O NMR shift of two lines (M and D) decomposed from the observed spectra for a powder of $\text{ZnCu}_3(\text{OH})_6\text{Cl}_2$. The M and D lines are considered to come from the oxygen sites depicted in the inset. The red curve represents the trace of a half of the value of the M line. The sketch in the lower left corner illustrates the environment of a Zn substituted on the Cu kagome plane, and thick lines represent Cu-Cu dimers.

trum follows a Curie-Weiss law down to 25 K, followed by a decrease at lower temperatures (Imai *et al.*, 2008). This is considered to indicate intrinsic magnetism for the kagome lattice (Imai *et al.*, 2008). The ^{17}O probes the kagome sites more preferentially than the nominal Zn sites due to larger hyperfine coupling with the kagome sites (Olariu *et al.*, 2008). The ^{17}O NMR spectra were decomposed into two components. One is from the ^{17}O sites coordinated by two Cu^{2+} ions, while the other is from the ^{17}O sites coordinated by a Cu^{2+} and a Zn^{2+} in the kagome plane. The relative fraction of the two components was consistent with a 6 % Zn admixture. The NMR shifts of the respective components, as shown in Fig. 30, are considered to be local susceptibilities at Cu sites with and without Zn^{2+} at the neighboring sites

(Olariu *et al.*, 2008). Both decrease below 50 K and saturate to finite values, indicating the gapless nature of the spin excitations. The low-temperature decrease in the shift at the Cu site with a Zn neighbor is in contrast to the enhancement commonly observed in the neighborhood of non-magnetic impurities (Olariu *et al.*, 2008). This behavior also suggests that the Curie-like upturn in the bulk susceptibility at low temperatures is not from the kagome plane. For the NMR relaxation rate, all of the O, Cl and Cu nuclear spins exhibit power-laws against temperature down to 0.47 K for O and 2 K or lower for Cl and Cu, indicating a gapless spin liquid (see Fig. 31) (Imai *et al.*, 2008; Olariu *et al.*, 2008). Although the power somewhat depends on the nuclear site, the relaxation profile is overall nuclear site-insensitive, which is filtered by the nuclear site-specific form-factor determined by its location relative to the kagome lattice, suggesting non-dispersive spin dynamics. Otherwise, the temperature profile of the relaxation rate would be site-dependent (Olariu *et al.*, 2008). This feature is potentially relevant to the spinon excitation with the continuum. More recently, NMR experiments performed at low temperatures have revealed an anomaly in the relaxation rate at a temperature depending on the applied field, which may signify field-induced spin freezing (Jeong *et al.*, 2011). Very recently, a ^{17}O NMR experiment performed with a single crystal has found different features from those observed so far in the powder samples (Fu *et al.*, 2015). According to the analysis of NMR spectra, there is no significant contamination of Zn in the Cu sites within the kagome plane, and the Knight shift shows appreciable temperature- and field-dependences, suggesting a spin gap of the order of 10 K, as shown in FIG 32, in contradiction with the consequences of the earlier NMR and neutron (see below) experiments.

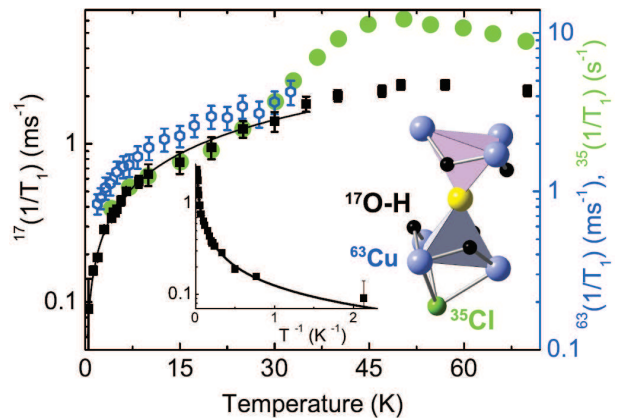


FIG. 31 (Imai *et al.*, 2008; Olariu *et al.*, 2008) ^{17}O , ^{63}Cu and ^{35}Cl nuclear spin-lattice relaxation rates $1/T_1$ for a powder of $\text{ZnCu}_3(\text{OH})_6\text{Cl}_2$. Inset shows ^{17}O $1/T_1$ versus $1/T$ plots.

The low-temperature specific heat was investigated under external magnetic fields (Helton *et al.*, 2007;

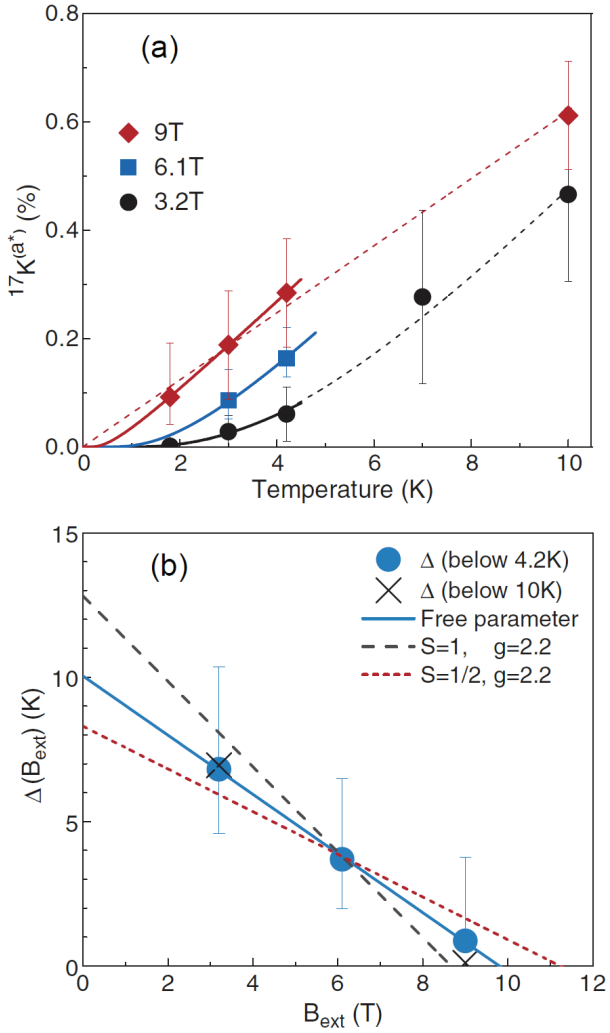


FIG. 32 (Fu *et al.*, 2015) Temperature dependence of ^{17}O Knight shift (a) and the field dependence of the spin gap deduced from the Knight shift for a single-crystal $\text{ZnCu}_3(\text{OH})_6\text{Cl}_2$.

de Vries *et al.*, 2008). As shown in Fig. 33(a) (Helton *et al.*, 2007), there is an enormous field dependence. The temperature dependence at a zero field is approximated by a power law T^α with α unity or smaller (see Fig. 33(b)). The broad peak present even at a zero field is shifted to higher temperatures under higher fields. Assuming that the field-dependent peak is a Schottky contribution associated with a field-induced gap, the data for different fields were analyzed in detail to reveal the intrinsic specific heat of the kagome lattice (de Vries *et al.*, 2008). The deduced Schottky component is consistent with Zeeman splitting of the 6% Cu impurities in the Zn sites at higher fields, and the intrinsic C/T follows a power law T^α with $\alpha = 1.3$ as the best estimate, suggesting gapless excitations (Helton *et al.*, 2007; Shaginyan *et al.*, 2011; de Vries *et al.*, 2008).

Neutron-scattering experiments, which are capable of

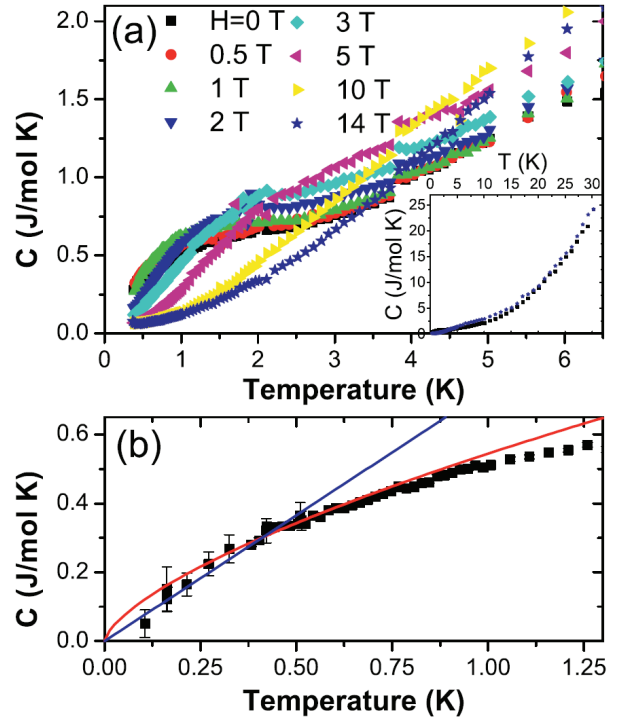


FIG. 33 (Helton *et al.*, 2007) (a) Specific heat C of $\text{ZnCu}_3(\text{OH})_6\text{Cl}_2$ in various applied fields. Inset shows C over a wider temperature range in applied fields of 0 T (square) and 14 T (star). (b) C in a zero field at low temperatures. The lines represent power law fits.

profiling spin excitations with respect to momentum and energy transfers, are available for herbertsmithite. One of the key issues of elementary excitations in spin liquids is the possible fractionalization of $S = 1$ spin excitations into $S = 1/2$ spinons, which could manifest themselves as a continuum in the spin excitation spectrum, *i.e.*, dynamic structure factor $S(\mathbf{Q}, \omega)$, where \mathbf{Q} and ω are momentum transfer and energy transfer divided by \hbar , respectively. Such a continuum is observed in a highly anisotropic triangular-lattice system, Cs_2CuCl_4 , ($J'/J \sim 3$ and $J' 0.34$ meV in Fig. 17), although it undergoes a magnetic transition into a spin-spiral order at 0.62 K (Coldea *et al.*, 2001, 2003). Several features signifying the continuum are found via neutron experiments of herbertsmithite, which were first performed for polycrystalline or powder samples. The inelastic scattering experiments exhibit no excitation gap at least down to 0.1 meV, which corresponds to $\sim J/170$, and insensitivity of the scattering strength to \mathbf{Q} , indicating gapless and local natures of spin fluctuations (Helton *et al.*, 2007). Furthermore, the scattering intensity is only weakly dependent on ω up to 25 meV and temperature up to 120 K and shifts toward lower \mathbf{Q} as temperature is increased (de Vries *et al.*, 2009). Some of the results are displayed in Fig. 34. All these features are suggestive of a continuum in spin excitations and the persistence of the short-

range nature of spin correlations even at low temperatures. Recent experiments on a large single crystal have succeeded in capturing the continuum nature, as seen in the green area in Fig. 35. The momentum profile of the excitation intensity (dynamic structure factor), $S(\mathbf{Q}, \omega)$, is approximately reproduced by the simulated structure factor of uncorrelated dimer-singlets, which indicates to the short-ranged spin correlations at least down to 1.6 K (Han *et al.*, 2012). The short-range nature that persists even at low temperatures, as suggested by the powder experiments as well, is generally in favor of a gapped state, whereas there is no indication of a spin gap down to 0.25 meV at any \mathbf{Q} values in the excitation spectra (Han *et al.*, 2012). It is puzzling that spin dynamic correlation exhibits short-range RVB nature while the spectrum is gapless. One possibility is that the Herbertsmithite is in a Z_2 spin liquid in close proximity to a critical point to the $U(1)$ Dirac liquid, as indicated by some recent numerical works (Li, 2016), although the true ground state of the isotropic Heisenberg model on a kagome lattice is still under debate (Iqbal *et al.*, 2016).

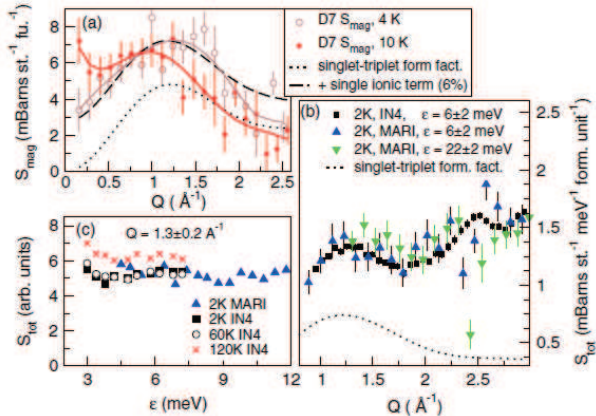


FIG. 34 (de Vries *et al.*, 2009) (a) Instantaneous magnetic correlations at 4 K and 10 K for a time scale corresponding to approximately 6.5 meV. The solid lines are a guide to the eye. (b) The Q dependence in the dynamic correlations with the energy integration interval indicated in the legend. The dotted line in panel (a) and (b) is the structure factor for dimer-like AF correlations. The dashed line, a single-ion contribution corresponding to the 6% antisite spins in this system, is added. (c) The energy and temperature dependence at $Q=1.3 \text{\AA}^{-1}$. D7, IN4 and MARI in the legends stand for the types of spectrometers used.

V.3. Hyperkagome-lattice system: $\text{Na}_4\text{Ir}_3\text{O}_8$

The hyperkagome lattice is a three-dimensional network of corner-sharing triangular lattices. In $\text{Na}_4\text{Ir}_3\text{O}_8$, the Ir^{4+} ion with $5d^5$ electrons likely takes on a low-spin state. These ions locate on the corners, forming a $S=1/2$ hyperkagome lattice (Okamoto *et al.*, 2007).

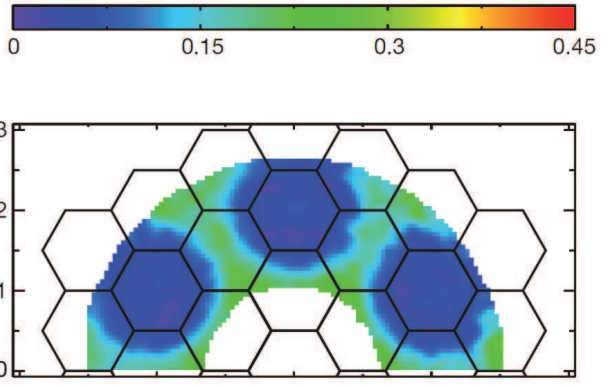


FIG. 35 (Han *et al.*, 2012) Contour plot of dynamical structure factor, $\text{Smag}(\mathbf{Q}, \omega)$, integrated over $1 \leq \hbar\omega \leq 9 \text{ meV}$ for a single-crystal $\text{ZnCu}_3(\text{OH})_6\text{Cl}_2$ at 1.6 K. The intense scattering is extended in a green-colored region, without peaking at any specific points.

The resistivity of the ceramic sample is 10 Ohmcm at room temperature. The samples are semiconducting, with a charge transport gap of 500 K, implying the proximity of this system to the Mott transition, which is different from the kagome materials reviewed above (Okamoto *et al.*, 2007). A connection between the spin liquid and the metal-insulator transition, similar to the case of $\kappa-(\text{ET})_2\text{Cu}_2(\text{CN})_3$, is shown (Podolsky *et al.*, 2009). A distinct feature of $\text{Na}_4\text{Ir}_3\text{O}_8$ among spin liquid candidates is its large spin-orbit coupling, which introduces additional interest to the physics of spin liquids (Chen and Balents, 2008; Zhou *et al.*, 2008). Several theoretical studies propose that $\text{Na}_4\text{Ir}_3\text{O}_8$ is a 3D QSL with fermionic spinons (Lawler *et al.*, 2008; Zhou *et al.*, 2008).

Fig. 36(a) shows the magnetic susceptibility of $\text{Na}_4\text{Ir}_3\text{O}_8$, which weakly increases with decreasing temperature, as characterized by the Curie-Weiss temperature of -650 K (Okamoto *et al.*, 2007). This implies an antiferromagnetic interaction of hundreds of Kelvin. There is no clear indication of magnetic ordering at least down to 2 K, whereas a small anomaly reminiscent of spin glass observed in the magnetization history against the field/temperature variation is attributed to a tiny fraction of the total spins (Okamoto *et al.*, 2007).

The electronic (magnetic) contribution to the specific heat of $\text{Na}_4\text{Ir}_3\text{O}_8$, as shown in Fig. 36(b), has a broad peak at 20 K. However, no anomaly signifying magnetic ordering is apparent (Okamoto *et al.*, 2007). The magnetic entropy estimated by integrating the C/T in Fig. 36(b) reaches 70–80% of $R \ln 2$ ($= 5.7 \text{ J/molK}$) at 100 K, a much lower temperature than the Weiss temperature of $\sim 600 \text{ K}$, which features frustrated magnetism. The C/T is characterized by a curious T^2 dependence at the lowest temperatures. The γ term, when present, appears on the order of $1 \text{ mJ/K}^2\text{mol Ir}$. Recent experiments extended down to 500 m K have found that C_m/T is well approximated by a form of $\gamma + \beta T^{2.4}$ with $\gamma = 2.5 \text{ mJ/K}^2\text{molIr}$

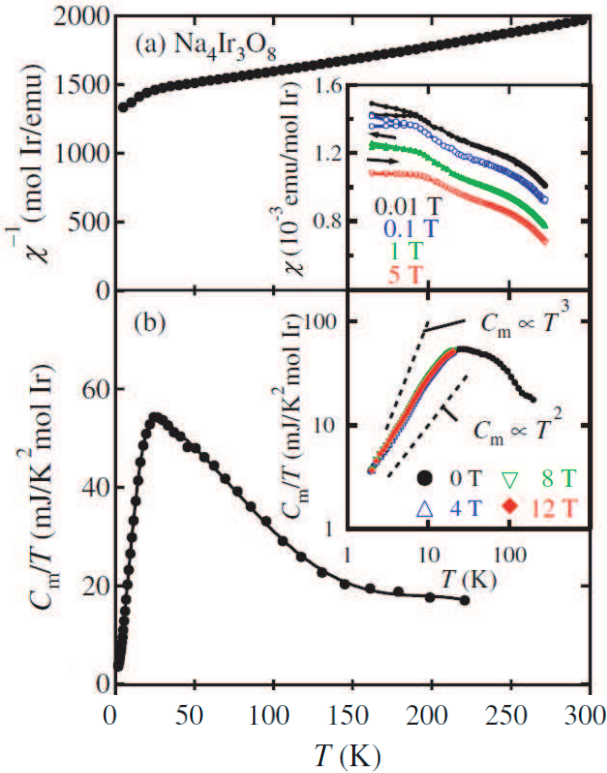


FIG. 36 (Okamoto *et al.*, 2007) (a) Temperature dependence of the inverse magnetic susceptibility χ^{-1} of polycrystalline $\text{Na}_4\text{Ir}_3\text{O}_8$ under 1 T. Inset shows magnetic susceptibility χ in various fields up to 5 T; for clarity, the curves are shifted by 3, 2, and 1×10^{-4} emu/mol Ir for 0.01, 0.1, and 1 T data, respectively. (b) Magnetic specific heat C_m divided by temperature T of polycrystalline $\text{Na}_4\text{Ir}_3\text{O}_8$. To estimate C_m , data for $\text{Na}_4\text{Sn}_3\text{O}_8$ is used as a reference of the lattice contribution. Inset shows C_m/T versus T in various fields up to 12 T.

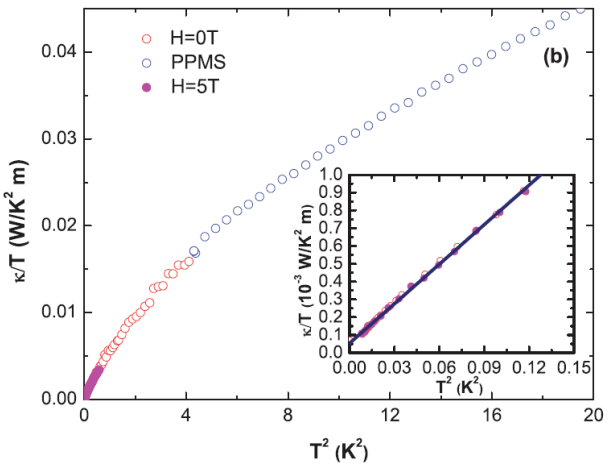


FIG. 37 (Singh *et al.*, 2013) Thermal conductivity κ of $\text{Na}_4\text{Ir}_3\text{O}_8$ in κ/T versus T^2 plots for magnetic fields of 0 T and 5 T. Inset shows the low-temperature part of the data.

(Singh *et al.*, 2013). As seen in the inset of Fig. 36(b), the applied field has no influence on the specific heat, at least up to 12 T.

The temperature dependence of thermal conductivity is shown in Fig. 37 (Singh *et al.*, 2013). At low temperatures down to 75 mK, κ/T is linear in T^2 . The κ/T value extrapolated to $T = 0$ is 6.3×10^{-2} mW/K²m, which is a vanishingly small value, compared with the value of $\text{EtMe}_3\text{Sb}[(\text{Pd}(\text{dmit})_2)_2]$, 0.2 W/K²m in Fig. 27. The suppression of the κ/T value by the extrinsic grain-boundary effect is not ruled out (Singh *et al.*, 2013). The feature that γ is diminished and κ/T is vanishing at low temperatures, while both are sizable at high temperatures of the order of Kelvin, appears to be in accordance with a theoretical picture of spinon Fermi surfaces that undergo a pairing instability at low temperatures (Zhou *et al.*, 2008). In this context, the magnetic susceptibility, remaining large even at low temperatures, can be due to the large spin-orbit interactions of Ir (Zhou *et al.*, 2008).

The substitution of non-magnetic Ti^{4+} ions at Ir sites will give rise to a Curie-like tail in the spin susceptibility curve (Okamoto *et al.*, 2007), similar to Zn substitution for Cu in high-T_c cuprates, indicating an RVB spin background. The scaling analysis of magnetic Gruneisen parameters is suggestive of the proximity of $\text{Na}_4\text{Ir}_3\text{O}_8$ to a zero-field quantum critical point (Singh *et al.*, 2013).

Very recent μ SR (Dally *et al.*, 2014) and NMR experiments (Shockley *et al.*, 2015) have found some indications that are not in accordance with the above claims. Both probes detected the emergence of local fields signifying the freezing of moments at low temperatures, as shown in Fig. 38. The muons are revealed to sense an inhomogeneous local field of electronic origin that appears at 6 K, where the irreversibility in magnetization occurs, and levels off to 70 G on average, which may correspond to 0.5 μ_B on Ir. It is suggested, however, that the spin correlation is short-ranged (of the order of one unit-cell) and quasi-static in that the slow dynamics captured by the relaxation rate persist down to 20 mK. The quasi-static nature is also seen in the S=1 triangular-lattice system, NiGa_2S_4 (MacLaughlin *et al.*, 2008; Nakatsuji *et al.*, 2005). ^{17}O and ^{23}Na NMR lines show broadening, which is roughly scaled to the μ SR results at low temperatures, as seen in Fig. 38; the moment is estimated at 0.27 μ_B on Ir. The NMR line profile also suggests inhomogeneous spin freezing and slow dynamics persisting down to low temperatures although the temperature dependencies of the relaxation rates on the muon and ^{23}Na differ. Noticeably, the ^{23}Na relaxation rate exhibits a peak indicative of the critical slowing down at approximately 7.5 K despite no anomaly in specific heat. The nature and origin of these anomalous properties are not clear at present; however, it is likely that disorder plays a vital role in this system, which can host configurationally degenerate phases with fluctuating order (Dally *et al.*, 2014). Considering that muon, ^{17}O

and ^{23}Na captured the behavior of the majority of spins in the sample, the disorder effect, if any, is such that it is not restricted to finite areas but extended over the system, being reminiscent of the quantum Griffiths effect given the inhomogeneity and slow dynamics.

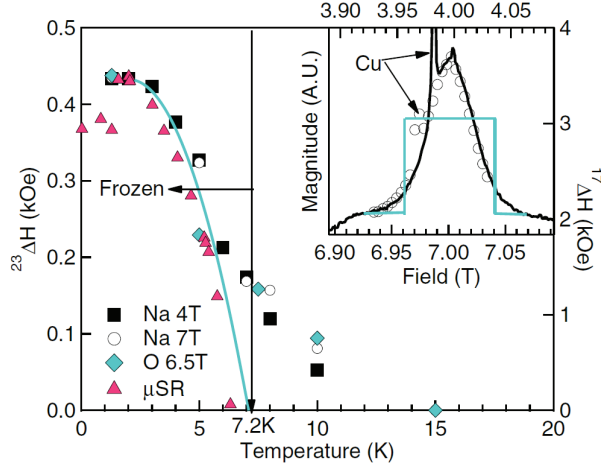


FIG. 38 (Shockley *et al.*, 2015) The line width (FWHM) of Gaussian-broadened ^{17}O and ^{23}Na NMR spectra and the mean value of the distributed local fields detected based on μSR (Dally *et al.*, 2014). For the NMR line width, its deviation from the value at 15 K is plotted. Inset: ^{23}Na spectra at 78.937 MHz for 7 T (empty circles) and 45.046 MHz for 4 T (solid line) with the horizontal axis shifted by 3.005 T at 1.3 K. The blue line shows the expected powder pattern of the spectrum, with every Ir-site carrying the same moment.

V.4. Experimental summary

Due to intensive experimental studies, unconventional thermodynamic and magnetic properties that evoke spin liquids have been found in several materials with anisotropic triangular lattices, kagome lattices and hyperkagome lattices as seen above. These materials exhibit no indications of conventional magnetic ordering. Their magnetic and thermodynamic properties are summarized in Table III. It appears that the gapless nature is a property that a class of frustrated lattices constructed with triangles possesses, although the thermal conductivity of κ -(ET)₂Cu₂(CN)₃ suggested a tiny excitation gap three orders of magnitude smaller than J . A recent NMR work on herbertsmithite insists on gapped spin excitations, and anomalous quasi-static spin freezing has recently been revealed by μSR and NMR studies of the hyperkagome system. This feature and the successful observation of fractionalized excitations in a kagome lattice (Han *et al.*, 2012) tempt ones to think about spinons as promising elementary excitations in spin liquids. How to detect the spinon Fermi surfaces, if they exist, is a

focus—smoking-gun experiments are awaited.

As seen in Table III, several experimental characteristics are seemingly inconsistent within given materials; understanding the apparently contradicting data in a consistent way requires clarification of the nature of the spin states. One of the key issues may be the randomness present in real materials. In particular, it has long been recognized that the effect of inevitable Zn/Cu admixtures in herbertsmithite has to be separated from the intrinsic magnetism. More recently, the issue of inhomogeneous quasi-static spin correlation with slow dynamics in the hyperkagome-lattice system has emerged as a consequence of disorder. Theoretically, it was proposed that as randomness is intensified, the 120-degree Néel order in the triangular-lattice Heisenberg model is changed to a sort of random singlets but not spin glass state. It is intriguing that randomness appears to enhance the quantum nature because the singlet is a purely quantum state (Shimokawa *et al.*, 2015; Watanabe *et al.*, 2014). In the case of kagome lattices, it was theoretically suggested that disorder could lead to a valence-bond glass state (Singh, 2010) or a gapless spin liquid state

TABLE III Spin liquid materials summary

Material	Triangular, κ -(ET) ₂ Cu ₂ (CN) ₃	Triangular M[Pd(dmit) ₂] ₂	Kagome ZnCu ₃ (OH) ₆ Cl ₂	Hyper-Kagome, Na ₄ Ir ₃ O ₈
Susceptibility	A broad peak at 60 K, Finite at 2 K, $J = 250$ K (*1)	A broad peak at 50 K, Finite at 2 K, $J = 220 \sim$ 280 K (*7)	Curie-Weiss at high-T $\Theta_W = -300$ K, $J = 230$ K, Upturn at low-T due to impurity sites (*11, *12)	Curie-Weiss $\Theta_W = -650$ K (*19, *20)
Specific heat	Gapless, $\gamma = 15$ mJ/K ² mol, Field-independent (*2)	Gapless, $\gamma = 20$ mJ/K ² mol, Field-independent (*8)	Gapless, $C \sim T^\alpha$ $\alpha = 1.3$ at high fields (*13)	Gapless, $C \sim T^2$ (*19), $C \sim \gamma T + \beta T^{2.4}$, $\gamma = 2$ mJ/K ² mol (*20), Field-independent (*21, *22)
Thermal conductivity	Gapped; $\Delta = 0.46$ K (*3)	Gapless; finite κ/T (*9)		Vanishingly small κ/T (*22)
NMR shift	Not precisely resolved (*4)	Not precisely resolved (*10)	High-T Broad peak at 50-60 K for ¹⁷ O (*14, *15), at 25-50 K for ³⁵ Cl (*16) Low-T gapless :finite value (*14) gapped : $\Delta \sim 10$ K (*15)	¹⁷ O shift — scales to χ_{bulk} in 100 K - 300 K but levels off below 80 K (*23) ¹⁷ O, ²³ Na- inhomogeneous line broadening at low- T (*23)
NMR 1/T₁	Inhomogeneous 1/T ₁ , Power law, ¹ H 1/T ₁ ; $\sim T / \sim T^2$ at $T < 0.3$ K (two components) (*1), ¹³ C 1/T ₁ ; $\sim 1/T^{1.5}$ at $T < 0.2$ K (stretched exponential) (*4)	Inhomogeneous 1/T ₁ , Power law, ¹³ C 1/T ² at < 0.5 K (stretched exponential) (*10)	1/T ₁ $\sim T^\alpha$ $\alpha \sim 0.73$ for ¹⁷ O (*14) $\alpha \sim 0.5$ for ⁶³ O (*16) Field-induced spin freezing (*17)	²³ Na 1/T ₁ — a peak formation typical of critical slowing down at 7.5 K (*23)
μSR	No internal field at 0 T (*5, *6)		No internal field at 0 T (*18)	Emergence of distributed local fields below 6 K Quasi-static short-ranged spin freezing with slow dynamics (*24)
Neutron			Powders \sim gapless (< 0.1 meV) (*11, *19) Single crystal \sim gapless (< 0.25 meV) (*20) Continuum in dynamic structure factor (*11, *19, *20)	
References	*1 Shimizu <i>et al.</i> , 2003, *2 Yamashita <i>et al.</i> , 2008 *3 Yamashita <i>et al.</i> , 2009, *4 Shimizu <i>et al.</i> , 2006, *5 Pratt <i>et al.</i> , 2011, *6 Goto <i>et al.</i> , 2012 *6 Goto <i>et al.</i> , 2012	*7 Kato, 2014, *8 Yamashita <i>et al.</i> , 2011, *9 Yamashita <i>et al.</i> , 2010, *10 Itou <i>et al.</i> , 2010	*11 Helton <i>et al.</i> , 2007, *12 Bert <i>et al.</i> , 2007, *13 de Vries <i>et al.</i> , 2008, *14 Olariu <i>et al.</i> , 2008, *15 Imai <i>et al.</i> , 2015 *16 Imai <i>et al.</i> , 2008 *17 Jeong <i>et al.</i> , 2011, *18 Mendels <i>et al.</i> , 2007 *19 de Vries <i>et al.</i> , 2009 *20 Han <i>et al.</i> , 2012	*21 Okamoto <i>et al.</i> , 2007 *22 Singh <i>et al.</i> , 2013 *23 Shockley <i>et al.</i> , 2015 *24 Dally <i>et al.</i> , 2014

(Kawamura *et al.*, 2014; Shimokawa *et al.*, 2015). Furthermore, a recent NMR experiment on an organic Mott insulator, i.e., κ -(ET)₂Cu[N(CN)₂]Cl, found that the antiferromagnetic ordering in the pristine crystal, when irradiated by X-rays, disappears. Spin freezing, spin gap and critical slowing down are not observed, but gapless spin excitations emerge, suggesting a novel role of disorder that brings forth a QSL from a classical ordered state (Furukawa *et al.*, 2015b). Whether the randomness is fatal or vital to the physics of a QSL is a non-trivial issue to be resolved.

The development of new materials, although not addressed in this article, is under way. Among them is a new type of hydrogen-bonded κ -H₃(Cat-EDT-TTF)₂ with a triangular lattice of one-dimensional anisotropy (Isono *et al.*, 2013) and κ -(ET)₂Ag₂(CN)₃, an analogue of κ -(ET)₂Cu₂(CN)₃ (Saito, 2014). Another compound with hyperkagome lattice structure, i.e., PbCuTe₂O₆, with Curie-Weiss temperature $\theta = -22$ K is also proposed to be a spin liquid candidate (Khuntia *et al.*, 2016; Koteswararao *et al.*, 2014). The entanglement of additional degrees of freedom with quantum spins may be another direction for future studies; e.g., Ba₃CuSb₂O₉ is proposed to host a spin-orbital coupled liquid state (Nakatsuji *et al.*, 2012; Zhou *et al.*, 2011).

It should be emphasized that the identification of QSL experimentally is a very important and challenging task. As a “featureless” Mott insulator, there exists no simple magnetic order for identifying QSL states, and so far, there exists only indirect experimental evidence for mobile fermionic spinons in some candidate compounds as discussed above.

To remedy this situation, theorists have proposed new experiments to identify QSLs through identifying nontrivial properties of spinons and gauge fields. For example, power law AC conductivity inside the Mott gap has been noted (Ng and Lee, 2007). A giant-magnetoresistance-like experiment was proposed to measure mobile spinons through oscillatory coupling between two ferromagnets via a QSL spacer (Norman and Micklitz, 2009). The thermal Hall effect in insulating quantum magnets was proposed as a probe for the thermal transport of spinons, where different responses were used to distinguish between magnon- and spinon- transports (Katsura *et al.*, 2010). Raman scattering was proposed as a signature to probe the $U(1)$ QSL state (Ko *et al.*, 2010). It was also proposed that the spinon life time and mass as well as gauge fluctuations can be measured through a sound attenuation experiment (Zhou and Lee, 2011), and neutron scattering can be used to detect scalar spin chirality fluctuations in the kagome system (Lee and Nagaosa, 2013). Low energy electron spectral functions were evaluated for future ARPES experiments (Tang *et al.*, 2013) and it was proposed that spin current flow through a metal-QSL-metal junction can be used to distinguish differ-

ent QSLs (Chen *et al.*, 2013). More recently, it was suggested that there exists a long-life surface plasmon mode propagating along the interface between a linear medium and a QSL with spinon Fermi surface at frequencies above the charge gap, which can be detected by the widely used Kretschmann-Raether three-layer configuration (Ma and Ng, 2015).

However, there exists an important discrepancy between existing experiments and theories in some of the above experiments.

1) Specific heat: Using the one-loop calculation supplemented by scaling analysis (Lee and Nagaosa, 1992; Polchinski, 1994), it is found that the strong coupling between the $U(1)$ gauge field and spinon Fermi surface leads to $T^{2/3}$ correction to the temperature dependence of specific heat in $U(1)$ gauge theory. This predicted $T^{2/3}$ behavior has never been observed in experiments. Instead, linear, Fermi-liquid-like specific heat is found to exists in a wide range of temperatures in both organic materials (κ -ET and dmit).

Some theories exist that try to explain this missing singular $T^{2/3}$ specific heat. For instance, Z_4 and Z_2 spin liquid states with a spinon Fermi surface have been proposed (Barkeshli *et al.*, 2013) as well as Z_2 spin liquid states with quadratic touched spinon bands (Mishmash *et al.*, 2013). However, all these proposals require fine-tuned parameters. A more natural way of explaining existing experiments is still missing.

2) Thermal Hall effect: Katsura, Nagaosa and Lee (Katsura *et al.*, 2010) have theoretically investigated the thermal Hall effect induced by the external magnetic field in a $U(1)$ spin liquid with a spinon Fermi surface and have predicted measurable electronic contributions. Their predicted sizable thermal Hall effect have never been observed in an experiment on dmit compounds (Yamashita *et al.*, 2010). This contradiction between experiment and theory remains unsolved, although an explanation that depends on fine-tuned parameters has been proposed (Mishmash *et al.*, 2013).

3) Power law AC conductivity: A power law AC conductivity inside the Mott gap was proposed by Ng and Lee (Ng and Lee, 2007). Indeed, power law behavior $\sigma(\omega) \sim \omega^\alpha$ has been observed in both κ -ET (Elsässer *et al.*, 2012) and Herbertsmithite (Pilon *et al.*, 2013). However, the power α observed in both compounds is smaller than predicted value, indicating that there exist more in-gap electronic excitations than those predicted in the $U(1)$ gauge theory.

Thus, despite all the theoretical efforts, the understanding and finding of realistic “smoking gun” evidence for QSLs remains the greatest challenge in the study of QSLs.

VI. SUMMARY

In this article, we provide a pedagogical introduction to the subject of QSLs and review the current status of the field. We first discuss the semi-classical approach to simple quantum antiferromagnets. We explain how it leads to the Haldane conjecture in one dimension and why it fails for frustrated spin models. We then focus on spin-1/2 systems with spin rotational symmetry and introduce the RVB concept and the slave-particle plus Gutzwiller-projected wavefunction approaches. We explain the technical difficulties associated with these approaches and why slave-particle approaches naturally lead to gauge theories for spin liquid states. The natures of $SU(2)$, $U(1)$ and Z_2 spin liquid states are explained, and the extensions of the approach to systems with spin-orbit coupling and $S > 1/2$ systems are introduced. We explain that because of the intrinsic limitations of the analytical slave-particle approach, many alternative approaches to spin liquid states have been developed, both numerically and analytically. These approaches complement each other and often lead to exotic possibilities not covered by the simple fermionic slave-particle approach. The experimental side of the story is also introduced with a review of the properties of several candidate spin liquid materials, including anisotropic triangular lattice systems (κ -(ET)₂Cu₂(CN)₃ and EtMe₃Sb[(Pd(dmit)₂)₂]), kagome lattice systems (ZnCu₃(OH)₆Cl₂) and hyperkagome lattice systems (Na₄Ir₃O₈). We note several outstanding difficulties with attempts to explain experimental results using existing theories. *These difficulties indicate that the field of QSLs is still wide open and immature and that important physics may still be missing in our present understanding of QSLs.*

While keeping the article at an introductory level, we are not able to cover many important developments in the study of spin liquid states, and many technical details have been neglected, both theoretically and experimentally. For example, the important techniques of renormalization groups and conformal field theory are not addressed in this article. We also do not discuss in detail the many developments related to MPSs and/or PEPSs and the corresponding numerical DMRG technique, the understanding of spin systems with broken rotational symmetry following the discovery of the Kitaev state, and the spin liquid physics of $S > 1/2$ systems. The role of topology in spin liquid states is not touched upon except as it is relevant to examples of spin liquid states. These are rapidly evolving areas in which new discoveries are expected.

In the following section, we outline a few other topics that are neglected in this article but either have played important historical roles in the development of the field of QSLs or shed light on future research:

Quantum dimer models: Quantum dimer models (QDMs) are a class of models defined in the Hilbert

space of nearest neighbor valence bond (or dimer) coverings over a lattice instead of the spin Hilbert space (Rokhsar and Kivelson, 1988). QDMs can be obtained in certain large- N limits of $SU(N)$ or $Sp(N)$ antiferromagnets (Read and Sachdev, 1989) and provide a simplified description of RVB states. This simplification allows researcher to proceed further in analytical treatments because of the close relations that arise to classical dimer problems, Ising models and Z_2 gauge theory (Fisher, 1961; Kasteleyn, 1961, 1963; Misguich *et al.*, 2002; Moessner and Sondhi, 2003; Moessner *et al.*, 2001). However, by construction, QMDs focus on the dynamics in the spin-singlet subspace and ignore spin-triplet excitations. Therefore, they are not directly relevant to spin systems in which the magnetic excitations are gapless.

An advantage of QDMs is that some QDMs are exactly solvable (Misguich *et al.*, 2002; Yao and Kivelson, 2012). Thus, many issues related to QSLs that are difficult to address, such as spinon deconfinement, Z_2 vortices and topological order, can be addressed explicitly in QDMs. Interestingly, some spin-1/2 Hamiltonians give rise to sRVB ground states defined in the dimer Hilbert space when the relationship between the spin and dimer configurations is properly chosen (Cano and Fendley, 2010; Fujimoto, 2005; Seidel, 2009). Readers who are interested in further details on QDMs can refer to Chapter 5.5 in reference (Diep, 2004) and Chapter 17 in reference (Lacroix *et al.*, 2011).

Chiral spin liquids: QSL states that break the parity (P) and time-reversal (T) symmetries while conserving the spin rotational symmetry have been proposed by Kalmeyer and Laughlin (Kalmeyer and Laughlin, 1987, 1989). These states are called chiral spin liquids.

Kalmeyer and Laughlin proposed that some frustrated Heisenberg antiferromagnets in 2D can be described by bosonic fractional quantum Hall wavefunctions. Soon afterward, Wen, Wilczek and Zee (Wen *et al.*, 1989) introduced a generic method of describing chiral spin liquids. They suggested that chiral spin states can be characterized in terms of the spin chirality $E_{123} = \vec{S}_1 \cdot (\vec{S}_2 \times \vec{S}_3)$, defined for three different spins, \vec{S}_1 , \vec{S}_2 and \vec{S}_3 . The expectation value of the spin chirality in fermionic RVB theory is given by $\langle E_{123} \rangle = \frac{1}{2} \text{Im} \langle \chi_{12} \chi_{23} \chi_{31} \rangle$, where the χ_{ij} are the short-range order parameters defined in Eq. (39).

Exactly solvable Hamiltonians hosting both gapful chiral spin liquid states (Laughlin, 1989; Schroeter *et al.*, 2007; Thomale *et al.*, 2009; Yao and Kivelson, 2007) and gapless chiral spin liquids (Chua *et al.*, 2011) have been found. There is also numerical evidence for chiral spin liquids on some 2D frustrated lattices (Bauer *et al.*, 2013; Gong *et al.*, 2015, 2014a; He and Chen, 2014; He *et al.*, 2014; Nielsen *et al.*, 2013; Sorella *et al.*, 2003; Zhu *et al.*, 2015). It has been suggested that the statistics of spinons in these chiral spin liquid states can be non-Abelian; see, e.g., (Greiter and Thomale, 2009; Yao and Kivelson,

2007).

Characterizing spin liquid states numerically: Because of rapid advancements in the power of numerical approaches to spin models, the characterization of spin liquid states for specific spin models from numerical data has become a rapidly evolving field. In addition to the MPS and/or PEPS approach and the corresponding numerical DMRG technique, Tang and Sandvik developed a quantum Monte Carlo method of characterizing spinon size and confinement length in quantum spin systems, which allows the spinon confinement-deconfinement issue to be studied numerically (Tang and Sandvik, 2013). Another important achievement is the use of entanglement entropy to characterize QSL states. Readers may consult reference (Grover *et al.*, 2013) for a brief review.

To conclude, the field of QSLs is still wide open, both theoretically and experimentally. The major difficulty in understanding QSLs is that they are intrinsically strongly correlated systems, for which no perturbative approach is available. Theorists have been using all of the available tools as well as inventing new theoretical tools to understand QSLs with the hope that novel emerging phenomena not covered by perturbative approaches can be uncovered. Thus far, there have been a few successes, and new experimental discoveries and theoretical ideas are rapidly emerging. However, a basic mathematical framework that can be used to understand QSLs systematically is still lacking. We expect that more new physics will be discovered in QSLs, posing a challenge to both theorists and experimentalists to construct a basic framework for the understanding of QSLs.

ACKNOWLEDGMENTS

Y.Z. and T.K.N. thank Patrick A. Lee, Zheng-Xin Liu, Naoto Nagaosa, Shaojin Qin, Zhaobin Su, Hong-Hao Tu, Tao Xiang, Xiao-Gang Wen, Zheng-Yu Weng, Guang-Ming Zhang, and Fu-Chun Zhang for their close collaboration on related issues over the years. K.K. is grateful to K. Miyagawa, Y. Shimizu, Y. Kurosaki, H. Hashiba, H. Kobashi, H. Kasahara, T. Furukawa, M. Maesato, G. Saito, F. Pratt, and M. Poirier for their collaboration on the topic of spin liquids. We benefited greatly from discussions with our colleagues Yan Chen, Yin-Chen He, Bruce Normand, Fa Wang, Cenke Xu, and Hong Yao. Y.Z. is supported by the National Key R&D Program of China (No.2016YFA0300202), the National Basic Research Program of China under Grant No. 2014CB921201 and by the National Natural Science Foundation of China under Grant No. 11374256. He also wishes to acknowledge the hospitality of the Max Planck Institute for the Physics of Complex Systems in Dresden, where this review article was finalized. K.K. is partially supported by JSPS KAKENHI under Grant Nos. 20110002, 25220709, and 24654101, by the US

National Science Foundation under Grant No. PHYS-1066293, and by the hospitality of the Aspen Center for Physics. T.K.N. acknowledges support from HKRGC through Grant No. 603913.

Appendix A: Path integral for a single spin

We consider the path integral for a single spin \mathbf{S} in a magnetic field \mathbf{B} ($H = \mathbf{S} \cdot \mathbf{B}$) in the coherent state representation. Spin coherent states are defined as

$$\hat{\mathbf{S}}|\mathbf{n}\rangle = S\mathbf{n}|\mathbf{n}\rangle,$$

where $\hat{\mathbf{S}}$ is the spin operator. The path integral can be derived by using the identity operator

$$\mathbf{I} = \left(\frac{2S+1}{4\pi} \right) \int d^3 n \delta(\mathbf{n}^2 - 1) |\mathbf{n}\rangle\langle\mathbf{n}| = \int D\mathbf{n} |\mathbf{n}\rangle\langle\mathbf{n}| \quad (\text{A1a})$$

and the corresponding inner product

$$\langle \mathbf{n}_1 | \mathbf{n}_2 \rangle = e^{iS\Phi(\mathbf{n}_1, \mathbf{n}_2, \mathbf{n}_0)} \left(\frac{1 + \mathbf{n}_1 \cdot \mathbf{n}_2}{2} \right)^S, \quad (\text{A1b})$$

where \mathbf{n}_0 is a fixed unit vector and is usually chosen to be $\mathbf{n}_0 = \hat{z}$, $\Phi(\mathbf{n}_1, \mathbf{n}_2, \mathbf{n}_0)$ is the area of the spherical triangle with vertices \mathbf{n}_1 , \mathbf{n}_2 , and \mathbf{n}_0 , and $S\Phi$ is the Berry's phase acquired by a particle traveling through a loop formed by the edges of the spherical triangle.

The partition function $Z = e^{-\beta H}$ can be written as a path integral using the standard procedure:

$$\begin{aligned} Z &= \lim_{N_t \rightarrow \infty, \delta t \rightarrow 0} (e^{-\delta t H})^{N_t} \\ &= \lim_{N_t \rightarrow \infty, \delta t \rightarrow 0} \left(\prod_{j=1}^{N_t} \int D\mathbf{n}_j \right) \left(\prod_{j=1}^{N_t} \langle \mathbf{n}_j | e^{-i\delta t H} | \mathbf{n}_{j+1} \rangle \right), \end{aligned} \quad (\text{A2})$$

with the periodic boundary condition $|\mathbf{n}(0)\rangle = |\mathbf{n}(\beta)\rangle$.

In the limit $\delta t \rightarrow 0$, we may approximate

$$\begin{aligned} \langle \mathbf{n}_j | e^{-i\delta t H} | \mathbf{n}_{j+1} \rangle &\sim \langle \mathbf{n}_j | \mathbf{n}_{j+1} \rangle - \delta t \langle \mathbf{n}_j | H | \mathbf{n}_{j+1} \rangle \\ &\sim \langle \mathbf{n}_j | \mathbf{n}_{j+1} \rangle \left(1 - \delta t \frac{\langle \mathbf{n}_j | H | \mathbf{n}_{j+1} \rangle}{\langle \mathbf{n}_j | \mathbf{n}_{j+1} \rangle} \right) \\ &\sim e^{iS\Phi(\mathbf{n}_j, \mathbf{n}_{j+1}, \mathbf{n}_0)} \left(\frac{1 + \mathbf{n}_j \cdot \mathbf{n}_{j+1}}{2} \right)^S \\ &\quad \times (1 - \delta t S \mathbf{B} \cdot \mathbf{n}_t), \end{aligned} \quad (\text{A3})$$

which is valid to the first order in δt . In deriving the last equality in Eq. (A3), we have made use of the result $\langle \mathbf{n} | \hat{\mathbf{S}} = \langle \mathbf{n} | \mathbf{n}$. Furthermore, we note that

$$\begin{aligned} \left(\frac{1 + \mathbf{n}_j \cdot \mathbf{n}_{j+1}}{2} \right)^S &\sim e^{S \ln(1 + \frac{\delta t}{2} \mathbf{n}(t) \cdot \partial_t \mathbf{n}(t))_{t=t_j}} \\ &\sim e^{S \delta t \partial_t [\mathbf{n}(t)]^2} = e^{(0)} \end{aligned} \quad (\text{A4})$$

to leading order in δt . Therefore,

$$\langle \mathbf{n}_j | e^{-i\delta t H} | \mathbf{n}_{j+1} \rangle \sim e^{iS\Phi(\mathbf{n}_j, \mathbf{n}_{j+1}, \mathbf{n}_0) - \delta t S \mathbf{B} \cdot \mathbf{n}_t} \quad (\text{A5})$$

and

$$Z \sim \int \mathbf{D}\mathbf{n}(t) e^{iS\Omega(\mathbf{n}(t)) - S \int_0^\beta dt \mathbf{B} \cdot \mathbf{n}(t)}, \quad (\text{A6})$$

where $\int \mathbf{D}\mathbf{n}(t) = \lim_{N_t \rightarrow \infty, \delta t \rightarrow 0} \left(\prod_{j=1}^{N_t} \int D\mathbf{n}_j \right)$ and

$$\Omega(\mathbf{n}(t)) = \sum_j \Phi(\mathbf{n}_j, \mathbf{n}_{j+1}, \mathbf{n}_0)$$

is the total area on the surface of the unit sphere covered by the (closed) path swept out by the spin $\mathbf{n}(t)$ from $t = 0$ to $t = \beta$.

The classical action of the system in real time is given by

$$S_{cl} = S\Omega(\mathbf{n}(t)) - S \int_0^T dt \mathbf{B} \cdot \mathbf{n}(t), \quad (\text{A7a})$$

and the classical equation of motion $\frac{\delta S_{cl}}{\delta' \mathbf{n}(t)} = 0$ leads to the Euler equation of motion

$$\mathbf{n} \times ((\mathbf{n} \times \partial_t \mathbf{n}) - \mathbf{B}) = 0, \quad (\text{A7b})$$

where we have used the result that a small variation $\delta \mathbf{n}$ leads to a change in $\Omega(C[\mathbf{n}])$ that is given by

$$\delta\Omega[\mathbf{n}(t)] = \int_0^\beta dt \delta\mathbf{n}(t) \cdot (\mathbf{n}(t) \times \partial_t \mathbf{n}(t)).$$

REFERENCES

Abdel-Jawad, M., I. Terasaki, T. Sasaki, N. Yoneyama, N. Kobayashi, Y. Uesu, and C. Hotta (2010), *Phys. Rev. B* **82**, 125119.

Abrikosov, A. A. (1965), *Physics* **2**, 5.

Affleck, I. (1986), *Nucl. Phys. B* **265** (3), 409.

Affleck, I. (1990), *Field Theory Methods and Quantum Critical Phenomena*, edited by E. Brezin and J. Zinn-Justin (North-Holland, Amsterdam).

Affleck, I., T. Kennedy, E. Lieb, and H. Tasaki (1988a), *Commun. Math. Phys.* **115** (3), 477.

Affleck, I., T. Kennedy, E. H. Lieb, and H. Tasaki (1987), *Phys. Rev. Lett.* **59**, 799.

Affleck, I., and J. B. Marston (1988), *Phys. Rev. B* **37**, 3774.

Affleck, I., Z. Zou, T. Hsu, and P. W. Anderson (1988b), *Phys. Rev. B* **38**, 745.

Anderson, P. (1973), *Mater. Res. Bull.* **8** (2), 153.

Anderson, P. W. (1959), *Phys. Rev. Lett.* **3**, 325.

Anderson, P. W. (1987), *Science* **235**, 1196.

Androes, G. M., and W. D. Knight (1959), *Phys. Rev. Lett.* **2**, 386.

Arovas, D. P. (2008), *Phys. Rev. B* **77**, 104404.

Arovas, D. P., and A. Auerbach (1988), *Phys. Rev. B* **38**, 316.

Arrachea, L., L. Capriotti, and S. Sorella (2004), *Phys. Rev. B* **69**, 224414.

Auerbach, A. (1994), *Interacting Electrons and Quantum Magnetism* (Springer-Verlag New York, Inc.).

Balents, L. (2010), *Nature* **464**, 199.

Balents, L., M. P. A. Fisher, and C. Nayak (1998), *Int. J. Mod. Phys. B* **12** (10), 1033.

Barkeshli, M., H. Yao, and S. A. Kivelson (2013), *Phys. Rev. B* **87**, 140402.

Baskaran, G., and P. W. Anderson (1988), *Phys. Rev. B* **37**, 580.

Baskaran, G., S. Mandal, and R. Shankar (2007), *Phys. Rev. Lett.* **98**, 247201.

Baskaran, G., G. Santhosh, and R. Shankar (2009), arXiv:0908.1614.

Baskaran, G., Z. Zou, and P. Anderson (1987), *Solid State Commun.* **63** (11), 973.

Bauer, B., B. P. Keller, M. Dolfi, S. Trebst, and A. W. W. Ludwig (2013), arXiv preprint arXiv:1303.6963.

Baym, G., and C. Pethick (2004), *Landau Fermi-Liquid Theory: Concepts and Applications* (WILEY-VCH Verlag GmbH & Co. KGaA, Weinheim).

Berry, M. V. (1984), *Proc. Roy. Soc. London A* **392** (1802), pp. 45.

Bert, F., S. Nakamae, F. Ladieu, P. L'Hôte, D. and Bonville, F. Duc, J.-C. Trombe, and M. P. (2007), *Phys. Rev. B* **76**, 132411.

Bieri, S., C. Lhuillier, and L. Messio (2016), *Phys. Rev. B* **93**, 094437.

Bieri, S., M. Serbyn, T. Senthil, and P. A. Lee (2012), *Phys. Rev. B* **86**, 224409.

Brézin, E., and J. Zinn-Justin (1976), *Phys. Rev. B* **14**, 3110.

Brinkman, W. F., and T. M. Rice (1970), *Phys. Rev. B* **2**, 4302.

Cano, J., and P. Fendley (2010), *Phys. Rev. Lett.* **105**, 067205.

Capriotti, L., F. Becca, A. Parola, and S. Sorella (2001), *Phys. Rev. Lett.* **87**, 097201.

Capriotti, L., A. E. Trumper, and S. Sorella (1999), *Phys. Rev. Lett.* **82**, 3899.

Ceperley, D., G. V. Chester, and M. H. Kalos (1977), *Phys. Rev. B* **16**, 3081.

Chaloupka, J. c. v., G. Jackeli, and G. Khaliullin (2010), *Phys. Rev. Lett.* **105**, 027204.

Chandra, P., and B. Doucot (1988), *Phys. Rev. B* **38**, 9335.

Chen, C. Z., Q. F. Sun, F. Wang, and X. C. Xie (2013), *Phys. Rev. B* **88**, 041405.

Chen, G., and L. Balents (2008), *Phys. Rev. B* **78**, 094403.

Chen, G., and Y. B. Kim (2013), *Phys. Rev. B* **87**, 165120.

Chen, H. D., and Z. Nussinov (2008), *J. Phys. A: Math. Theor.* **41** (7), 075001.

Chen, H. D., B. Wang, and S. Das Sarma (2010), *Phys. Rev. B* **81**, 235131.

Chen, X., Z. C. Gu, Z. X. Liu, and X. G. Wen (2012), *Science* **338** (6114), 1604.

Chen, X., Z. C. Gu, and X. G. Wen (2011a), *Phys. Rev. B* **83**, 035107.

Chen, X., Z. C. Gu, and X. G. Wen (2011b), *Phys. Rev. B* **84**, 235128.

Cheng, J. G., G. Li, L. Balicas, J. S. Zhou, J. B. Goodenough, C. Xu, and H. D. Zhou (2011), *Phys. Rev. Lett.* **107**, 197204.

Choy, T. P., and Y. B. Kim (2009), *Phys. Rev. B* **80**, 064404.

Chua, V., H. Yao, and G. A. Fiete (2011), *Phys. Rev. B* **83**, 180412.

Cirac, J. I., and F. Verstraete (2009), *J. Phys. A: Math. Theor.* **42** (50), 504004.

Coldea, R., D. A. Tennant, A. M. Tsvelik, and Z. Tyliczynski (2001), *Phys. Rev. Lett.* **86**, 1335.

Coldea, R., D. A. Tennant, and Z. Tyliczynski (2003),

Phys. Rev. B **68**, 134424.

Dally, R., T. Hogan, A. Amato, H. Luetkens, C. Baines, J. Rodriguez-Rivera, M. J. Graf, and S. D. Wilson (2014), Phys. Rev. Lett. **113**, 247601.

Dayal, S., R. T. Clay, H. Li, and S. Mazumdar (2011), Phys. Rev. B **83**, 245106.

Depenbrock, S., I. P. McCulloch, and U. Schollwöck (2012), Phys. Rev. Lett. **109**, 067201.

Diep, H. T. (2004), *Frustrated spin systems* (World Scientific).

Dodds, T., S. Bhattacharjee, and Y. B. Kim (2013), Phys. Rev. B **88**, 224413.

Dombre, T., and N. Read (1988), Phys. Rev. B **38**, 7181.

Dusuel, S., K. P. Schmidt, J. Vidal, and R. L. Zaffino (2008), Phys. Rev. B **78**, 125102.

Eggert, S., and I. Affleck (1992), Phys. Rev. B **46**, 10866.

Elsässer, S., D. Wu, M. Dressel, and J. A. Schlueter (2012), Phys. Rev. B **86**, 155150.

Fannes, M., B. Nachtergael, and R. F. Werner (1992), Commun. Math. Phys. **144** (3), 443.

Farnell, D. J. J., R. F. Bishop, and K. A. Gernoth (2001), Phys. Rev. B **63**, 220402.

Fazekas, P., and P. Anderson (1974), Philos. Mag. **30** (2), 423.

Feng, X. Y., G. M. Zhang, and T. Xiang (2007), Phys. Rev. Lett. **98**, 087204.

Fisher, M. E. (1961), Phys. Rev. **124**, 1664.

Florens, S., and A. Georges (2004), Phys. Rev. B **70**, 035114.

Fradkin, E., and S. H. Shenker (1979), Phys. Rev. D **19**, 3682.

Fradkin, E., and M. Stone (1988), Phys. Rev. B **38**, 7215.

Frigeri, P. A., D. F. Agterberg, A. Koga, and M. Sigrist (2004), Phys. Rev. Lett. **92**, 097001.

Fu, M., T. Imai, T.-H. Han, and Y. S. Lee (2015), Science **350**, 655.

Fujimoto, S. (2005), Phys. Rev. B **72**, 024429.

Furukawa, T., K. Miyagawa, H. Taniguchi, R. Kato, and K. Kanoda (2015a), Nature Physics **11**, 221.

Furukawa, T., K. Miyagawa, H. Taniguchi, R. Kato, and K. Kanoda (2015b), Physical Review Letters **115**, 077001.

Galitski, V., and Y. B. Kim (2007), Phys. Rev. Lett. **99**, 266403.

Gebhard, F., and D. Vollhardt (1987), Phys. Rev. Lett. **59**, 1472.

Giamarchi, T. (2003), *Quantum Physics in One Dimension* (Oxford University Press).

Glarum, S. H., S. Geschwind, K. M. Lee, M. L. Kaplan, and J. Michel (1991), Phys. Rev. Lett. **67**, 1614.

Gong, S.-S., W. Zhu, L. Balents, and D. N. Sheng (2015), Phys. Rev. B **91**, 075112.

Gong, S.-S., W. Zhu, and D. Sheng (2014a), Scientific reports **4**, 10.1038/srep06317.

Gong, S.-S., W. Zhu, D. N. Sheng, O. I. Motrunich, and M. P. A. Fisher (2014b), Phys. Rev. Lett. **113**, 027201.

Gor'kov, L. P., and E. I. Rashba (2001), Phys. Rev. Lett. **87**, 037004.

Greiter, M., and R. Thomale (2009), Phys. Rev. Lett. **102**, 207203.

Griffiths, R. B. (1964), Phys. Rev. **133**, A768.

Gros, C. (1989), Ann. Phys. (N.Y.) **189** (1), 53.

Gros, C., R. Joyst, and T. M. Rice (1987), Phys. Rev. B **36**, 381.

Grover, T., N. Trivedi, T. Senthil, and P. A. Lee (2010), Phys. Rev. B **81**, 245121.

Grover, T., Y. Zhang, and A. Vishwanath (2013), New J. Phys. **15**, 025002.

Gu, Z. C., and X. G. Wen (2009), Phys. Rev. B **80**, 155131.

Hahn, T. (1996), *International tables for crystallography, Volume A, Space-Group Symmetry*, 4th ed., Vol. A (Kluwer Academic Publishers, Dordrecht, Netherlands).

Haldane, F. (1985), J. Appl. Phys. **57** (8), 3359.

Haldane, F. D. M. (1983a), Phys. Lett. A **93** (9), 464.

Haldane, F. D. M. (1983b), Phys. Rev. Lett. **50**, 1153.

Haldane, F. D. M. (1988a), Phys. Rev. Lett. **60**, 635.

Haldane, F. D. M. (1988b), Phys. Rev. Lett. **61**, 1029.

Han, T.-H., J. S. Helton, S. Chu, D. G. Nocera, J. A. Rodriguez-Rivera, C. Broholm, and Y. S. Lee (2012), Nature **492**, 406.

Hastings, M. B. (2000), Phys. Rev. B **63**, 014413.

Hastings, M. B. (2007), J. Stat. Mech. **2007**, P08024.

He, Y. C., and Y. Chen (2014), arXiv preprint arXiv:1407.2740.

He, Y. C., D. Sheng, and Y. Chen (2014), Phys. Rev. Lett. **112**, 137202.

Helton, J. S., K. Matan, M. P. Shores, E. A. Nytko, B. M. Bartlett, Y. Yoshida, Y. Takano, A. Suslov, Y. Qiu, J. H. Chung, D. G. Nocera, and Y. S. Lee (2007), Phys. Rev. Lett. **98**, 107204.

Herbut, I. F., and B. H. Seradjeh (2003), Phys. Rev. Lett. **91**, 171601.

Herbut, I. F., B. H. Seradjeh, S. Sachdev, and G. Murthy (2003), Phys. Rev. B **68**, 195110.

Hermeme, M., T. Senthil, M. P. A. Fisher, P. A. Lee, N. Nagaosa, and X. G. Wen (2004), Phys. Rev. B **70**, 214437.

Hohenberg, P. C. (1967), Phys. Rev. **158**, 383.

Horsch, P., and T. A. Kaplan (1983), J. Phys. C **16** (35), L1203.

Hotta, C. (2010), Phys. Rev. B **82**, 241104.

Hu, W.-J., F. Becca, A. Parola, and S. Sorella (2013), Phys. Rev. B **88**, 060402.

Huse, D. A., and V. Elser (1988), Phys. Rev. Lett. **60**, 2531.

Imai, T., E. A. Nytko, B. Bartlett, S. M.P., and D. G. Nocera (2008), Phys. Rev. Lett. **100**, 077203.

Iqbal, Y., F. Becca, S. Sorella, and D. Poilblanc (2013), Phys. Rev. B **87**, 060405.

Iqbal, Y., D. Poilblanc, and F. Becca (2014), Phys. Rev. B **89**, 020407.

Iqbal, Y., D. Poilblanc, and F. Becca (2016), arXiv:1606.02255 , 5.

Isono, T., H. Kamo, A. Ueda, A. Takahashi, K. Nakao, R. Kumai, H. Nakano, K. Kobayashi, Y. Murakami, and H. Mori (2013), Nature Commun. **4**, 1344.

Itoh, K., H. Itoh, M. Naka, S. Saito, I. Hosako, N. Yoneyama, S. Ishihara, T. Sasaki, and S. Iwai (2013), Phys. Rev. Lett. **110**, 106401.

Itou, T., A. Oyamada, S. Maegawa, and R. Kato (2010), Nature Phys. **6**, 673.

Itou, T., A. Oyamada, S. Maegawa, M. Tamura, and R. Kato (2008), Phys. Rev. B **77**, 104413.

Itou, T., K. Yamashita, M. Nishiyama, A. Oyamada, S. Maegawa, K. Kubo, and R. Kato (2011), Phys. Rev. B **84**, 094405.

Jackeli, G., and G. Khaliullin (2009), Phys. Rev. Lett. **102**, 017205.

Jeong, M., F. Bert, P. Mendels, F. Duc, J. C. Trombe, M. A. de Vries, and A. Harrison (2011), Phys. Rev. Lett. **107**, 237201.

Jiang, H. C., Z. C. Gu, X. L. Qi, and S. Trebst (2011), Phys. Rev. B **83**, 245104.

Jiang, H. C., Z. Wang, and L. Balents (2012a), *Nature Phys.* **8** (12), 902.

Jiang, H. C., Z. Y. Weng, and D. N. Sheng (2008), *Phys. Rev. Lett.* **101**, 117203.

Jiang, H.-C., H. Yao, and L. Balents (2012b), *Phys. Rev. B* **86**, 024424.

Kagawa, F., K. Miyagawa, and K. Kanoda (2005), *Nature* **436**, 534.

Kalmeyer, V., and R. B. Laughlin (1987), *Phys. Rev. Lett.* **59**, 2095.

Kalmeyer, V., and R. B. Laughlin (1989), *Phys. Rev. B* **39**, 11879.

Kandpal, H. C., I. Opahle, Y.-Z. Zhang, H. O. Jeschke, and R. Valenti (2009), *Phys. Rev. Lett.* **103**, 067004.

Kanoda, K. (1997a), *Physica C* **287**, 299.

Kanoda, K. (1997b), *Hyperfine Interact.* **104**, 235.

Kanoda, K. (2006), *J. Phys. Soc. Jpn.* **75**, 051007.

Kanoda, K., and R. Kato (2011), *Annu. Rev. Condens. Matter Phys.* **2**, 167.

Kasteleyn, P. (1961), *Physica* **27** (12), 1209.

Kasteleyn, P. (1963), *4*, 10.1063/1.1703953.

Kato, R. (2014), *Bull. Chem. Soc. Jpn.* **87**, 355.

Kato, R., A. Tajima, A. Nakao, A. Tajima, and M. Tamura (2007), *Multifunctional Conducting Molecular Materials*, p. 32. *Erratum: Caption of Fig. 4 in p. 35 should be corrected for right; 'Cation =EtMe₃Sb left; Cation=EtMe₃As'*. (RSC, Cambridge).

Katsura, H., N. Nagaosa, and P. A. Lee (2010), *Phys. Rev. Lett.* **104**, 066403.

Kawamoto, A., Y. Honma, K. Kumagai, N. Matsunaga, and K. Nomura (2006), *Phys. Rev. B* **74**, 212508.

Kawamura, H., K. Watanabe, and T. Shimokawa (2014), *J. Phys. Soc. Jpn.* **83**, 103704.

Kells, G., J. K. Slingerland, and J. Vala (2009), *Phys. Rev. B* **80**, 125415.

Kézsmárki, I., Y. Shimizu, G. Mihály, Y. Tokura, K. Kanoda, and G. Saito (2006), *Phys. Rev. B* **74**, 201101.

Khuntia, P., F. Bert, P. Mendels, B. Koteswararao, A. V. Mahajan, M. Baenitz, F. C. Chou, C. Baines, A. Amato, and Y. Furukawa (2016), *Phys. Rev. Lett.* **116**, 107203.

Kimchi, I., and A. Vishwanath (2014), *Phys. Rev. B* **89**, 014414.

Kimchi, I., and Y. Z. You (2011), *Phys. Rev. B* **84**, 180407.

Kino, H., and H. Fukuyama (1995), *J. Phys. Soc. Jpn.* **64**, 2726.

Kitaev, A. (2003), *Ann. Phys.* **303** (1), 2.

Kitaev, A. (2006), *Ann. Phys.* **321** (1), 2, january Special Issue.

Klümper, A., A. Schadschneider, and J. Zittartz (1993), *Europhys. Lett.* **24** (4), 293.

Ko, W. H., P. A. Lee, and X. G. Wen (2009), *Phys. Rev. B* **79**, 214502.

Ko, W. H., Z. X. Liu, T. K. Ng, and P. A. Lee (2010), *Phys. Rev. B* **81**, 024414.

Komatsu, Y., N. Matsukawa, T. Inoue, and G. Saito (1996), *J. Phys. Soc. Jpn.* **65**, 1340.

Koretsune, T., and C. Hotta (2014), *Phys. Rev. B* **89**, 045102.

Koteswararao, B., R. Kumar, P. Khuntia, S. Bhowal, S. K. Panda, M. R. Rahman, A. V. Mahajan, I. Dasgupta, M. Baenitz, K. H. Kim, and F. C. Chou (2014), *Phys. Rev. B* **90**, 035141.

Kotliar, G. (1988), *Phys. Rev. B* **37**, 3664.

Kou, S. P., and X. G. Wen (2009), *Phys. Rev. B* **80**, 224406.

Kurosaki, Y., Y. Shimizu, K. Miyagawa, and K. Kanoda (2005), *Phys. Rev. Lett.* **95**, 177001.

Kyung, B., and A.-M. S. Tremblay (2006), *Phys. Rev. Lett.* **97**, 046402.

Lacroix, C., P. Mendels, and F. Mila (2011), *Introduction to Frustrated Magnetism: Materials, Experiments, Theory*, Vol. 164 (Springer).

Lai, H.-H., and O. I. Motrunich (2011), *Phys. Rev. B* **84**, 085141.

Larkin, A. I. (1964), *Sov. Phys. JETP* **19** (6), 1478.

Laubach, M., R. Thomale, C. Platt, W. Hanke, and G. Li (2015), *Phys. Rev. B* **91**, 245125.

Laughlin, R. B. (1989), *Annals of Physics* **191** (1), 163.

Lawler, M. J., A. Paramekanti, Y. B. Kim, and L. Balents (2008), *Phys. Rev. Lett.* **101**, 197202.

Lecheminant, P., B. Bernu, C. Lhuillier, L. Pierre, and P. Sindzingre (1997), *Phys. Rev. B* **56**, 2521.

Lee, D. H., G. M. Zhang, and T. Xiang (2007a), *Phys. Rev. Lett.* **99**, 196805.

Lee, E. K. H., R. Schaffer, S. Bhattacharjee, and Y. B. Kim (2014), *Phys. Rev. B* **89**, 045117.

Lee, P. A. (2008a), *Science* **321**, 1306.

Lee, P. A., and N. Nagaosa (1992), *Phys. Rev. B* **46**, 5621.

Lee, P. A., and N. Nagaosa (2013), *Phys. Rev. B* **87**, 064423.

Lee, P. A., N. Nagaosa, and X.-G. Wen (2006), *Rev. Mod. Phys.* **78**, 17.

Lee, S.-S. (2008b), *Phys. Rev. B* **78**, 085129.

Lee, S. S., and P. A. Lee (2005), *Phys. Rev. Lett.* **95**, 036403.

Lee, S. S., P. A. Lee, and T. Senthil (2007b), *Phys. Rev. Lett.* **98**, 067006.

Lefebvre, S., P. Wzietek, S. Brown, C. Bourbonnais, D. Jerome, C. Mezire, M. Fourmigue, and P. Batail (2000), *Phys. Rev. Lett.* **85**, 5420.

Leggett, A. J. (1965), *Phys. Rev.* **140**, A1869.

Leggett, A. J. (1975), *Rev. Mod. Phys.* **47**, 331.

Leung, P. W., and V. Elser (1993), *Phys. Rev. B* **47**, 5459.

Li, T. (2016), arXiv:1601.0216 , 5.

Li, T., and H.-Y. Yang (2007), *Phys. Rev. B* **75**, 172502.

Liang, S., B. Doucot, and P. W. Anderson (1988), *Phys. Rev. Lett.* **61**, 365.

Lieb, E. H. (1994), *Phys. Rev. Lett.* **73**, 2158.

Lieb, E. H., and F. Y. Wu (1968), *Phys. Rev. Lett.* **20**, 1445.

Liu, Z. X., Y. Zhou, and T. K. Ng (2010a), *Phys. Rev. B* **82**, 144422.

Liu, Z. X., Y. Zhou, and T. K. Ng (2010b), *Phys. Rev. B* **81**, 224417.

Liu, Z. X., Y. Zhou, and T. K. Ng (2014), *New J. Phys.* **16**, 083031.

Liu, Z. X., Y. Zhou, H. H. Tu, X. G. Wen, and T. K. Ng (2012), *Phys. Rev. B* **85**, 195144.

Lu, Y. M., Y. Ran, and P. A. Lee (2011), *Phys. Rev. B* **83**, 224413.

Luther, A., and I. Peschel (1975), *Phys. Rev. B* **12**, 3908.

Ma, M. (1988), *Phys. Rev. B* **38**, 6813.

Ma, Y.-F., and T.-K. Ng (2015), *Phys. Rev. B* **91**, 075106.

MacLaughlin, D. E., Y. Nambu, S. Nakatsuji, R. H. Heffner, L. Shu, O. O. Bernal, and K. Ishida (2008), *Phys. Rev. B* **78**, 220403.

Mandal, S., S. Bhattacharjee, K. Sengupta, R. Shankar, and G. Baskaran (2011), *Phys. Rev. B* **84**, 155121.

Mandal, S., R. Shankar, and G. Baskaran (2012), *J. Phys. A* **45** (33), 335304.

Manna, R. S., M. de Souza, A. Brühl, J. A. Schlueter, and M. Lang (2010), *Phys. Rev. Lett.* **104**, 016403.

Manousakis, E. (1991), Rev. Mod. Phys. **63**, 1.

Marshall, W. (1955), Proc. Roy. Soc. London A. **232** (1188), 48.

Marston, J., and C. Zeng (1991), J. Appl. Phys. **69** (8), 5962.

Mendels, P., F. Bert, M. A. de Vries, A. Olariu, A. Harrison, F. Duc, J. C. Trombe, J. S. Lord, and A. a. C. B. Amato (2007), Phys. Rev. Lett. **98**, 077204.

Mermin, N. D., and H. Wagner (1966), Phys. Rev. Lett. **17**, 1133.

Mila, F. (1998), Phys. Rev. Lett. **81**, 2356.

Misguich, G., B. Bernu, C. Lhuillier, and C. Waldtmann (1998), Phys. Rev. Lett. **81**, 1098.

Misguich, G., and C. Lhuillier (2004), *Frustrated spin systems*, edited by T. H. Diep (World Scientific, Singapore).

Misguich, G., D. Serban, and V. Pasquier (2002), Phys. Rev. Lett. **89**, 137202.

Mishmash, R. V., J. R. Garrison, S. Bieri, and C. Xu (2013), Phys. Rev. Lett. **111**, 157203.

Miyagawa, K., K. Kanoda, and A. Kawamoto (2004), Chem. Rev. **104**, 5635.

Miyagawa, K., A. Kawamoto, Y. Nakazawa, and K. Kanoda (1995), Phys. Rev. Lett. **75**, 1174.

Moessner, R., and J. T. Chalker (1998), Phys. Rev. Lett. **80**, 2929.

Moessner, R., and S. L. Sondhi (2003), Phys. Rev. B **68**, 054405.

Moessner, R., S. L. Sondhi, and E. Fradkin (2001), Phys. Rev. B **65**, 024504.

Mori, T., A. Kobayashi, Y. Sasaki, H. Kobayashi, G. Saito, and H. Inokuchi (1984), Bull. Chem. Soc. Jpn **57**, 627.

Mori, T., H. Mori, and S. Tanaka (1999), Bull. Chem. Soc. Jpn **72**, 179.

Morita, H., S. Watanabe, and M. Imada (2002), J. Phys. Soc. Jpn. **71**, 2109.

Motrunich, O. I. (2005), Phys. Rev. B **72**, 045105.

Mudry, C., and E. Fradkin (1994a), Phys. Rev. B **50**, 11409.

Mudry, C., and E. Fradkin (1994b), Phys. Rev. B **49**, 5200.

Naka, M., and S. Ishihara (2010), J. Phys. Soc. Jpn. **79**, 063707.

Nakajima, S., T. Suzuki, Y. Ishii, K. Ohishi, I. Watanabe, T. Goto, A. Oosawa, N. Yoneyama, N. Kobayashi, F. L. Pratt, and T. Sasaki (2012), J. Phys. Soc. Jpn. **81**, 063706.

Nakamura, K., Y. Yoshimoto, T. Kusugi, R. Arita, and I. M. (2009), J. Phys. Soc. Jpn. **78**, 083710.

Nakatsuji, S., K. Kuga, K. Kimura, R. Satake, N. Katayama, E. Nishibori, H. Sawa, R. Ishii, M. Hagiwara, F. Bridges, T. U. Ito, W. Higemoto, M. Karaki, Y. Halim, A. A. Nugroho, J. A. Rodriguez-Rivera, and C. B. M. A. Green (2012), Science **336**, 559.

Nakatsuji, S., Y. Nambu, H. Tonomura, O. Sakai, S. Jonas, C. Broholm, H. Tsunetsugu, Y. Qiu, and Y. Maeno (2005), Science **309**, 1697.

Nave, C. P., and P. A. Lee (2007), Phys. Rev. B **76**, 235124.

Nayak, C., S. H. Simon, A. Stern, M. Freedman, and S. Das Sarma (2008), Rev. Mod. Phys. **80**, 1083.

Ng, T. K. (1994), Phys. Rev. B **50**, 555.

Ng, T. K. (1999), Phys. Rev. Lett. **82**, 3504.

Ng, T. K., and P. A. Lee (2007), Phys. Rev. Lett. **99**, 156402.

Nielsen, A. E., G. Sierra, and J. I. Cirac (2013), Nature communications **4**.

Nogueira, F. S., and H. Kleinert (2005), Phys. Rev. Lett. **95**, 176406.

Norman, M. R., and T. Micklitz (2009), Phys. Rev. Lett. **102**, 067204.

Nussinov, Z., and Z. van den Brink (2013), arXiv:1303.5922 .

Nussinov, Z., and G. Ortiz (2009), Phys. Rev. B **79**, 214440.

Okamoto, Y., M. Nohara, H. Aruga-Katori, and H. Takagi (2007), Phys. Rev. Lett. **99**, 137207.

Olariu, A., P. Mendels, F. Bert, F. Duc, J. C. Trombe, M. A. de Vries, and A. Harrison (2008), Phys. Rev. Lett. **100**, 087202.

Orus, R. (2014), Ann. Phys. **349**, 117.

Östlund, S., and S. Rommer (1995), Phys. Rev. Lett. **75**, 3537.

Pauling, L. (1949), Proc. Roy. Soc. London A. **196** (1046), 343.

Pilon, D. V., C. H. Lui, T. H. Han, D. Shrekenhamer, A. J. Frenzel, W. J. Padilla, Y. S. Lee, and N. Gedik (2013), Phys. Rev. Lett. **111**, 127401.

Podolsky, D., A. Parameshwari, Y. B. Kim, and T. Senthil (2009), Phys. Rev. Lett. **102**, 186401.

Poilblanc, D., and N. Schuch (2013), Phys. Rev. B **87**, 140407.

Poirier, M., M. de Lafontaine, K. Miyagawa, K. Kanoda, and Y. Shimizu (2014), Phys. Rev. B **89**, 045138.

Poirier, M., S. Parent, A. Cote, K. Miyagawa, K. Kanoda, and Y. Shimizu (2012), Phys. Rev. B **85**, 134444.

Polchinski, J. (1994), Nucl. Phys. B **422** (3), 617.

Pollmann, F., E. Berg, A. M. Turner, and M. Oshikawa (2012), Phys. Rev. B **85**, 075125.

Polyakov, A. (1977), Nucl. Phys. B **120** (3), 429 .

Polyakov, A. (1987), *Gauge Fields and Strings (Contemporary Concepts in Physics)* (Harwood Academic Publishers, Switzerland).

Polyakov, A. M. (1975), Phys. Lett. B **59** (1), 79.

Potter, A. C., T. Senthil, and P. A. Lee (2013), Phys. Rev. B **87**, 245106.

Powell, B. J., and R. H. McKenzie (2011), Reports Prog. Phys. **74**, 056501.

Pratt, F. L., P. J. Baker, S. J. Blundell, T. Lancaster, S. Ohira-Kawamura, C. Baines, Y. Shimizu, K. Kanoda, I. Watanabe, and G. Saito (2011), Nature **471**, 612.

Price, C. C., and N. B. Perkins (2012), Phys. Rev. Lett. **109**, 187201.

Qi, Y., C. Xu, and S. Sachdev (2009), Phys. Rev. Lett. **102**, 176401.

Qin, S., T. K. Ng, and Z. B. Su (1995), Phys. Rev. B **52**, 12844.

Ran, Y., M. Hermele, P. A. Lee, and X. G. Wen (2007), Phys. Rev. Lett. **98**, 117205.

Read, N., and B. Chakraborty (1989), Phys. Rev. B **40**, 7133.

Read, N., and S. Sachdev (1989), Nucl. Phys. B **316** (3), 609 .

Read, N., and S. Sachdev (1990), Phys. Rev. B **42**, 4568.

Reuther, J., R. Thomale, and S. Trebst (2011), Phys. Rev. B **84**, 100406.

Ribeiro, P., and P. A. Lee (2011), Phys. Rev. B **83**, 235119.

Rigol, M., and R. R. P. Singh (2007), Phys. Rev. Lett. **98**, 207204.

Rokhsar, D. S., and S. A. Kivelson (1988), Phys. Rev. Lett. **61**, 2376.

Ryu, S. (2009), Phys. Rev. B **79**, 075124.

Sachdev, S. (1992), Phys. Rev. B **45**, 12377.

Saito, G. (2014), unpublished.

Schaffer, R., S. Bhattacharjee, and Y. B. Kim (2012), Phys. Rev. B **86**, 224417.

Schmidt, K. P., S. Dusuel, and J. Vidal (2008), Phys. Rev. Lett. **100**, 057208.

Schollwöck, U. (2005), Rev. Mod. Phys. **77**, 259.

Schroeter, D. F., E. Kapit, R. Thomale, and M. Greiter (2007), Phys. Rev. Lett. **99**, 097202.

Schuch, N., D. Poilblanc, J. I. Cirac, and D. Pérez-García (2012), Phys. Rev. B **86**, 115108.

Seidel, A. (2009), Phys. Rev. B **80**, 165131.

Senthil, T. (2008), Phys. Rev. B **78**, 045109.

Senthil, T., and M. P. A. Fisher (2000), Phys. Rev. B **62**, 7850.

Shaginyan, V. R., A. Z. Msezane, and K. G. Popov (2011), Phys. Rev. B **84**, 0640401(R).

Shankar, R., and N. Read (1990), Nucl. Phys. B **336** (3), 457.

Shastry, B. S. (1988), Phys. Rev. Lett. **60**, 639.

Shimizu, Y., K. Miyagawa, K. Kanoda, M. Maesato, and G. Saito (2003), Phys. Rev. Lett. **91**, 107001.

Shimizu, Y., K. Miyagawa, K. Kanoda, M. Maesato, and G. Saito (2006), Phys. Rev. B **73**, 140407.

Shimokawa, T., K. Watanabe, and H. Kawamura (2015), Phys. Rev. B **92**, 134407.

Shockley, A. C., F. Bert, J.-C. Orain, Y. Okamoto, and P. Mendels (2015), Phys. Rev. Lett. **115**, 047201.

Shores, M. P., E. A. Nytko, B. M. Bartlett, and D. G. Nocera (2005), J. Am. Chem. Soc **127**, 13462.

Sigrist, M., and K. Ueda (1991), Rev. Mod. Phys. **63**, 239.

Sindzingre, P., P. Lecheminant, and C. Lhuillier (1994), Phys. Rev. B **50**, 3108.

Singh, R. R. P. (2010), Phys. Rev. Lett. **104**, 177203.

Singh, Y., S. Manni, J. Reuther, T. Berlijn, R. Thomale, W. Ku, S. Trebst, and P. Gegenwart (2012), Phys. Rev. Lett. **108**, 127203.

Singh, Y., Y. Tokiwa, J. Dong, and P. Gegenwart (2013), Phys. Rev. B **88**, 220413.

Sorella, S., L. Capriotti, F. Becca, and A. Parola (2003), Phys. Rev. Lett. **91**, 257005.

Stephenson, J. (1970), J. Math. Phys. **11** (2), 420.

Sze, W. P., Y. Zhou, and T.-K. Ng (2016), Phys. Rev. Lett..

Tamura, M., and R. Kato (2002), J Phys. Condens. Matter **14**, L729.

Tang, E., M. P. A. Fisher, and P. A. Lee (2013), Phys. Rev. B **87**, 045119.

Tang, Y., and A. W. Sandvik (2013), Phys. Rev. Lett. **110**, 217213.

Thomale, R., E. Kapit, D. F. Schroeter, and M. Greiter (2009), Phys. Rev. B **80**, 104406.

Tikhonov, K. S., and M. V. Feigel'man (2010), Phys. Rev. Lett. **105**, 067207.

Tocchio, L. F., H. Feldner, F. Becca, V. R., and C. Gros (2013), Phys. Rev. B **87**, 035143.

Toulouse, G. (1977), Commun. Phys **2** (4), 115.

Tsumuraya, T., H. Seo, H. Tsuchizawa, R. Kato, and T. Miyazaki (2013), J. Phys. Soc. Jpn. **82**, 033709.

Vannimenus, J., and G. Toulouse (1977), J. Phys. C **10** (18), L537.

Verstraete, F., and J. I. Cirac (2004a), arXiv:0407066 .

Verstraete, F., and J. I. Cirac (2004b), Phys. Rev. A **70**, 060302.

Verstraete, F., and J. I. Cirac (2006), Physical Review B **73**, 094423.

Verstraete, F., V. Murg, and J. Cirac (2008), Adv. Phys. **57** (2), 143.

Verstraete, F., M. M. Wolf, D. Perez-Garcia, and J. I. Cirac (2006), Phys. Rev. Lett. **96**, 220601.

Vidal, J., K. P. Schmidt, and S. Dusuel (2008), Phys. Rev. B **78**, 245121.

Villain, J., Bidaux, R., Carton, J.-P., and Conte, R. (1980), J. Phys. France **41** (11), 1263.

de Vries, M. A., K. V. Kamenev, W. A. Kockelmann, J. Sanchez-Benitez, and A. Harrison (2008), Phys. Rev. Lett **100**, 157205.

de Vries, M. A., J. R. Stewart, P. P. Deen, J. O. Piatek, G. J. Nilsen, H. M. Rønnow, and A. Harrison (2009), Phys. Rev. Lett **103**, 237201.

Walldtmann, C., H. U. Everts, B. Bernu, C. Lhuillier, P. Sindzingre, P. Lecheminant, and L. Pierre (1998), Eur. Phys. J. B **2** (4), 501.

Wang, F. (2010a), Phys. Rev. B **81**, 184416.

Wang, F. (2010b), Phys. Rev. B **82**, 024419.

Wang, F., and A. Vishwanath (2006), Phys. Rev. B **74**, 174423.

Wang, L., D. Poilblanc, Z. C. Gu, X. G. Wen, and F. Verstraete (2013), Phys. Rev. Lett. **111**, 037202.

Wannier, G. H. (1950), Phys. Rev. **79**, 357.

Watanabe, D., M. Yamashita, S. Tonegawa, Y. Oshima, H. Yamamoto, R. Kato, I. Sheikin, K. Behnia, T. Terashima, S. Uji, et al. (2012), Nature Commun. **3**, 1090.

Watanabe, K., H. Kawamura, H. Nakano, and T. Sakai (2014), J. Phys. Soc. Jpn. **83**, 034714.

Watanabe, T., H. Yokoyama, Y. Tanaka, and J. Inoue (2008), Phys. Rev. B **77**, 214505.

Wen, X. G. (1989), Phys. Rev. B **39**, 7223.

Wen, X. G. (1991), Phys. Rev. B **44**, 2664.

Wen, X. G. (2002), Phys. Rev. B **65**, 165113.

Wen, X. G., F. Wilczek, and A. Zee (1989), Phys. Rev. B **39**, 11413.

Wen, X. G., and A. Zee (1988), Phys. Rev. Lett. **61**, 1025.

White, S. R. (1992), Phys. Rev. Lett. **69**, 2863.

White, S. R., and A. L. Chernyshev (2007), Phys. Rev. Lett. **99**, 127004.

Wu, C., D. Arovas, and H.-H. Hung (2009), Phys. Rev. B **79**, 134427.

Wu, T. T., and C. N. Yang (1976), Nucl. Phys. B **107** (3), 365.

Xie, Z., J. Chen, J. F. Yu, X. Kong, B. Normand, and T. Xiang (2014), Phys. Rev. X **4**, 011025.

Xu, C., F. Wang, Y. Qi, L. Balents, and M. P. A. Fisher (2012), Phys. Rev. Lett. **108**, 087204.

Yamashita, M., N. Nakata, Y. Kasahara, T. Sasaki, N. Yoneyama, N. Kobayashi, S. Fujimoto, T. Shibauchi, and Y. Matsuda (2008a), Nature Phys. **5** (1), 44.

Yamashita, M., N. Nakata, Y. Senshu, M. Nagata, H. M. Yamamoto, R. Kato, T. Shibauchi, and Y. Matsuda (2010), Science **328** (5983), 1246.

Yamashita, S., Y. Nakazawa, M. Oguni, Y. Oshima, H. Nojiri, Y. Shimizu, K. Miyagawa, and K. Kanoda (2008b), Nature Phys. **4** (6), 459.

Yamashita, S., T. Yamamoto, Y. Nakazawa, M. Tamura, and R. Kato (2011), Nature Commun. **2** (Aug), 275.

Yan, S., D. Huse, and S. White (2011), Science **332** (6034), 1173.

Yang, H. Y., A. M. Läuchli, F. Mila, and K. P. Schmidt (2010), Phys. Rev. Lett. **105**, 267204.

Yang, S., D. L. Zhou, and C. P. Sun (2007), Phys. Rev. B **76**, 180404.

Yao, H., and S. A. Kivelson (2007),

Phys. Rev. Lett. **99**, 247203.

Yao, H., and S. A. Kivelson (2012), Phys. Rev. Lett. **108**, 247206.

Yao, H., and D. H. Lee (2011), Phys. Rev. Lett. **107**, 087205.

Yao, H., S.-C. Zhang, and S. A. Kivelson (2009), Phys. Rev. Lett. **102**, 217202.

Yokoyama, H., and H. Shiba (1987), J. Phys. Soc. Jpn. **56**, 3570.

Yu, Y. (2008), Nucl. Phys. B **799** (3), 345 .

Yu, Y., L. Liang, Q. Niu, and S. Qin (2013), Phys. Rev. B **87**, 041107.

Yu, Y., and Z. Wang (2008), EPL **84**, 57002.

Yunoki, S., and S. Sorella (2006), Phys. Rev. B **74**, 014408.

Zhou, H. D., E. S. Choi, G. Li, L. Balicas, C. R. Wiebe, Y. Qiu, J. R. D. Copley, and J. S. Gardner (2011), Phys. Rev. Lett. **106**, 147204.

Zhou, Y., and P. A. Lee (2011), Phys. Rev. Lett. **106**, 056402.

Zhou, Y., P. A. Lee, T. K. Ng, and F. C. Zhang (2008), Phys. Rev. Lett. **101**, 197201.

Zhou, Y., and T. K. Ng (2013), Phys. Rev. B **88**, 165130.

Zhou, Y., and X.-G. Wen (2002), arXiv:cond-mat/0210662 .

Zhu, W., S. S. Gong, and D. N. Sheng (2015), Phys. Rev. B **92**, 014424.